

Title of thesis

**ASSESSMENT OF ULCER WOUNDS USING 3D SKIN
SURFACE IMAGING**

I, NEJOOD MOHAMMED ELTEGANI,

hereby allow my thesis to be placed at the Information Resource Center (IRC) of Universiti Teknologi PETRONAS (UTP) with the following conditions:

1. The thesis becomes the property of UTP.
2. The IRC of UTP may make copies of the thesis for academic purposes only.
3. This thesis is classified as

Confidential

Non-confidential

If this thesis is confidential, please state the reason:

The contents of the thesis will remain confidential for 2 years.

Remarks on disclosure:

Endorsed by

Signature of Author

Signature of Supervisor
Universiti Teknologi PETRONAS

Date :

Date :

UNIVERSITI TEKNOLOGI PETRONAS

Approval by Supervisor (s)

The undersigned certify that they have read, and recommend to The Postgraduate Studies Programme for acceptance, a thesis entitled “**ASSESSMENT OF ULCER WOUNDS USING 3D SKIN SURFACE IMAGING**” submitted by **NEJOOD MOHAMMED ELTEGANI** for the fulfillment of the requirements for the degree of Master of Science in Electrical and Electronics Engineering.

Date

Signature : _____

Main supervisor : Prof. Ir. Dr. Ahmad Fadzil M. Hani

Date : _____

Signature : _____

Co-Supervisor : _____

Date : _____

UNIVERSITI TEKNOLOGI PETRONAS

ASSESSMENT OF ULCER WOUNDS USING 3D SKIN SURFACE IMAGING

By

NEJOOD MOHAMMED ELTEGANI

A THESIS

SUBMITTED TO THE POSTGRADUATE STUDIES PROGRAMME

AS A REQUIREMENT FOR THE

DEGREE OF MASTER OF SCIENCE

ELECTRICAL AND ELECTRONICS ENGINEERING

BANDAR SERI ISKANDAR,

PERAK

October 2009

DECLARATION

I hereby declare that the thesis is based on my original work except for quotations and citations which have been duly acknowledged. I also declare that it has not been previously or concurrently submitted for any other degree at UTP or other institutions.

Signature : _____

Name : NEJOOD MOHAMMED ELTEGANI

Date : _____

Acknowledgement

First and foremost I thank Allah without whom none of this work would have been done.

Special thanks to Prof Ahmad Fadzil, my supervisor, for his help and guidance along the way and his family for their hospitality. I am glad to have the opportunity to work with him and to be a member of the Intelligent Imaging lab and to have the opportunity to use all the advance facilities of the lab.

I would like to thank my family for their support and understanding, and my friends/colleagues at SUST/UTP for their support during my study period.

I would like to thank my colleagues and friends at the Intelligent Imaging lab (Batool, Esa, Wawan, Fitri, Dani, Hanung, Lila and Maryam) for their support and discussion and their collaboration in the process of data collection. I want to extend my thanks to friends (Tamiru) for offering training on AutoCAD software and the valuable discussions.

I would like to thank the Rapid Prototyping unit at UTP for allowing me to use their utilities and their help during the process. I would also like to thank the PG office staff (Fadil, Wahida, Haslina, Norma, Kamalia, Kahar).

And Finally I would like to thank the HKL specialists, staff for their help during the process of data collection and the ulcer patients for their inspiring attitude and collaboration.

Abstract

In medical care, ulcer wound refers to open wound or sore in which certain conditions exist that impede healing. Nonhealing wounds can cause economical and psychological distress for patients. Wound size measurement (top area, true surface area, depth, and volume) is an objective indicator for wound healing. Top area measurement is useful for the follow up of shallow wounds, while true surface area if done accurately can work for all types of wounds. Calculating ulcer volume is crucial since studies showed that wounds start healing from the bottom. Overestimation in top area and true surface area measurement can be solved by digitizing the traced part. The objective of this research is to develop computer algorithms to measure ulcer wound size using 3D surface imaging. The wounds of interest are the wounds located at the leg. The algorithms should construct wound models and compute volume without getting affected by irregularities on wound surface and they should model leg curvature. Two algorithms for constructing wound models and volume computation are developed and evaluated; namely midpoint projection and convex hull approximation (Delaunay tetrahedralization). Parameters that describe the wounds are developed based on real ulcer wound surface images for wound modelling. Wound models representing possible ulcer wounds developed using AutoCAD software are used to investigate the performance of solid reconstruction methods. Results and analysis show that, for volume computation midpoint and convex hull methods can compute volume of leg ulcer without getting affected by irregularities in the healthy skin around the wound. The results show that, for convex hull low errors are produced in cases of regular boundary models excluding the elevated base models. Overestimation in volume for convex hull method can either be due to irregular boundary and/or elevation at the base (both global and local). Surface division is performed prior to convex hull approximation so that the high curvature of the leg and irregularity at the boundary can be represented using a number of linear segments. With the increase in surface division, error due to irregular boundary is reduced. In the case of global curvature, the reconstructed model using convex hull preceded by surface division simulates the leg curvature. Midpoint outperforms convex hull for models excluding elevated base models. Midpoint can construct solids for wound surfaces with local curvature while for surfaces with high global curvature the error is high. Midpoint method is not suitable for shallow and very large wounds.

Abstrak

Ulser dalam istilah perubatan merujuk kepada luka fizikal yang terdedah atau lepuh di bahagian luar kulit yang melalui proses penyembuhan yang sangat lambat. Lebih membimbangkan, ulser bukan sahaja boleh memberi kesan dari segi ekonomi, malah ia juga memberi tekanan psikologi kepada pesakit. Antara penunjuk aras peningkatan penyembuhan luka ialah saiz luka itu sendiri yang terdiri daripada bahagian atas, permukaan nyata dan isipadu luka tersebut. Pengukuran bahagian atas luka adalah sangat berguna bagi pemeriksaan luka ringan manakala permukaan nyata boleh menyembuhkan semua jenis luka. Pengiraan isipadu ulser adalah sangat penting bagi menentukan fasa penyembuhan luka dari bawah kulit. Kebarangkalian pengukuran bahagian atas dan keluasan permukaan yang kurang tepat boleh diselesaikan melalui pendigitan luka tersebut. Objektif kajian ini ialah untuk membina algoritma komputer supaya pengukuran saiz ulser boleh dilakukan melalui pengimejan permukaan 3D. Luka dalam kajian ini bertumpu pada bahagian kaki. Algoritma ini mampu membina model luka dan menjana data isipadu tanpa mengambil kira permukaan luka yang tidak sekata. Sistem ini menghasilkan model sebuah kaki yang sempurna. Dua algoritma untuk membina model luka dan pengiraan isipadu telah dibangunkan dan dinilai iaitu unjuran titik tengah dan penganggaran hull cembung (Delaunay tetrahedralization). Parameter yang menggambarkan luka dibina berdasarkan imej permukaan luka ulser yang asal. Perisian AutoCAD telah digunakan untuk menentukan keberkesanan kaedah pembinaan model luka yang mantap. Hasil kajian dan daripada perolehan analisa menunjukkan yang model luka ini boleh meramal ulser yang bakal terjadi. Penentuan isipadu ulser kaki boleh dikomputasikan melalui gabungan komputasi titik tengah isipadu beserta kaedah Hull. Ketidaksamaan hasil daripada kulit sihat disekitar ulser tidak memberi kesan terhadap penilaian komputasi ini. Gabungan kaedah Hull menghasilkan ralat yang sangat rendah apabila model yang berlainan daripada biasa digunakan. Ralat ini biasanya berpunca daripada ketidaksamaan jalur pemisah dan/atau kedalaman dasar ulser itu sendiri (secara menyeluruh atau setempat). Pembahagian permukaan luka dibuat berdasarkan penaakulan Hull. Hal ini supaya susuk bentuk kaki dan ketidaksamaan jalur pemisah dapat dibuat menggunakan jujukan segmen yang linear. Ralat pada jalur pemisah yang tidak sekata dapat dikurangkan apabila pembahagian permukaan luka ditingkatkan. Bagi kes susuk bentuk yang umum, model yang dibina menggunakan gabungan kaedah Hull

menjurus kepada pembahagian permukaan supaya dapat menghasilkan simulasi susuk bentuk kaki yang baik. Titik tengah pada model hanya dilakukan menggunakan gabungan kaedah Hull tanpa mengambil kira model asas. Titik tengah menghasilkan permukaan luka yang jelas dengan susuk luka setempat. Manakala susuk luka yang menyeluruh atau berselerak akan menghasilkan ralat yang sangat tinggi. Kaedah titik tengah tidak sesuai bagi luka ringan/nipis dan terlalu besar.

Table of Contents

Acknowledgement.....	v
Abstract.....	vi
Abstrak.....	vii
Table of Contents	ix
List of Tables	xii
List of Figures	xiii
CHAPTER 1: INTRODUCTION	1
1.1 BACKGROUND OF THE STUDY	1
1.2 PROBLEM STATEMENT	5
1.3 RESEARCH OBJECTIVE AND SCOPE	9
1.4 OVERVIEW OF THESIS STRUCTURE	11
CHAPTER 2: WOUND ANALYSIS IN MEDICAL PRACTICE	12
2.1 ULCER WOUNDS.....	12
2.1.1 Leg Ulcers.....	14
2.1.2 Documentation and Treatment.....	16
2.2 WOUND MEASUREMENT IN CLINICAL PRACTICE.....	19
2.2.1 Area and Surface Area Measurement.....	19
2.2.2 Depth Measurement	21
2.2.3 Volume Estimation.....	22
2.4 SUMMARY	23
CHAPTER 3: WOUND ANALYSIS USING DIGITAL IMAGING TECHNIQUES.....	25
3.1 IMAGING TECHNIQUES FOR WOUNDS.....	25
3.1.1 2D Photography in Dermatology and Wound Assessment	25
3.1.1.1 Wound Bed Tissue Classification Using Coloured Images	25
3.1.1.2 Digitization of Wound Area/Surface Area	26
3.1.1.3 Depth measurement	26
3.1.1.3.1 Optical Coherence Tomography (OCT)	26
3.1.1.3.2 Ultrasound	27
3.1.2 Three-dimensional (3D) Surface Scanning Techniques.....	28
3.1.2.1 Structured Light.....	28
3.1.2.2 Photogrammetry.....	28
3.1.2.3 Laser Scanning.....	29

3.2 SURFACE REPRESENTATION	31
3.3 CURRENT METHODS for COMPUTING ULCER WOUND VOLUME from 3D SURFACE SCANS	32
3.3.1 Fitting a Plane to Wound Boundary.....	33
3.3.2 Surface Interpolation using Cubic Spline.....	34
3.4 SURFACE FITTING MODELS	35
3.4.1 Analytic Surfaces	35
3.4.2 Synthetic Surfaces.....	36
3.5 SOLID RECONSTRUCTION FROM SURFACES	38
3.5.1 Building Solid/Model from Surface Patches	38
3.5.2 Projection.....	39
3.5.2.1 <i>Projecting surface to a plane</i>	39
3.5.2.2 <i>Projecting surface faces to origin point /reference point</i>	41
3.5.3 Convex Hull Approximation	41
3.6 VOLUME COMPUTATION.....	43
3.6.1 Morphological Approach to Volume Calculation – Cross sectioning	43
3.6.2 Integration and Divergence Theorem.....	44
3.6.3 Projecting Surface Boundaries to Centre Point / Origin Point, Tertahedralization	46
3.6.4 Dividing the Solid to Equal Size Elements	47
3.7 SUMMARY	48
CHAPTER 4: ALGORITHM DEVELOPMENT AND WOUND MODELING FOR NONINVASIVE WOUND ASSESSMENT	50
4.1 ALOGRITHM DESIGN CONSIDERATIONS.....	50
4.2 3D LASER SCANNING.....	52
4.2.1 Surface Scanning Setup.....	54
4.2.2 Registering Multiple Scans.....	55
4.2.3 Segmenting Wound Area	57
4.3 ENHANCEMENT	57
4.4 ALIGNMENT AND COORDINATE SYSTEM.....	58
4.5.1 Wound Shape Attributes.....	62
4.5.2 Developing Wound Models	64
4.6 CALCULATING WOUND TOP AREA AND TRUE SURFACE AREA ...	67
4.6.1 Top Area.....	68

4.6.2 True Surface Area	69
4.7 SURFACE RECONSTRUCTION: CREATING SOLID BY PROJECTING SURFACE FACES TO MIDPOINT	70
4.8 SURFACE RECONSTRUCTION: CREATING SOLID USING CONVEX HULL APPROXIMATION (Delaunay Tetrahedralization).....	75
4.9 SURFACE DIVISION FOR MODELLING LEG CURVATURE.....	78
4.10 VOLUME COMPUTATION FROM RECONSTRUCTED SOLIDS.....	83
4.11 VALIDATING THE PERFORMANCE OF SOLID RECONSTRUCTION ALGORITHMS USING SOLID MODELS	84
4.12 SUMMARY	86
CHAPTER 5: RESULTS AND ANALYSIS	88
5.1 SIMULATION RESULTS OF VOLUME COMPUTATION	88
5.2 SURFACE DIVISION PRIOR TO CONVEX HULL APPROXIMATION (Delaunay tetrahedralization)	95
5.3 MEASUREMENTS on REAL WOUNDS SCANS.....	99
5.4 RESULTS of REAL SCANS COMPARED to MOLDED SURFACES	106
CHAPTER 6: CONCLUSION.....	111
REFERENCES.....	116
APPENDIX A: IMAGES OF THE SCANNED WOUNDS	122
APPENDIX B: WOUND MODELING USING AutoCAD	131
APPENDIX C: ALGORITHMS CODE	134
APPENDIX D: CD.....	145

List of Tables

Table 3.1: Analytic surfaces	36
Table 3.2: Synthetic surfaces	37
Table 4.1: Wound attributes and their descriptors	62
Table 4.2: Wound Models	64
Table 5.1: The results of volume computation using midpoint projection and convex hull approximation	89
Table 5.2: The effect of base elevation on volume computation	93
Table 5.3: The measurement of the DB wounds scans	99
Table 5.4: The top are, true surface area, average depth and volume results obtained by applying the algorithms on real wound scans	100
Table 5.5: Size measurement on two moulded wounds	110

List of Figures

Figure 1.1: A lesion with a square lattice on top for area measurement [Wilhelm <i>et al.</i> 2006].....	1
Figure 1.2: Quantification of wrinkles [Serup <i>et al.</i> 2006]	2
Figure 1.3: Examples of leg ulcers.....	3
Figure 1.4: VIVD 3D laser scanner and examples of wound scans.....	5
Figure 1.5: Invasive methods for volume measurement	7
Figure 1.6: Curvature of the leg and surface irregularities surrounding the wound	8
Figure 1.7: Error in surface reconstruction.....	9
Figure 2.1: Schematic illustration of a wound involves the epidermis and at least part of the dermis [Shai & Maibach 2005]	12
Figure 2.2: Examples of leg ulcer wounds	15
Figure 2.3: Distribution of nonvenous and venous ulcers of lower limb [London & Donnelly 2000]	16
Figure 2.4: Schematic diagram of the timing of the wound healing phases [HARTMANN 2006].....	17
Figure 2.5: Compression bandage [London & Donnelly 2000]	18
Figure 2.6: Measuring wound based on maximum length and width [Ahn & Salcido 2008]	19
Figure 2.7: Defining wound boundary manually [Langemo <i>et al.</i> 2008].....	20
Figure 2.8: Acetate sheet tracing [Baranoski & Ayello 2007]	21
Figure 2.9: Approximate measurement of wound depth using a simple probe [Flanagan 2003].....	21
Figure 2.10: The Kunding gauge [Baranoski & Ayello 2007]	22
Figure 2.11: Alginate paste method for volume estimation [Plassman <i>et al.</i> 1994].....	22
Figure 2.12: Filling wound surface with saline solution for volume estimation [HARTMANN 2006]	23
Figure 3.1: Colour analysis for wound tissue classification.....	26
Figure 3.2: Visitrak Wound Measurement System [Smith & Nephew 2009].....	26
Figure 3.3: Optical coherence tomography of wound healing of an incision [Wilhelm <i>et al.</i> 2006].....	27
Figure 3.4: Venous ulcer (left) and its cross section scan using ultrasound (right) [Wendelken <i>et al.</i> 2003]	27
Figure 3.5: Example of the distortion of originally parallel stripes due to wrinkle structure [Wilhelm <i>et al.</i> 2006]	28
Figure 3.6: Photogrammetry method for 3D scanning.....	29
Figure 3.7: Laser triangulation concept.....	30
Figure 3.8: Point cloud and the corresponding triangular mesh surface	32
Figure 3.9: The inner volume computed by closing the 3D model of the wound surface with a plane defined from the wound boundary [Albouy & Treuillet 2007]	33
Figure 3.10: Cross section illustration of wound surface	34
Figure 3.11: Reconstructed model out of wound scan [Plassman <i>et al.</i> 1995].....	35
Figure 3.12: Stitching surfaces [Kazhdan, 2005].....	38
Figure 3.13: Projecting a triangular face to the origin	39
Figure 3.14: Projecting scanned surface faces to a plane	40
Figure 3.15: Calibration cube for scanner measurement validation [Zhang <i>et al.</i> 2005]..	40
Figure 3.16: Projecting faces to origin point [Ohanian 2003]	41
Figure 3.17: Enclosing a model in convex polyhedron.....	42

Figure 3.18: Convex decomposition [Lien & Amato 2008].....	42
Figure 3.19: Ten generated vertical 2D electrical resistivity sections [Sirakov <i>et al.</i> 2003]	44
Figure 3.20: Illustration of the Method of Direct Integration [Lee & Requicha 1982]	45
Figure 3.21: Projecting faces to centre point	46
Figure 3.22: Subdivision of a model into tetrahedra [Hoffmann 1989].....	46
Figure 3.23: Dividing an object into identical cubes [Lee & Requicha 1982]	47
Figure 4.1: Obtaining wound surface scan using 3D laser scanner	53
Figure 4.2: Liquids at wound surface (date: 4-12-08; patient: P-9; hospital: HKL).....	55
Figure 4.3: Ray refraction due to shiny surface [LEVOY 1999].....	55
Figure 4.4: Surface registration using two surface scans	57
Figure 4.5: Wound surface selection.....	57
Figure 4.6: Wound surface with noise.....	58
Figure 4.7: Surface translation and aligning	59
Figure 4.8: Wound surface with different coordinates.....	60
Figure 4.9: Surface acquisition and pre-processing steps.....	61
Figure 4. 10: Illustrations of the geometrical attributes of ulcer wounds.....	62
Figure 4.11: Union and subtraction commands [AutoCAD 2007]	64
Figure 4.12: Extrude command [AutoCAD 2007].....	65
Figure 4.13: Creating solid models using AutoCAD	65
Figure 4.14: Models M1, M2a, M3b and M4b	66
Figure 4.15: Overview of the system diagram.....	67
Figure 4.16: Extracting surface boundary	68
Figure 4.17: Surface alignment.....	69
Figure 4.18: Midpoint calculation.....	70
Figure 4.19: Midpoint solid reconstruction for a model and a skin surface	72
Figure 4.20: L shaped wound.....	73
Figure 4.21: Flow chart diagram of mid-point projection algorithm	74
Figure 4.22: The horizon of a polytope [Berg <i>et al.</i> 2008].....	76
Figure 4.23: Adding a point to the convex hull [Berg <i>et al.</i> 2008].....	76
Figure 4.24: Convex hull solid reconstruction for a model and a skin surface	78
Figure 4.25: Tabulated surface reconstruction.....	79
Figure 4.26: Constructing the model by performing division union.....	79
Figure 4.27: Constructing solids out of surfaces using surface division prior to convex hull approximation (Delaunay teraheralization)	80
Figure 4.28: Representing models using different point density	81
Figure 4.29: Flow diagram of convex hull reconstruction with surface division	82
Figure 4.30: Solid reconstruction using convex hull approximation algorithm	85
Figure 4.31: Solid reconstruction using midpoint algorithm.....	85
Figure 5.1: Percentage errors of volume computation using midpoint projection and convex hull approximation	90
Figure 5.2: The top view of a model and its convex hull approximation.....	91
Figure 5.3: The effect of base elevation on solid reconstruction algorithms.....	91
Figure 5.4: Percentage errors of volume computation excluding elevated base wound models.....	92
Figure 5.5: Elevation at the wound base	94
Figure 5.6: Results of volume computation using convex hull and convex hull with 2,5,10 and 20 divisions	95
Figure 5.7: Percentage error in volume computation using convex hull, convex hull with 2,5,10 and 20 divisions	96

Figure 5.8: Solid Reconstructionf for regular boundary model(m1h)	96
Figure 5.9: Solid Reconstructionf for irregular boundary model (m2h)	97
Figure 5.10: Solid Reconstructionf for irregular boundary model (m4h)	97
Figure 5.11: Solid Reconstruction for irregular boundary model (m6h).....	97
Figure 5.12: Global base elevation.....	98
Figure 5.13: The results of solid reconstruction for a large wound	98
Figure 5.14: Large wound model reconstruction (Ulcer 18)	101
Figure 5.15: Wound model reconstructed from wound surface (Ulcer 16).....	103
Figure 5.16: Foot ulcers (Ulcer 9).....	103
Figure 5.17: Wounds with large area	104
Figure 5.18: Representing leg shape using 8 faces	105
Figure 5.19: Foot ulcers.....	105
Figure 5.20: Steps for measuring wound volume using flexible material.....	107
Figure 5.21: Wound model reconstructed from wound surface (Ulcer 6)	108
Figure 5.22: Wound model reconstructed from wound surface (Ulcer 14).....	109

CHAPTER 1: INTRODUCTION

1.1 BACKGROUND OF THE STUDY

Noninvasive imaging techniques are becoming an essential part of the medical care. It is used for obtaining data that can be further analyzed to obtain information which is helpful in the diagnosis and/or assessment of a disease or condition [Wilhelm *et al.* 2006].

Photographic data, in addition to its being a noninvasive criterion is also valuable for storing patients' records that can easily be retrieved whenever needed. Documenting different stages of the medical history can be used for assessment/reassessment and for improving the quality of medical care [Dealey 1999].

In dermatology, 2D photography is an essential tool since the skin is a visible organ of the body which can be directly accessed and scanned. Skin diseases evolve in a range of visible changes. Thus photographic recording allows the integration of objective noninvasive methods for assessment and follow up in different skin diseases. Photography is used for telemedicine applications and for studying patterns of skin diseases in addition to its advantage in record keeping. 2D imaging is used to produce assessment of the extent of some diseases based on the colour analysis. 2D images can also be used for computing area of skin lesion as shown in Figure 1.1 [Wilhelm *et al.* 2006].

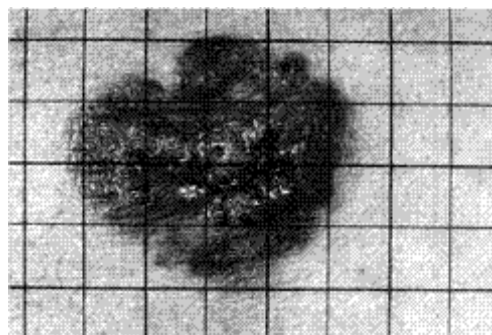


Figure 1.1: A lesion with a square lattice on top for area measurement [Wilhelm *et al.* 2006]

Some diseases require more sophisticated data than 2D images. For example when the disease has some sort of texture changes like the skin aging effects [Wilhelm *et al.* 2006] or when the continuity of the skin is interrupted as in the case of wounds. These diseases require data which provide details of the depth changes. In addition, 3D representations that can be manipulated by the observer convey information not obtainable from 2D images [Séquin 2005]. Quantification of wrinkles is an area that requires 3D surface scans as shown in Figure 1.2. This can be used to proof the efficacy of specific treatment in reducing the aging effect [Serup *et al.* 2006].



Figure 1.2: Quantification of wrinkles [Serup *et al.* 2006]

Wound is defined as any discontinuity in the skin and probably the underlying tissue due to various factors. Ideally wound will heal normally within the expected time given the overall wellbeing of the person is not disturbed. However for people with some other medical complications wound might not heal normally. Most physicians would agree that a wound which is not healing within 3-4 months may be regarded as chronic. Ulcer wound is considered a chronic wound that has underlying causes that prevents it from healing. In some ulcer cases, wounds can take up to two years to heal. Nonhealing wounds can cause economical and psychological distress for patients [Ahn & Salcido 2008]. Figure 1.3 displays two cases of leg ulcers obtained from Hospital Kuala Lumpur (HKL).



Figure 1.3: Examples of leg ulcers

Ulcer wound is a worldwide problem, generating high morbidity and medical expenses. Assessment of an ulcer wound involves surveying a range of physical parameters, which is time consuming, and often results in inconsistencies in patient care [Simonsen *et al.* n.d.]. Chronic wounds are common 8% of bedridden / chairbound patients develop pressure ulcers [Plassman *et al.* 1994]. Another type of chronic wound is ulceration of the lower limb. Leg ulcers affect 1% of the adult population and 3.6% of people older than 65 years [Shai & Maibach 2005; HARTMANN 2006].

When assessing wounds, several steps need to be performed namely (a) recording history, (b) physical examination, (c) laboratory tests/biopsy, (d) ulcer measurement and (e) patient assessment. Because different types of ulcer wounds exist, the cause of the ulcer is the key for treatment selection [Shai & Maibach 2005].

Establishing the cause of the wound or skin condition will help identify the correct classification and management process. Underlying medical conditions (etiology) such as poor nutrition, diabetes (neuropathy), venous hypertension (can result in leg swelling), arterial insufficiency (can result in scales) and mixed etiology (can result in scales at the leg and swelling) may explain why the wound may be healing slowly. These conditions need to be treated concurrently [Hess 2005]. The effectiveness of a treatment regime can be estimated by measuring changes in the ulcer wound. And thus identifying appropriate treatment regime will reduce the healing time [Ahn & Salcido 2008].

Documenting wounds and obtaining several quantitative measurements is not only useful for wound assessment and follow up but it is also a useful tool in forensic medicine. In forensic medicine, documenting or determining the wound size at the time of the incident is necessary or the wound will heal, over time. Photographic data can be used as evidence [KONICA 2004; Sansoni *et al.* 2007]. Quantitative wounds measurement is essential parameter in wound documentation which can state weather the wound is progressing or regressing. Early changes in the wound size can be determined from the wound volume compared to other measurements since wound starts healing from the bottom [Plassman *et al.* 1994].

Invasive methods for volume estimation might cause infection or disturbance to the wound tissue, and therefore are limited in practical use [Zhu 2007].

Noninvasive 3D scanners based on different technologies (photogrammetry, structured light and laser) are used to capture the skin surface [Malian *et al.* 2004; Plassman *et al.* 1995; KONICA 2004]. The availability of different types of 3D scanners that are capable of capturing depth at various locations on a surface make diagnosis and assessment for various skin diseases possible [Wilhelm *et al.* 2006].

The noninvasive method for documentation is preferable for different reasons. It is used in:

- (a) art preservation and archeology since the objects are fragile [Kampel & Sablatnig 2006; Li *et al.* 2003],
- (b) in crime scenes to keep the exact location of every object in the scene [Sansoni *et al.* 2007]
- (c) and in wounds care since invasive methods cause pain, discomfort or infections for patients [Zhu 2007].

Figure 1.4 (a) displays the Vivid 910 3D laser scanner which is used in this research to capture a variety of 3D surfaces scans and Figure 1.4(b) display two ulcer wounds captured by the scanner.

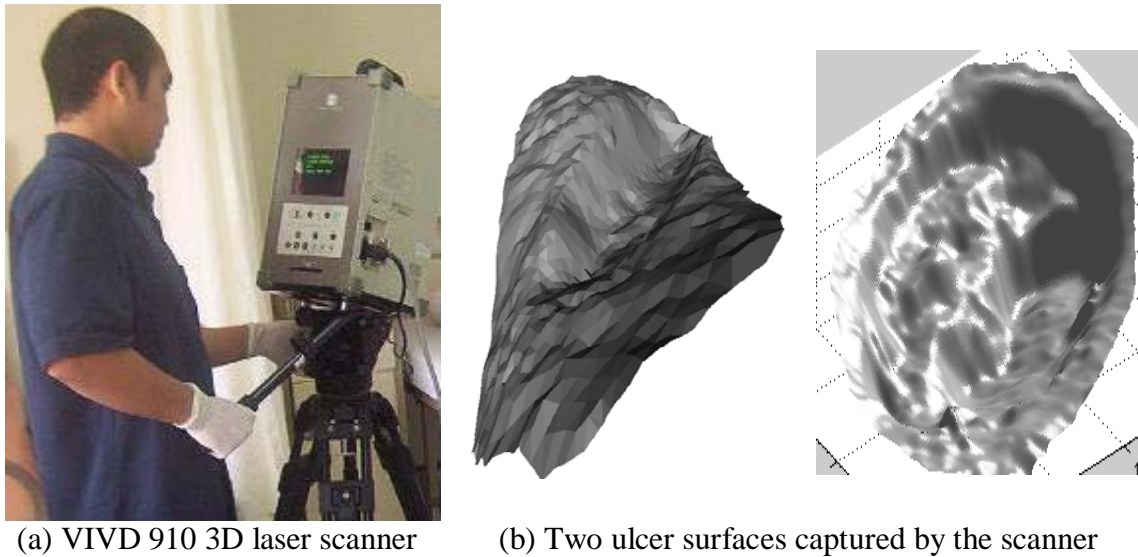


Figure 1.4: VIVD 3D laser scanner and examples of wound scans

1.2 PROBLEM STATEMENT

When assessing ulcer wounds, the effectiveness of a treatment regime can be estimated by measuring changes in the ulcer wound. Wound measurement is useful if performed accurately. Wound documentation is necessary for later use by interdisciplinary team in the assessment/reassessment process. The primary purpose of wound assessment should be to monitor the progress of healing and to detect nonhealing wounds early [Flanagan 2003]. Early detection of wound response to a treatment is not only applicable to reduce treatment time but it is also valuable for evaluating new treatments in pharmaceutical research [Thomson & Miles 2006]. There is a need for measuring ulcer wounds size using noninvasive techniques including 2D and 3D accompanied by programs which can obtain measurement to higher precision. This will also help in identifying the appropriate treatment regime by detecting changes, and hence reduces the healing time.

Multiple references are present today for physicians that give several recommendations and protocols when dealing with ulcer wounds. These sources give different approaches and procedures that might be confusing even for health professionals [Ahn & Salcido 2008]. Diversity in wound care extends throughout the whole procedure, starting from diagnosis to the assessment and wound size measurement. The current methods of wound assessment are often subjective. There is a need to standardize assessment to enable accurate data collection and detection of clinically relevant improvement in patient

outcome [Flanagan 2003 ; Fette 2006]. A topical subject in wound research is to find a standardized procedure and protocol for wound care.

Different parameters might be used for assessing ulcer wounds progression towards healing; such as maximum length, width, depth, top area, true surface area and volume. Wound top area measurement can indicate healing for wounds that have superficial tissue loss, are shallow and do not extend under the skin edge. Surface tracing if performed accurately work for both deep and shallow wounds. Volume measurement is useful measurement in case of wounds that are deep and extend under the skin edge [Baranoski & Ayello 2007].

For wound top area determination, the outer wound boundary is traced on a sheet and this traced boundary will be placed over a gridded paper for top area calculation. Surface true area can be obtained by tracing a wound using acetate sheet placed directly onto the surface of a wound. The wound true surface area is then calculated in a similar way to top area measurement. Inaccuracy in measuring wound top area and true surface area could result if the wound extends over several half or quarter squares in the gridded sheet for measurement [Baranoski & Ayello 2007].

Calculating ulcer volume is crucial since studies show that wounds start healing from the bottom followed by area changes in more advanced stages of the healing process [Plassman *et al.* 1994]. The current methods for evaluating ulcer volumes are subjective and require direct contact with the wound, which might cause pain and discomfort for patients. Figure 1.5 shows two methods used to compute ulcer wounds volume. The first method is by filling the wound cavity with a liquid as shown in Figure 1.5 (a). The second method is by filling the wound with a moulding material which will have equal volume to the wound volume as in Figure 1.5 (b).



(a) Filling with liquid [HARTMANN 2006]



(b) Alginate paste [Plassman *et al.* 1994]

Figure 1.5: Invasive methods for volume measurement

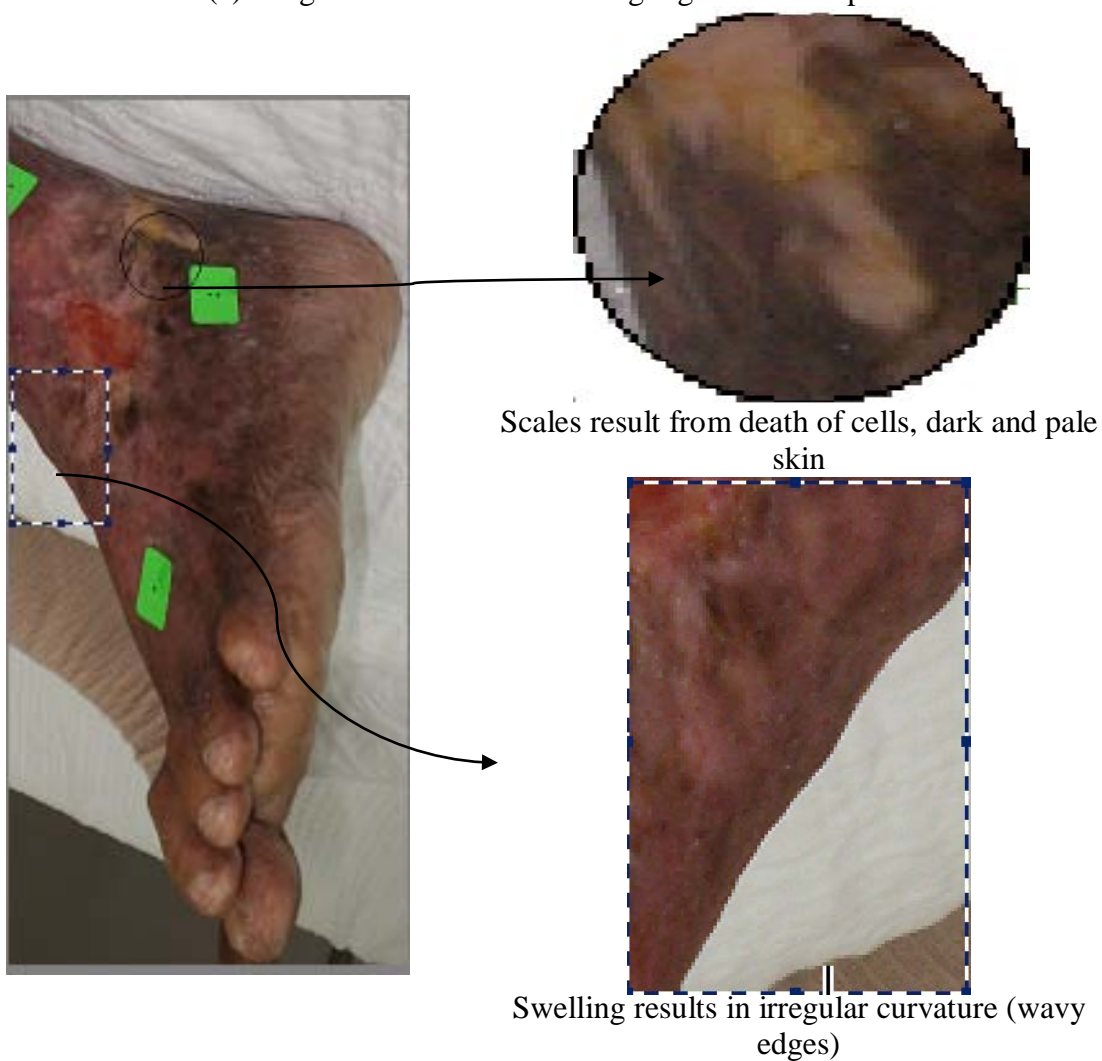
The invasive methods described earlier for measuring ulcer wound size might be difficult to obtain due to the curvature of the leg. Noninvasive methods that contain photographic data are preferable and more objective for wound measurement. Although 2D photograph can give accurate estimation of top area, length, width and perimeter in addition to its low cost, but it does not give depth and volume estimation. 3D surface recording techniques produce data which can be used for measuring 2D and 3D measurement; therefore it is the method of choice.

Yet computing volume of leg ulcers is in very challenging. This is because the leg is highly curved and reconstructing the skin surface at the ulcer wound needed for volume computation is affected by irregularities (swelling and existence of scales) of the skin surrounding the wound. As a result it is difficult to obtain the data around the skin necessary for surface reconstruction. The following Figure 1.6 shows some cases of leg ulcers with irregularity on the surface. Figure 1.6 (a) shows a wound spanning high

curvature area and Figure 1.6 (b) displays a case with swelling and scales surrounding the wound.



(a) Large wound surface covering high curvature part



(b) Irregularities surrounding the wound

Figure 1.6: Curvature of the leg and surface irregularities surrounding the wound

Reconstructing the missing skin surface at the wound area is affected by leg curvature and irregularities on the leg surface. When reconstructing a large wound surface a small reconstruction error will result in a bigger volume compared to when reconstructing over a smaller wound surface. The schematic diagram in Figure 1.7 shows the errors in volume computation that occur when constructing the missing skin surface over the wound area. X in both Figures 1.7(a) and 1.7(b) represents the true volume obtained when the top skin is reconstructed in the correct location and Y is the overestimation when the place of the top surface is displaced due to the effect of irregularities around the wound.

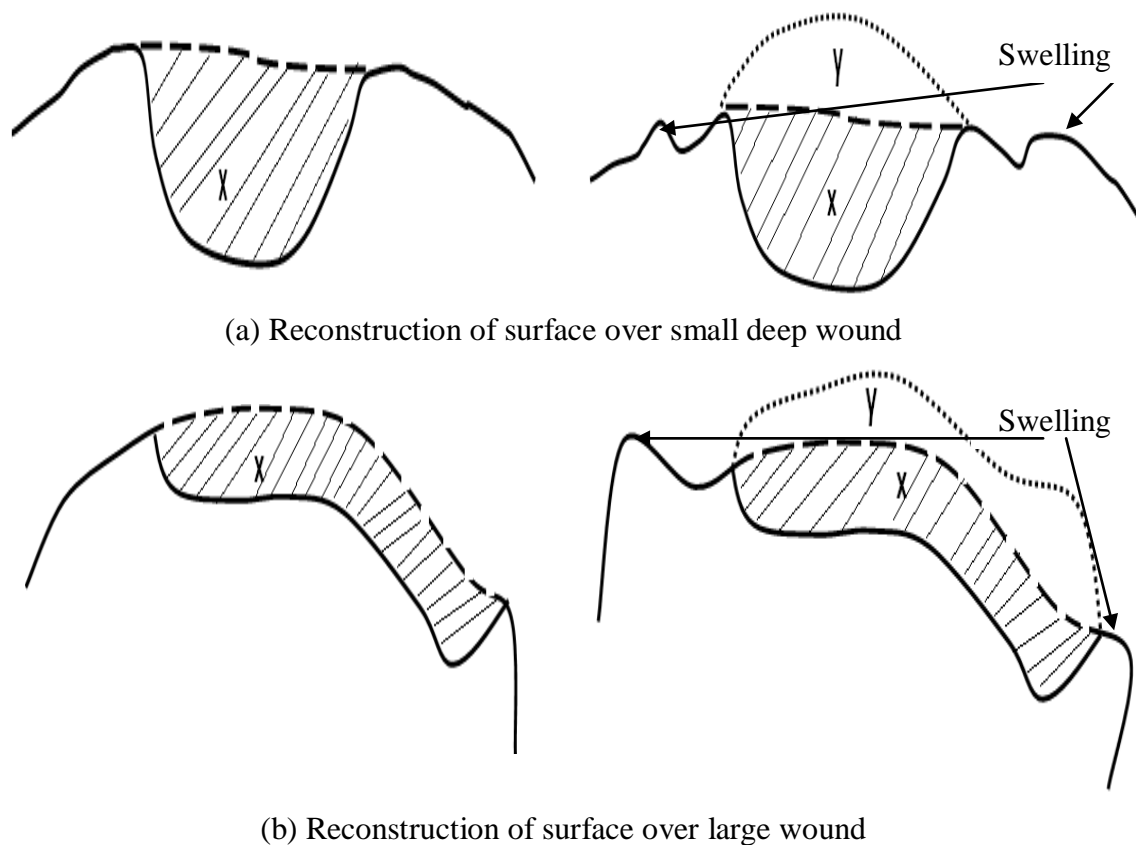


Figure 1.7: Error in surface reconstruction

1.3 RESEARCH OBJECTIVE AND SCOPE

From the literature, it is found that errors in estimating wound top area and true surface area of the wound bed can be solved by digitizing the traced top area formed by the wound boundary or the true surface area corresponding to the wound bed.

Two types of methods are available for assessing wound volume; that is invasive and noninvasive methods.

Invasive methods are performed by filling the wound volume by either a liquid (saline) or alginate paste. Difficulties arise when using the invasive methods for volume computation, namely:

- a. The methods can cause discomfort to patients and have a risk of infecting the wound [Plassman *et al.* 1995].
- b. Both techniques tend to give overestimation since people tend to overfill the wound with material [Plassman *et al.* 1994].
- c. The methods are not suitable for large wounds, wound lay on limb with high curvature, and shallow wounds.
- d. Irreproducibility of the results.

Noninvasive methods are performed on 3D wound surface scans. When obtaining the wound surface it is possible to compute wound volume by means of surface reconstruction and volume computation. Difficulties when performing these techniques are:

- a. Inaccuracy when reconstructing the missing surface on top of the wound due to the effect of irregularities (swelling and scales) on the surrounding skin.
- b. Dealing with the leg curvature when surface fitting of the missing wound top.
- c. Wounds that have depressed edges resulting in undermined wounds in which case the top of the wound is smaller than the wound bed.

In either case it is clear wound volume computation is significantly affected by the ability to reconstruct the missing surface (due to ulcer) from the skin around the wound.

The objective of this research is to develop noninvasive computer algorithms that objectively determine ulcer wound parameters such as top area, true surface area, average depth, and volume. The algorithms are based on 3D surface scans and the wound of interest is limited to leg ulcers. In achieving this objective, the algorithms are developed to overcome both the problems of invasive and noninvasive methods.

1.4 OVERVIEW OF THESIS STRUCTURE

Chapter 2 covers several aspects related to the work. It is divided into two sections. Section 1 covers the medical review of ulcer wounds and in more details leg ulcers. Section 2 demonstrates the different method for wound measurement used in clinical practice.

Chapter 3 contains seven sections. In sections 1 and 2, wound imaging techniques (2D and 3D) and surface representation scheme are discussed. Section 3 presents the current solid construction and volume computation methods applied on 3D skin surface scans. Possible alternative methods of surface fitting, solid reconstruction and volume computation are also given in sections 4, 5, 6. A summary of the chapter is given in the last section.

Chapter 4 presents the different processes and tools used in the work. Firstly, it presents the scanner and the scanning set up in addition to the surface pre-processing steps. Secondly, development of solid models using AutoCAD for ulcer wounds governed by 3 parameters is also presented. And finally, the development of algorithms for wound size measurement is explained.

Chapter 5 presents the investigation of the methods performance in computing ulcer wound size. It also shows in details the performance of surface reconstruction methods needed for volume computation on model and real wound surface scans.

Chapter 6 summarizes the achievements and contribution of this work.

CHAPTER 2: WOUND ANALYSIS IN MEDICAL PRACTICE

This chapter discusses several medical aspects related to this work. The first part discusses wounds and ulcer wounds with detailed description of leg ulcers, causes, treatment, and the importance of wound documentation. The second part demonstrates the different techniques used for wound measurements that are essential for the treatment.

2.1 ULCER WOUNDS

Any damage leading to a break in the continuity of the skin is called a wound. Wounds are classified as full thickness wound if it involves total loss of the skin layers (epidermis and dermis) and it might go to other tissue layers. While partial thickness wound is the one where some of the dermis remains. There are several causes of wounding: (a) traumatic (e.g mechanical, chemical, physical), (b) intentional (e.g surgery), (c) ischaemia (e.g arterial leg ulcer) and (d) pressure (pressure ulcer [Dealey 1999]). Figure 2.1 displays a schematic figure of a wound.

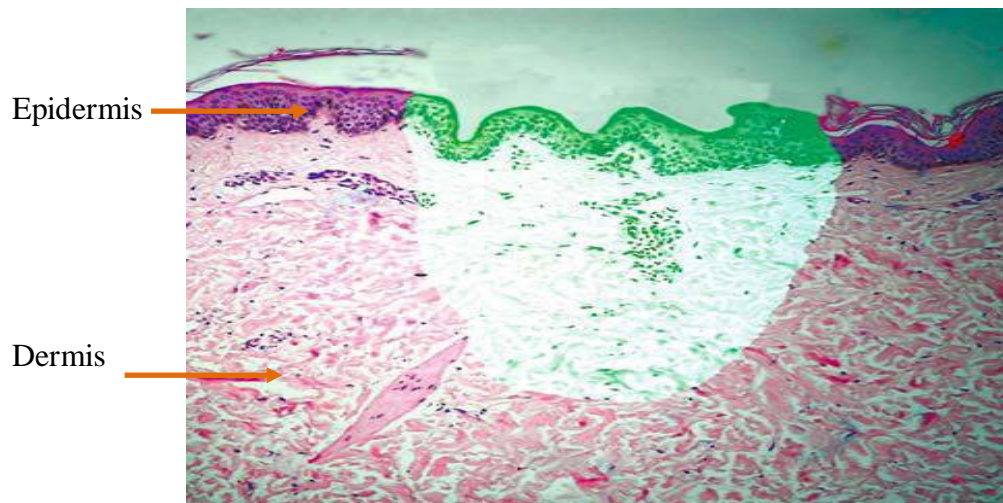


Figure 2.1: Schematic illustration of a wound involves the epidermis and at least part of the dermis [Shai & Maibach 2005]

Chronic wound are any wound that take long to heal. There is no specific border between the time taken by normal and chronic wound. Most physicians would agree that a wound that is not healing within 3-4 months may be regarded as chronic [Ahn & Salcido 2008].

Ulcer wounds are chronic wound with underlying cause/causes that prevents it from healing. In some ulcer cases, wounds can take up to two years to heal. Identifying an appropriate treatment regime will facilitate the healing process [Thomson & Miles 2006]. Establishing the cause of the wound or skin condition will help identify the correct classification and treatment process. Underlying medical conditions (etiology) such as poor nutrition and diabetes (neuropathy) may explain why the wound may be healing slowly. These conditions need to be treated concurrently. Non healing wounds can cause economical and psychological distress for patients [Hess 2005].

The following are the most common medical conditions (etiology) that can cause delaying in wound healing:

1. Diabetes: For wound healing delayed due to diabetes, the reason mostly reported for delaying is infection. The reason is high glucose levels encourage proliferation of bacteria [Dealey 1999].
2. Venous ulcers: Weakening of the vein walls by hereditary conditions, advanced age, obesity or pregnancy results in enlargement of the veins that result in valve leakage. This is known as venous insufficiency or reflux. With longstanding venous insufficiency and the effects of gravity, blood flows backward and pools or collects in the veins in the lowest portion of the leg. This often leads to aching and swelling of the feet, ankles and lower leg, which can be relieved by elevating the leg or wearing support stockings. The skin will be sensitive and stretched and the slightest trauma can cause wound [Thomson & Miles 2006].
3. Arterial ulcers/ peripheral vascular disease: Arterial ulcers are the result of inadequate tissue perfusion to the feet or legs. This is due to complete or partial blockage of the arterial supply to the legs. The lumen of the vessels gradually narrows, causing ischaemia in the surrounding tissue and ultimately resulting in death of the cells [Dealey 1999].

4. Ulcers of mixed aetiology: In some patients a mixed etiology might present in which both an arterial and a venous component exists. It is important to define the predominant factor, so that appropriate treatment may be given [Dealey 1999].

Ulcer wound is a worldwide problem, generating high morbidity and medical expenses. Assessment of an ulcer wound involves surveying a range of physical parameters, which is time consuming, and often results in inconsistencies in patient care [Simonsen *et al.* n.d.]. Chronic wounds are common, according to [Plassman *et al.* 1995] 8% of bedridden / chairbound patients develop pressure ulcers. Another type of chronic wound is ulceration of the lower limb, and according to [Shai & Maibach 2005; HARTMANN 2006] leg ulcers affects 1% of the adult population and 3.6% of people older than 65 years.

Ulcer wounds, such as pressure ulcers, venous ulcers, and diabetic ulcers, pose a significant challenge to patient rehabilitation both in terms of the high prevalence and the effort required for their management [Ahn & Salcido 2008].

When assessing wounds, these steps need to be performed: (a) recording history, (b) physical examination, (c) laboratory tests/biopsy, (d) ulcer measurement and, (e) patient assessment. Different types of ulcer wounds exist, and the cause of the ulcer is the main key for treatment selection [Shai & Maibach 2005].

2.1.1 Leg Ulcers

Ulcerations, particularly on the lower legs or the feet, commonly occur from arterial insufficiency, venous hypertension, neuropathy (any pathology of the peripheral nerves), trauma, obesity, immobility or a combination of these conditions. A common cause is decrease in blood supply to the area. The anatomic location of the ulcer, and distinctive wound characteristics help to distinguish among ulcers of the lower extremities [London & Donnelly 2000; Hess 2005].

According to [Shai & Maibach 2005; HARTMANN 2006] venous disease, arterial disease, and neuropathy cause over 90% of lower limb ulcers. It is therefore necessary to have an exact diagnosis and a detailed medical history since different causes of ulcer

wounds need to be treated differently. Figure 2.2 shows typical images of ulcer wounds at the leg (Figure 2.2(a)) and at the bottom of the foot of patients (Figure 2.2(b)).

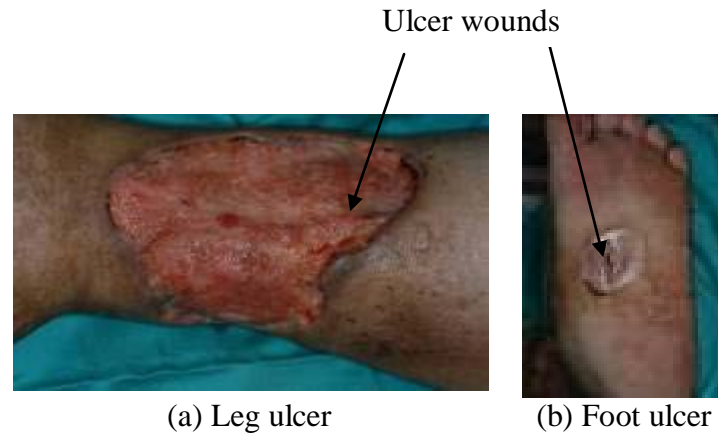


Figure 2.2: Examples of leg ulcer wounds

Lower limb ulceration tends to be recurrent [Shai & Maibach 2005]. Treatment history is significant because the clinician may learn which management modalities have been tried and which have succeeded or failed. The anatomic location of the wound should be documented consistently. A patient might have several ulcers and identifying each ulcer is necessary for the follow up [Hess 2005].

Following ulcer wounds is a tedious task and it requires handling the wound and the patients since the long ulcer period causes distress for patients. Leg ulcers are debilitating and painful, and greatly reduce patients' quality of life. The whole treatment plan should be explained to the patient. Both patient and physician should not lose patience when treating ulcer wounds. Leg ulcers reoccur within five years in up to 40% of the cases; therefore preventing reoccurrence is very important. Leg ulcers take long duration to heal and it is costly since it utilizes the hospital facilities for long. The duration for ulcer healing depends on: the patient's case, severity of the ulcer and the underlying etiology [London & Donnelly 2000; HARTMANN 2006].

Questions like how to treat venous ulcers and where, is still being debated. It has recently been suggested that patients with leg ulcers should have an initial assessment in a hospital vascular clinic, with patients who are unlikely to benefit from surgery then being cared for in the community [London & Donnelly 2000].

Patients with foot ulceration should be sent to hospital for investigation because most of them might need prompt intervention. While, patients with venous ulceration can be

managed either primarily in the community by trained nurses or referred to hospital for further investigation into the underlying venous abnormality. However, cases should be referred to dermatology in case of complications as indicated by: (a) no improvements after 12 weeks of treatment, (b) ulcer appears abnormal, (c) sudden deterioration in the condition of the leg, (e) patient has associated skin problems which complicate treatment, (f) uncontrolled pain, and (g) mixed etiology [London & Donnelly 2000].

2.1.2 Documentation and Treatment

A documentation form with diagrams of different anatomic sites is a helpful tool. For investigating ulcer cases, the location of ulcer wound in the body should be documented carefully. Usually patients will have multiple ulcers, it is therefore necessary to identify each wound for follow up purposes [London & Donnelly 2000; Hess 2005]. Figure 2.3 depicts the distribution of nonvenous and venous ulcers of lower limb. The majority of venous ulcers are in the gaiter area and the majority of nonvenous ulcers are at the foot [London & Donnelly 2000].

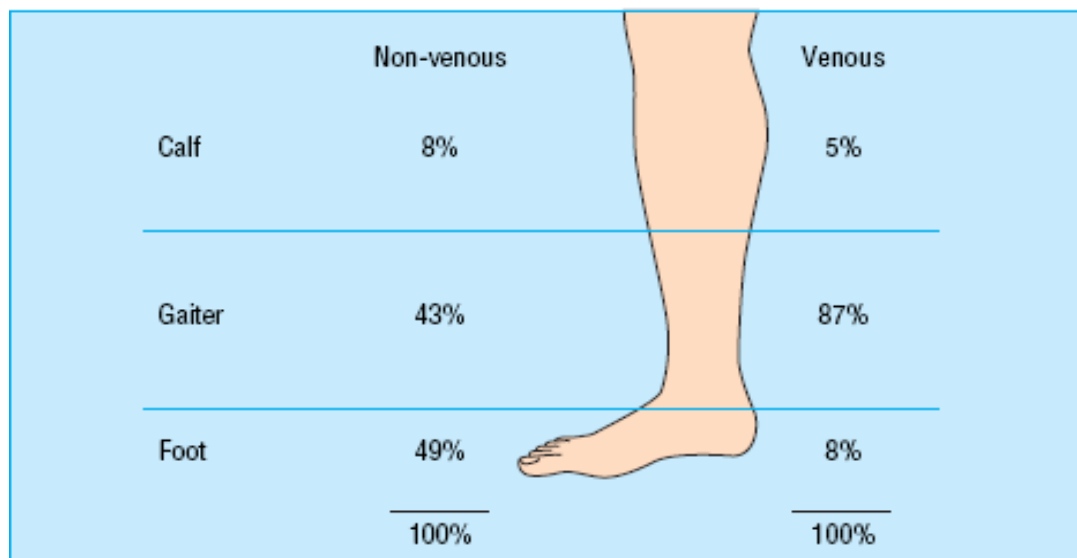


Figure 2.3: Distribution of nonvenous and venous ulcers of lower limb [London & Donnelly 2000]

The wound healing process consists of 3-4 overlapping stages (that cannot be clearly separated from each other) regardless of the type of wound and the extent of tissue loss. These stages are: (a) inflammatory and exudative (cleansing) phase to stop the bleeding and cleanse the wound, (b) proliferative phase (granulation) where blood vessels and replacement tissue, known as granulation tissue, are produced to fill the defect, and (c)

maturation (epithelisation) of the new tissue concluding scar formation. The stages last for variable lengths of time and any stage may be prolonged because of local factors such as ischaemia or lack of nutrients. Thus, different wound management routines are recommended for each phase [Dealey 1999; HARTMANN 2006]. Figure 2.4 contains a schematic diagram of the timing of each wound healing phase (time is in days post wounding).

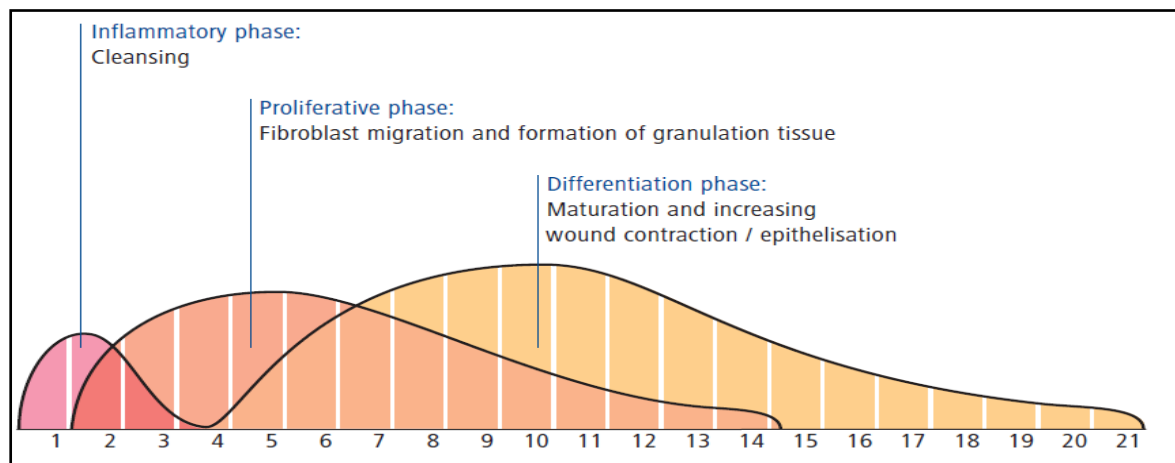


Figure 2.4: Schematic diagram of the timing of the wound healing phases [HARTMANN 2006]

Documented details that comprise a patient's chart are used to measure and benchmark clinical outcomes. Proper documentation provides guidance for appropriate treatment decisions, and evaluation of the healing process. Providing an accurate description of the wound and the skin around it is critical during each patient's visit. [Hess 2005].

Wound follow-up, which is a description of wound at different visits, can identify wounds that are not responding to treatment and this can reduce the risk of complications. Wound follow-up indicates whether the wound is healing or not and describes the different tissues covering the wound. Measuring different parameters might be used for assessing ulcer wounds. Measurements should be undertaken on a regular basis and the frequency depends on the type of wound [Dealey 1999]. Quantitatively measuring and evaluating wound healing is of great importance for both clinical use and in pharmaceutical research [Plassman *et al.* 1994]. Consistent units of measure are essential when documenting and describing wound measurements [Hess 2005].

In addition to treating the etiology behind the ulcer wound the wound it self need to be managed. General wound management products include topical agents as well as dressings. A topical agent is the one which is applied to a wound. A dressing is a covering on a wound that is intended to promote healing and protect from further injury. Two types of wound dressing exist: a primary dressing is the one which is used in direct contact with the wound and a secondary dressing is placed over the primary dressing [Dealey 1999].

The following are the common guidelines for patients with different etiology that prevent wound healing:

1. Diabetes patients: They should protect their feet from injuries. This is done by wearing comfortable shoes, paying attention when cutting foot nails, keeping the feet clean, and dry [Dealey 1999].
2. Venous hypertension: Patients should work in improving blood flow to the legs. Elevating leg whenever sitting or laying and walks for 30-60 minutes without stopping is encouraged. Current evidence suggests that the management of venous ulceration should be graduated compression bandaging (see Figure 2.5) [Dealey 1999]. Compression is effective for controlling wound exudate in leg ulceration as compression reduces chronic venous hypertension [London & Donnelly 2000].



Figure 2.5: Compression bandage [London & Donnelly 2000]

3. Arterial etiology: Surgical intervention to remove the blockage might be necessary [London & Donnelly 2000].
4. Mixed etiology: the dominate factor should be identified and response accordingly.

The management of unusual causes of lower leg ulceration is based on treating the cause. If the cause is unknown, correcting the cause is not possible. For example compression treatment is often used for ulcers with venous etiology, never used for ulcers with arterial etiology, and might be used with modification with ulcers with diabetes etiology [Dealey 1999; Shai & Maibach 2005].

2.2 WOUND MEASUREMENT IN CLINICAL PRACTICE

For effective wound management, objective measurement of wound dimensions is critical. To describe ulcer wounds, dermatologists set the diagnosis and description about the particular wound. Description about wound such as pattern, morphology, area, perimeter, maximum depth and volume are the different criteria included in patients report. Repeated determination of different measurement over time helps the practitioner in evaluating wound progress or regress, and the effectiveness of treatments [Ahn & Salcido 2008].

The following sections discuss the wound quantitative size measurement including: Length/ width, top area/ true surface area, depth, and volume.

2.2.1 Area and Surface Area Measurement

The length and width of any wound are measured as linear distances from one wound edge to another. To ensure accurate and consistent measurements, landmarks must be established for wound measurements. A simple method of measuring a wound is by measuring its greatest length and breadth as shown in Figure 2.6 [Dealey 1999; Ahn & Salcido 2008].

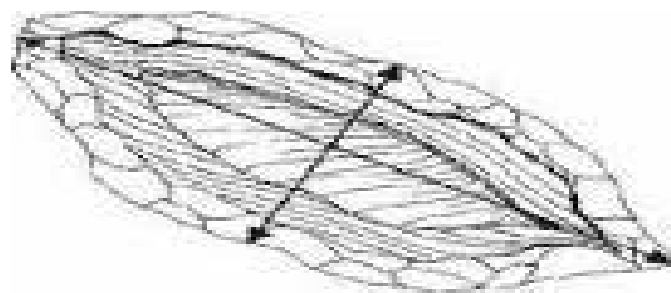


Figure 2.6: Measuring wound based on maximum length and width [Ahn & Salcido 2008]

Measurement of the longest length and width is independent of direction, and the measured length and width are measured perpendicular to one another [Ahn & Salcido 2008]. Multiplying the longest length by the perpendicular width gives an approximation of the wound area. This method of calculating wound area approximates the wound shape to be a rectangle that gives larger wound area than the actual size [Dealey 1999; Ahn & Salcido 2008].

Another way of calculating area of a wound is by tracing wound boundary on marked paper with the fixed size of squares as in Figure 2.7. The tracing should be placed in a plastic bag (for infection control purposes) and may be kept in the patient's file for reference throughout treatment. If the wound is healing normally, subsequent tracings will show a progressive decrease in size [Hess 2005]. Counting the number of squares inside the wound boundary gives an estimate of the wound area [Ohanian 2003].



Figure 2.7: Defining wound boundary manually [Langemo *et al.* 2008]

The results of the wound area obtained by square counting can be optimized by digitizing the traced wound surface and obtain the area by dividing it to very small units [Wilhelm *et al.* 2006]. When measuring wound area, it is expected that the area get reduced with the improvement of the wound.

Wound surface area (true wound area) can be obtained in a similar way to the tracing method. The different is that an acetate sheet should be placed into the wound (touching the wound bed directly). The plastic will be directly placed in the wound surface. Figure 2.8 below shows the method of measuring surface area by tracing the perimeter of a wound on an acetate sheet [Baranoski & Ayello 2007].

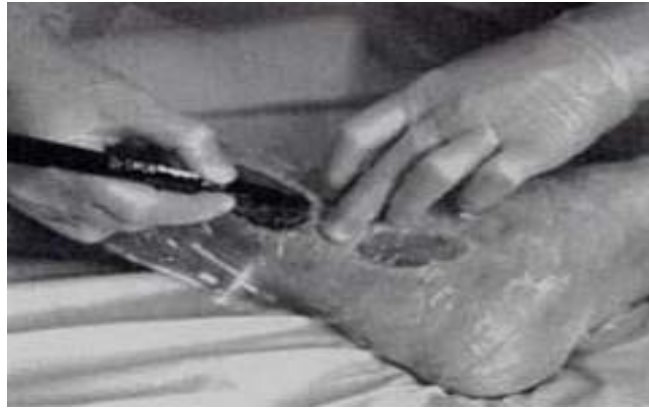


Figure 2.8: Acetate sheet tracing [Baranoski & Ayello 2007]

It is found that true area measurement and percentage of area reduction of wounds can differentiate between wounds that are responding to treatment or not [Flanagan 2003].

2.2.2 Depth Measurement

The depth of a wound can be described as the distance from the visible surface to the deepest point in the wound base. One way of measuring the depth is by using moistened cotton tip applicator placed into the depth of the wound and putting a marker in the healthy skin level as in Figure 2.9. If the depth varies, different areas of the wound bed have to be measured to confirm the deepest site [Zhang *et al.* 2005; Hess 2005; Flanagan 2003]. For ulcer lesions, maximum depth reduces with healing which affects the volume computation.



Figure 2.9: Approximate measurement of wound depth using a simple probe [Flanagan 2003]

Another tool for measuring width, length, and depth simultaneously is by using the Kundin gauge that is placed into the wound cavity. The Kundin gauge is a disposable paper measurement tool having three rulers at right angle to each other as shown in Figure 2.10 [Baranoski & Ayello 2007].

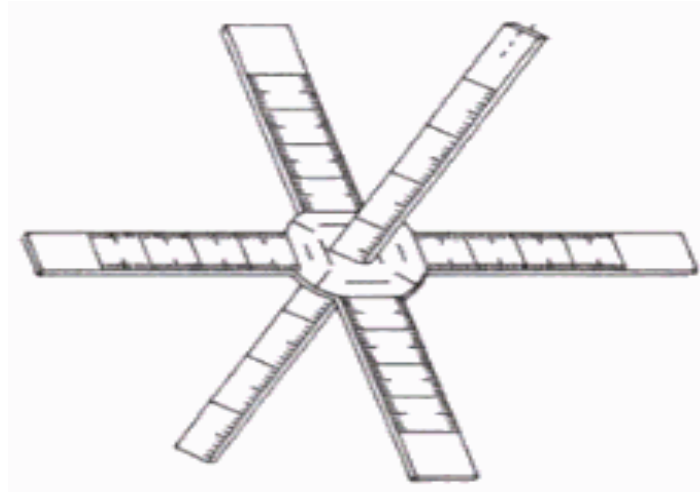


Figure 2.10: The Kundin gauge [Baranoski & Ayello 2007]

2.2.3 Volume Estimation

Calculating ulcer volume is crucial since studies showed that wounds start healing from the bottom followed by area changes in more advanced stages of the healing process. This is well pronounced in case of deep wounds. Area measurements do not reflect early changes in deep wounds as they start the healing process by building up granulation tissue from the base of the wound. To measure the volume in wounds it is often filled with measured amount of alginate paste or saline. In the alginate paste method, the paste will take the wound shape after it dries and its volume can be determined. Figure 2.11 illustrates the alginate paste method [Plassman *et al.* 1994; HARTMANN 2006].

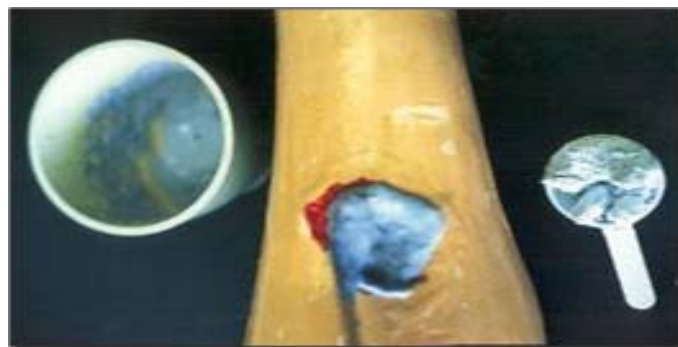


Figure 2.11: Alginate past method for volume estimation [Plassman *et al.* 1994]

Another method for measuring wound volume is by filling the wound with measured amount of saline solution. The wound is covered with foil (Figure 2.12(a)) and filled with a saline solution using a syringe (Figure 2.12(b)). When filling the wound with the saline solution, the volume dispensed from the syringe equals the wound volume. In this method, the accuracy of the volume estimation is affected by two factors: first the wound absorbs the saline solution and secondly it is difficult to ensure that the plastic cover takes up the shape of the original healthy skin [HARTMANN 2006].

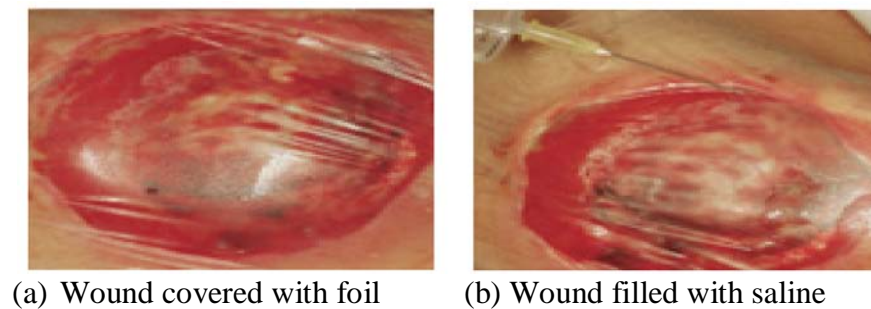


Figure 2.12: Filling wound surface with saline solution for volume estimation [HARTMANN 2006]

These methods for volume measurement are more applicable in areas of the body that is not having high curvature. The two methods are not easily applied for curved body parts. There is a risk that the alginate paste will dry out when applying it to wound with large area and for the liquid method it might spill out in case of wounds in area with curvature. It is also difficult to obtain the volume of shallow wounds. Thus for shallow wounds surface area measurements is preferable [Shai & Maibach 2005]

2.4 SUMMARY

Nonhealing wounds can cause economical and psychological distress for patients. Identifying appropriate treatment regime will reduce healing time. The effectiveness of a treatment regime can be estimated by measuring changes in the ulcer wound. Wound size measurements are objective and they can indicate whether the wound is healing normally or whether obstacles exist. Accurate wound measurements assist in designing an appropriate care plan. The effectiveness of a particular treatment regime can be determined by measuring changes of ulcer wounds during the course of a treatment. The wound size is determined by measuring length, width, depth, area (top area), surface area

(true surface area) or volume. Several methods exist for measuring wounds; these include linear measurement, wound tracings, and wound moulds.

Wound top area and true surface area are useful for assessing the progress of shallow ulcer wound over time. The inaccuracy with manual (invasive) approach for determining top area, true surface area can be solved by digitizing the traced area and computing the area using computer algorithm.

For volume measurement the two methods (saline and alginate paste) are not easily applied for curved body parts. There is a risk that the alginate paste will dry out when applying it to wound with large area and for the liquid method it might spill out in case of wounds in area with curvature. Both methods cannot be kept as a record for future reference and to check new ways of measurement.

Several factors affect the selection of particular wound measurement technique and this includes the ease of use cost and time required. Although invasive methods are not costly yet it can cause discomfort for patients and wound infection in addition to variation in results when the procedure is performed by different observers or the same observer at different visits.

CHAPTER 3: WOUND ANALYSIS USING DIGITAL IMAGING TECHNIQUES

This chapter covers the use of photography (2D and 3D) in wound analysis. The current solid construction and volume computation methods applied on 3D skin surface scans is presented and their limitation is discussed. Possible alternative methods for solid reconstruction and volume computation are also given.

3.1 IMAGING TECHNIQUES FOR WOUNDS

Noninvasive methods have been introduced to the wound care. In the noninvasive methods photographic equipment are used. In addition to their advantage of being noninvasive, the data can be kept as record for follow up and documentation.

3.1.1 2D Photography in Dermatology and Wound Assessment

2D images are of great use in wound assessment since both color and spatial information can be used to observe wound status. Colored images can be used to analyze different tissue composing wound bed [Wannous *et al.* 2008]. Spatial analysis of 2D images can be done when using the traced boundary of the wound to calculate wound area [Dealey 1999]. Cross sectional scans can be considered as 2D images and this can be used to obtain the depth of the wound across a line. Two methods for obtaining cross-sectional data of the surface or wound surface are Ultrasound and Optical Coherence Tomography (OCT).

3.1.1.1 Wound Bed Tissue Classification Using Coloured Images

Color images are analyzed for wound status investigation. The colors of the wound bed can indicate whether the wound is healthy or infected. The 3-color concept classifies wounds as red, yellow or black. Red may indicate a clean, healthy granulation tissue covering wound bed. Yellow may indicate the presence of exudate or slough. Black may indicate the presence of eschar (necrotic tissue), which slows healing and provides a site for microorganisms to proliferate [Hess 2005]. Using wound bed color information, the wound bed can be segmented into the constituent tissue classes. Current method for wound segmentation requires user intervention to accomplish the classification [Callieri *et al.* 2003; Wannous *et al.* 2008]. Figure 3.1 demonstrate the use of images for wound

tissue classification. Figure 3.1(a) shows a leg ulcer composed of different tissues and Figure 3.1(b) gives the desired output of the tissue classification.

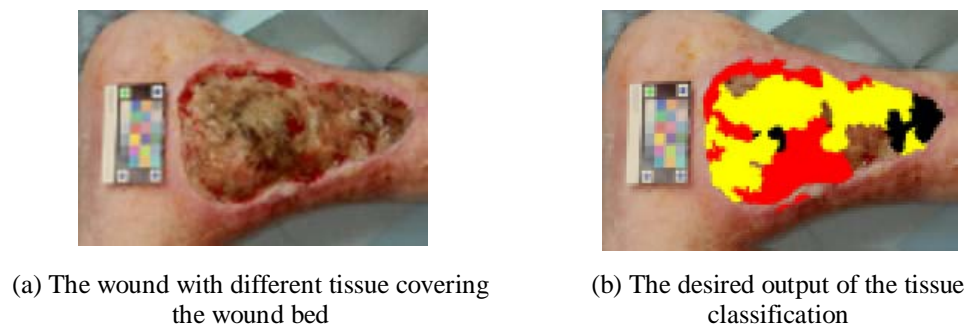


Figure 3.1: Colour analysis for wound tissue classification

3.1.1.2 Digitization of Wound Area/Surface Area

Inaccuracy in area measurement can happen due to two factors, error when tracing the wound and errors in computing the area by counting squares in a grid. The error in area computation can occur when the traced boundary cross partial squares this might result in variation in computing the wound area. Digitizing the wound with a tool like Visitrak as shown in Figure 3.2 can solve the second problem. After the digitization computer programs which can divide the area to small squares giving high precision compared to the manual method [Smith & Nephew 2009; Dealey 1999].



Figure 3.2: Visitrak Wound Measurement System [Smith & Nephew 2009]

3.1.1.3 Depth measurement

3.1.1.3.1 Optical Coherence Tomography (OCT)

Optical Coherence Tomography (OCT) is a noninvasive imaging method, producing two-dimensional (2D) cross-sectional images. It is a tool for imaging superficial layers of the

skin. In the cross-sectional images, a determination of the thickness of the skin layers is possible. Therefore, OCT is proposed for monitoring of inflammatory skin diseases and wound healing as well as for the quantification of treatment effects [Wilhelm *et al.* 2006]. Figure 3.3 shows optical coherence tomography of wound healing of an incision. Figure 3.3(a) displays a scan of a fresh cut and Figure 3.3(b) displays the same cut after 13 days (reduction in the depth happen because of the growing of granulation tissue).

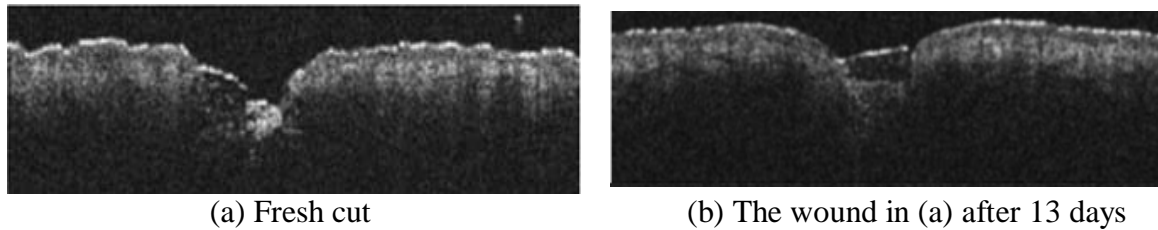


Figure 3.3: Optical coherence tomography of wound healing of an incision [Wilhelm *et al.* 2006]

3.1.1.3.2 Ultrasound

The work by [Wendelken *et al.* 2003] suggests the use of ultrasound as a diagnostic tool for wound assessment and detecting abnormalities in the surrounding tissues. Ultrasound requires a physical medium through which to travel such as liquid. It can not transmit through a vacuum. Thus prior to scanning the wound cavity is filled with a wound ultrasound transmission gel and then covered with an ultrasound film dressing. Figure 3.4 displays a venous ulcer in which the dark areas show low reflectivity in the placed filled with liquid. This is seen in places filled with the gel in the ulcer location and dark pockets filled with pooled blood. The advantage of this method is that it can be used for assessing undermined wounds.

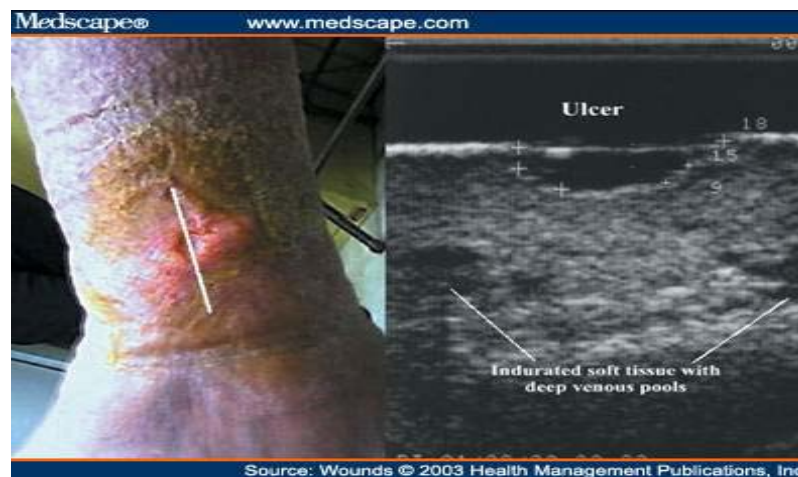


Figure 3.4: Venous ulcer (left) and its cross section scan using ultrasound (right) [Wendelken *et al.* 2003]

3.1.2 Three-dimensional (3D) Surface Scanning Techniques

3D surface scanning techniques can produce data suitable for a variety of applications. These techniques produce depth information along a surface not obtainable using 2D imaging. For wound assessment, noninvasive methods for obtaining the wound size measurement are of great value. 3D surface scanning can be used to assess wound true surface area and volume.

The techniques that can provide depth measurement and 3D surface profile noninvasively are structured light [Plassman *et al.* 1995], optical photogrammetry [Malian *et al.* 2004; Boersma *et al.* 2000; Albouy & Treuillet 2007] and laser scanning [KONICA 2004].

3.1.2.1 Structured Light

In case of structured light, a projector illuminates the wound area with a set of parallel stripes of light. In this method a pattern will be projected onto the surface of the skin at a certain angle of incidence. This enables measurement of an entire area without having any contact with the skin. This principle is illustrated in Figure 3.5. A pattern of parallel stripes in a reference plane, as depicted in Figure 3.5(a), is projected onto a wrinkle structure Figure 3.5(b), and the height information of the structured surface is coded in the distorted intensity pattern Figure 3.5(c), which is recorded by means of CCD video technology [Wilhelm *et al.* 2006]. Depth and surface information are calculated from the deformation of the light patterns in the scene [Plassman *et al.* 1995].

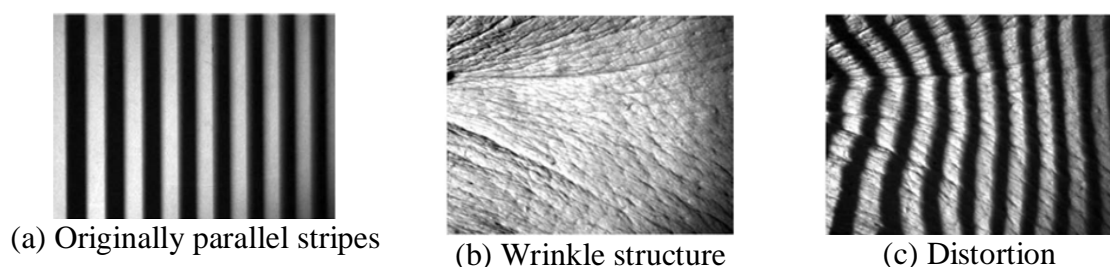


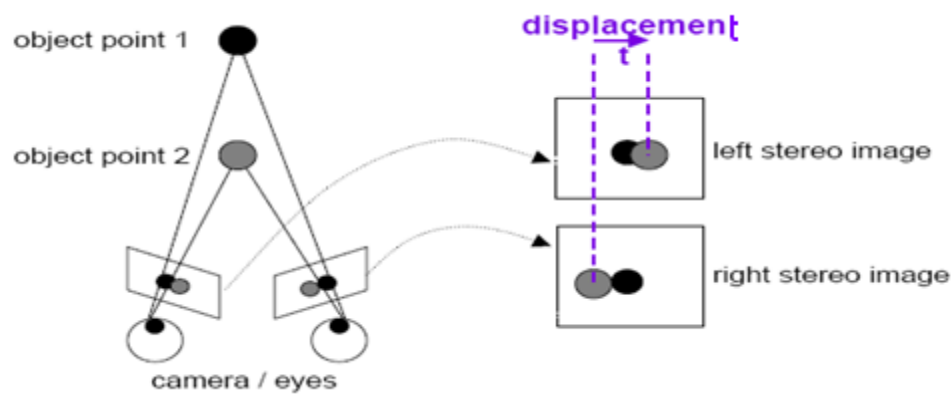
Figure 3.5: Example of the distortion of originally parallel stripes due to wrinkle structure [Wilhelm *et al.* 2006]

3.1.2.2 Photogrammetry

Photogrammetry indicates the use of photography in surveying and mapping to ascertain measurements. Photogrammetry method relies on creation of a 3D model from uncalibrated views. The model is created by analyzing the differences between the images taken from different views [Malian *et al.* 2004]. Photogrammetry method uses

different number of cameras such as: (a) two cameras [Albouy & Treuillet 2007], (b) three cameras [Boersma *et al.* 2000] and (c) four cameras [Malian *et al.* 2004], the fourth camera is for consistency checking of results covering different angles.

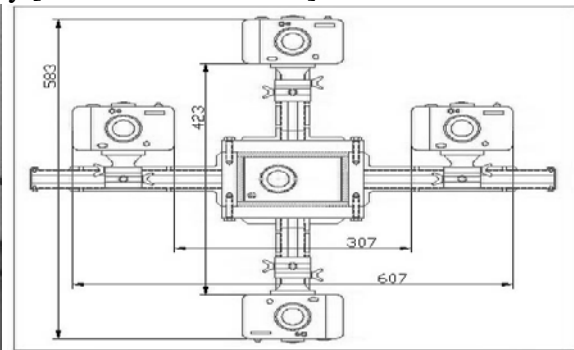
When using 2 cameras system, depth is the displacement between corresponding points in stereo images as shown in Figure 3.6(a). Figure 3.6(b) and Figure 3.6(c) show systems consisting of three and four cameras respectively.



(a) Stereo –Photogrammetry [Plassman *et al.* 1995]



(b) Three camera system [Boersma *et al.* 2000]



(c) Front view of 4 camera system [Malian *et al.* 2004]

Figure 3.6: Photogrammetry method for 3D scanning

3.1.2.3 Laser Scanning

In laser scanning, a surface is scanned by projecting laser light on the object. The light reflected from the object then enters the CCD camera. The distance to the object can be obtained by the angle of reflection of the laser, the angle of incidence of the reflected light from the object into the CCD and the fixed distance between the laser emitter and the CCD camera [KONICA 2004].

Laser scanning in general uses triangulation method to calculate the depth for various points at the surface. In this case depth is obtained given base length and two angles. This procedure will give dense point cloud, with each of the points indicating particular location at the surface. This dense point cloud can be further meshed to give the specific surface. Figure 3.7 explains the laser triangulation method. The distance to the object D can be obtained by the angle of reflection of the laser b , the angle of incidence of the reflected light from the object into the CCD a , and the distance B between Laser and CCD camera [KONICA 2004].

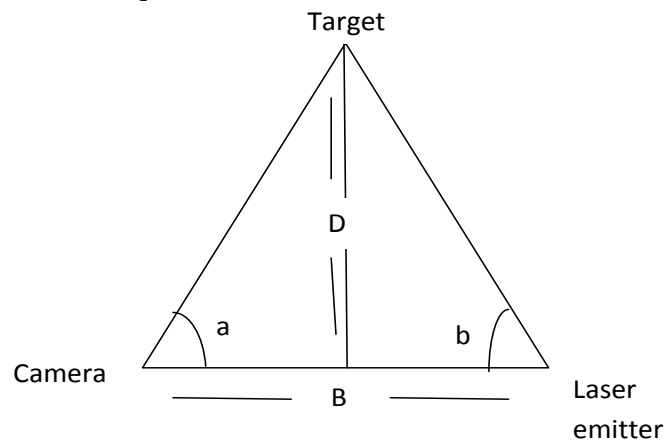
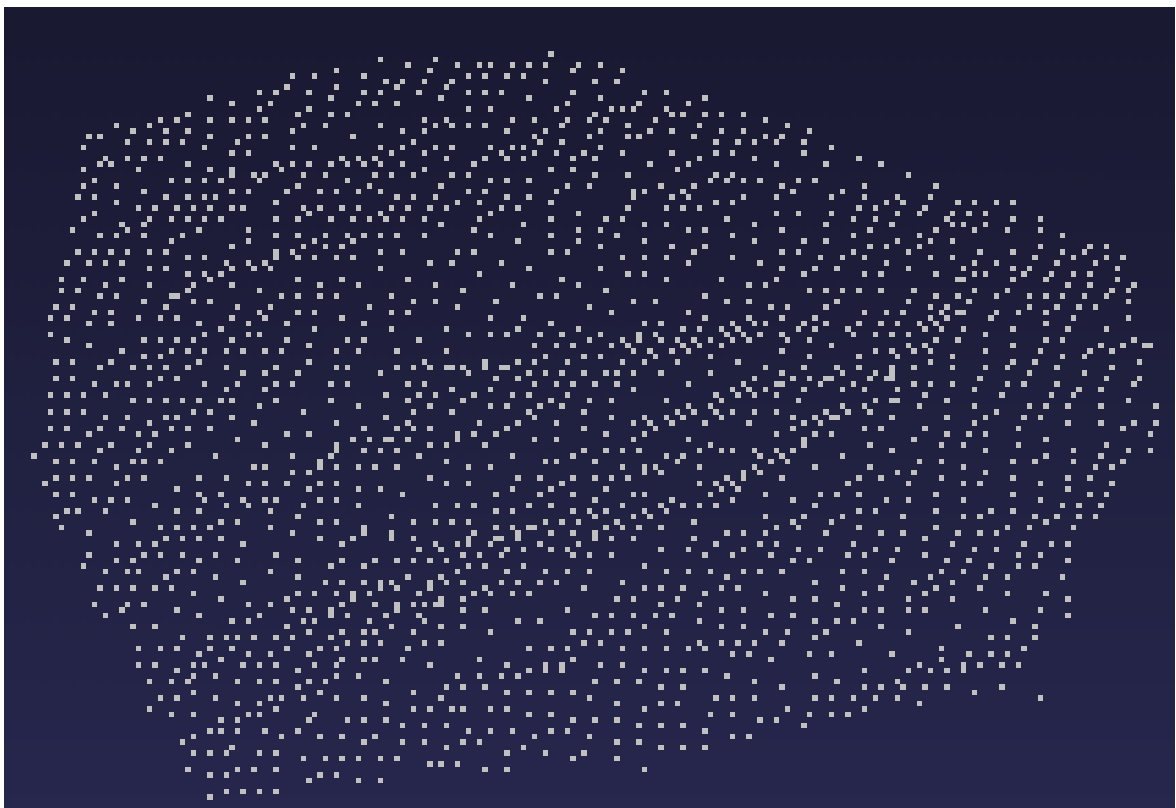


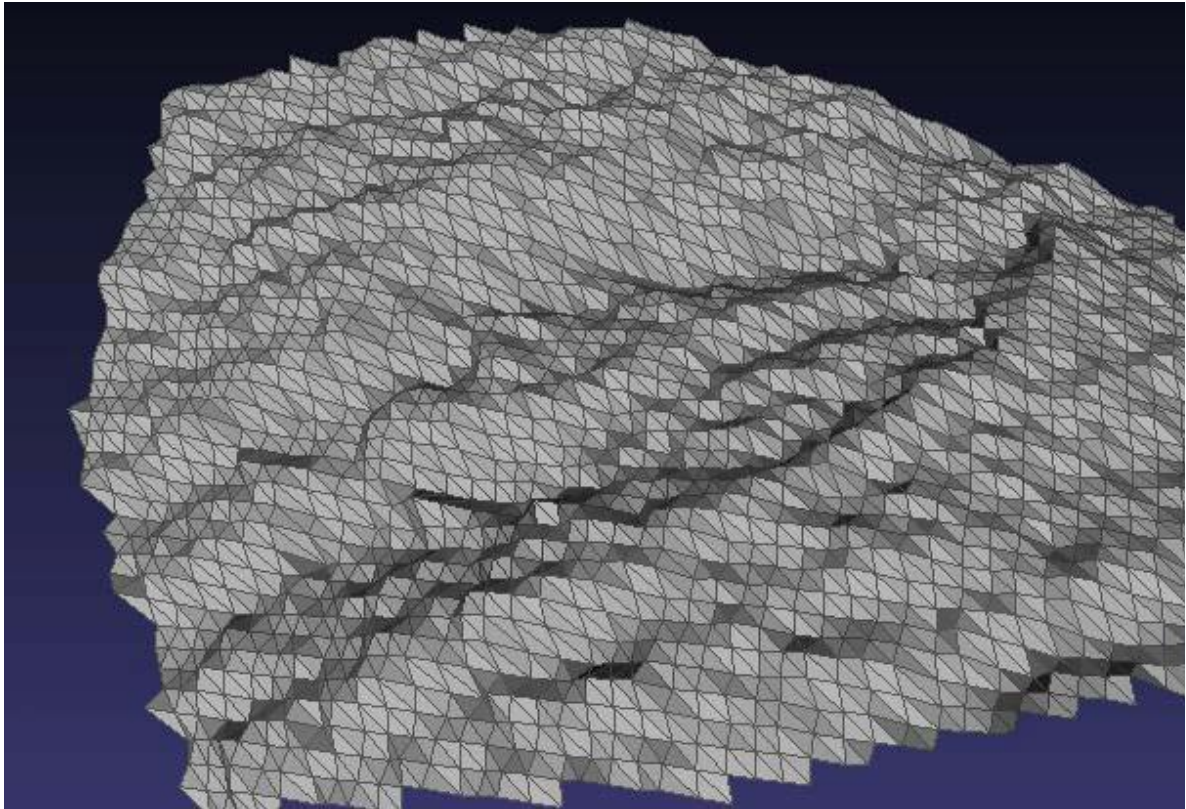
Figure 3.7: Laser triangulation concept

3.2 SURFACE REPRESENTATION

The data captured from 3D scanners are in the form of dense points and they are called “*point cloud*” which represents several accurate points’ coordinates at the object surfaces [KONICA 2004]. In order to obtain useful information from the dense point cloud (e.g. surface area), these points need to be connected in a process called meshing. The points can be connected in a form of triangles/quadrilaterals (in two dimensions) or tetrahedra/hexahedral bricks (in three dimensions). These polygon shapes are called “faces” each face is enclosed by a set of bounding “edges” [Shewchuck 1999]. Figure 3.8 (a) illustrates the data acquired using 3D scanner and Figure 3.8 (b) shows the corresponding polygons mesh.



(a) Point cloud



(b) triangular mesh

Figure 3.8: Point cloud and the corresponding triangular mesh surface

These surfaces are meshed and defined by the collection of vertices, edges and faces. The faces consist of triangles or quadrilaterals. Mostly, surface scans are represented using triangular mesh. In triangular mesh the dense points from the surface scan are connected using triangle of various sizes. Each of these triangles is called a face and the points composing the face are called vertices [Shewchuck 1999].

3.3 CURRENT METHODS for COMPUTING ULCER WOUND VOLUME from 3D SURFACE SCANS

Currently the development of ulcer wound measurement tools and software is being conducted by few groups using 3D surface scanning techniques. The systems are mostly concerned with pressure ulcers and they are:

- 1- ESCALE (**ES**Carre **A**nalyse **L**isibilité **E**valuation) it is a system designed for bed sore analysis and evaluation. The work is divided to three main parts: (a) developing the scanning techniques using photogrammetry [Albouy & Treuillet

2007], (b) Measuring wound volume from surface scan [Albouy *et al.* 2005] and (c) wound bed tissue analysis [Wannous *et al.* 2008].

- 2- MAVIS (**M**asurement of **A**rea and **V**olume **I**nstrument **S**ystem): Volume, circumference and depth of the wound are calculated from data grid.
- 3- MEDPHOS (**MED**ical **PHO**togrammetric **S**ystem) the system is focusing on the device for surface measurement [Malian *et al.* 2004].
- 4- DERMA, colour analysis is given based on semi automated region growing other parts of the system are not described [Callieri *et al.* 2003].

The following sections described the current methods used for volume computation.

3.3.1 Fitting a Plane to Wound Boundary

The method in [Albouy& Treuillet 2007] for calculating wound volume is based on closing the wound surface with a plane as in Figure 3.9. This plane is fitted to 3D points on a strip of healthy skin around the wound. A manual tracing of the wound outline is required on color images used for 3D reconstruction.

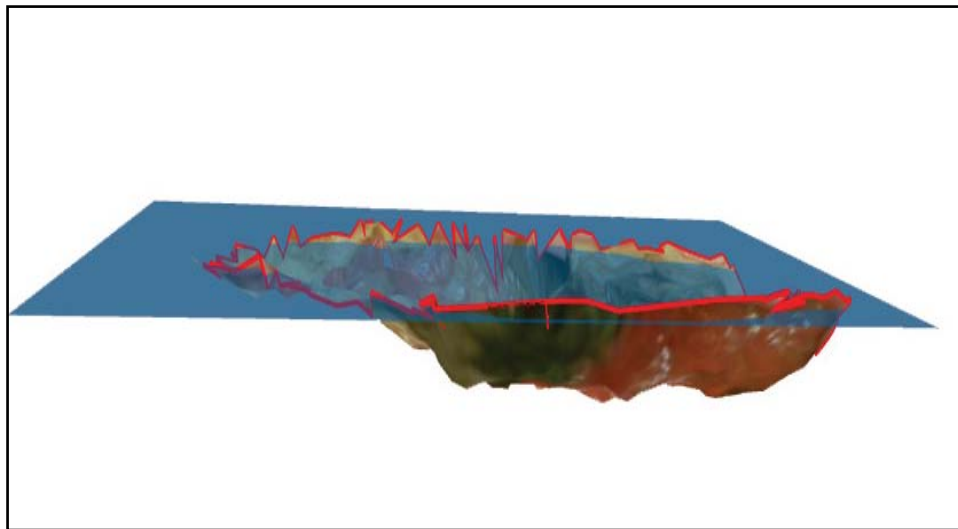


Figure 3.9: The inner volume computed by closing the 3D model of the wound surface with a plane defined from the wound boundary [Albouy& Treuillet 2007]

This method is triangulation based volume estimation; it create solid out of surface scan by projecting surface faces to a plane fitted on the wound boundary. The triangulation based volume calculation consists of the sum of the elementary volumes under each prism formed by facets and their orthogonal projections on a reference plane

For best fit plane method, the plane might fall below some of the surface parts. This method was reported for calculating the volume of pressure ulcers that its top surface can be approximated by a flat surface. Pressure ulcers are deep and the wound will be located of one side of the body, the limb curvature is not high.

3.3.2 Surface Interpolation using Cubic Spline

The volume of the wound is sandwiched between the wound surface and the wound missing surface that will be reconstructed on top of the wound. Figure 3.10 displays measured surface and the reconstructed surfaces of a wound.

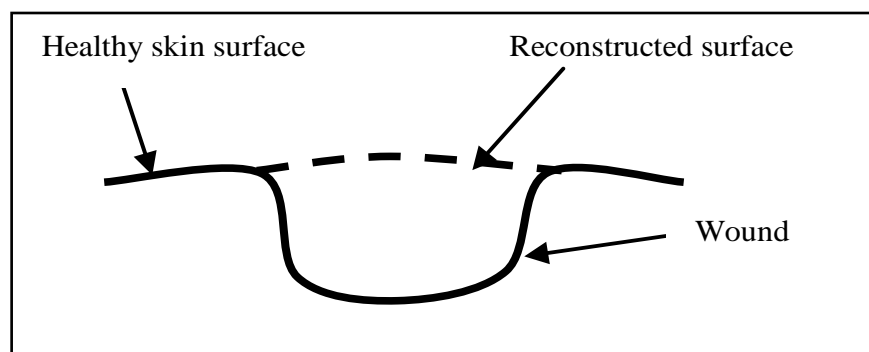


Figure 3.10: Cross section illustration of wound surface

To reconstruct a solid model out of the wound cavity, surface interpolation using cubic splines was proposed. Interpolation of healthy skin surface is obtained using the information from the skin surrounding the wound. Cubic splines have a tendency to generate curves with minimum curvature. In order to apply surface interpolation using this method the data should be arranged in a grid. The grid is created by taking a sample of the points composing the surface in a discrete steps of approximately 2 mm in each direction in the space. The volume of the resulting model can be calculated by integrating the distance between the base of the wound and a minimal surface attached to the wound edges [Plassman *et al.* 1995]. Figure 3.11 display a model created using this method out of a wound scanned surface.

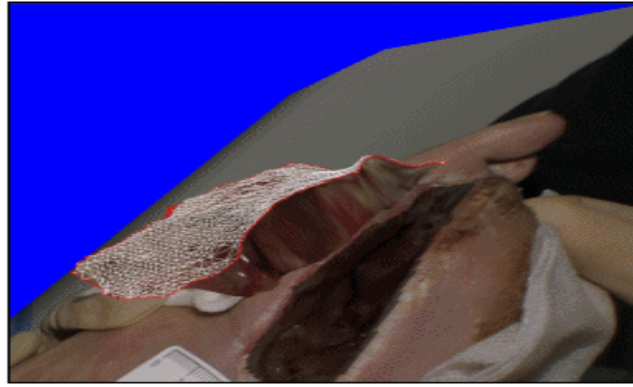


Figure 3.11: Reconstructed model out of wound scan [Plassman *et al.* 1995]

It is easier to reconstruct accurately over a small wound area while for larger wounds the reconstruction becomes increasingly more inaccurate [Plassman *et al.* 1995].

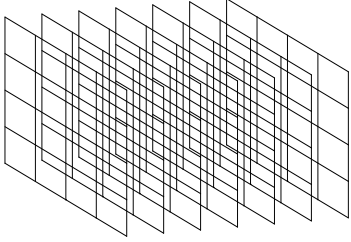
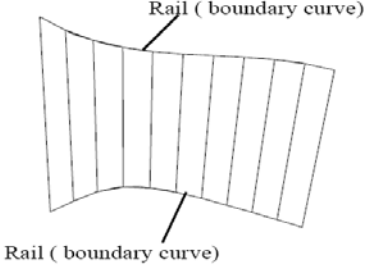

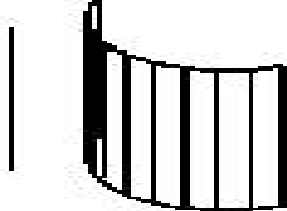
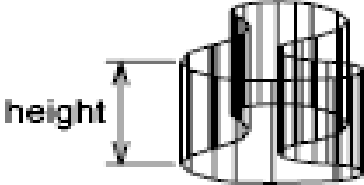
3.4 SURFACE FITTING MODELS

Surfaces can be generated using different fitting algorithm and the choice of the appropriate fitting algorithm depends on the required shape [Sirakov *et al.* 2003]. There are two types of surfaces: specifically analytic surfaces and synthetic surfaces [Hsu 1998].

3.4.1 Analytic Surfaces

Analytic surfaces are based on wireframe entities. These include the plane surface, ruled surface, surface of revolution and tabulated cylinder [Hsu 1998]. Table 3.1 list analytic surface generation methods.

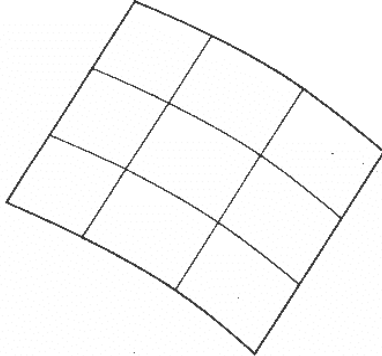
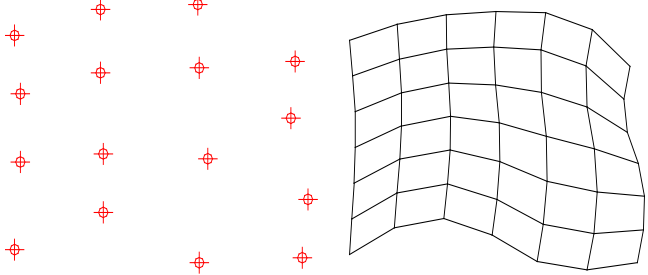
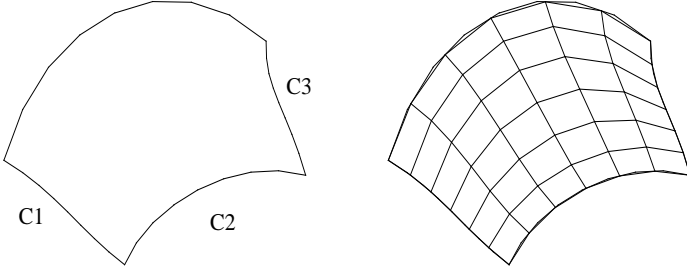
Table 3.1: Analytic surfaces

Fitting models	Required data	Figure
Plane surface	3-Corner point - It requires three non-coincident points to define an infinite plane. The plane surface can be used to generate cross-sectional views by intersecting a surface model with it [Hsu 1998].	 <p>[Hsu 1998]</p>
Ruled/ Lofted surfaces	2-boundary curves - that interpolate surface linearly between 2 boundary parallel curves that define the surface (rails) [Hsu 1998].	 <p>[Hsu 1998]</p>
Revolution	Curve rotating around an axis.	 <p>[Weisstein 2000]</p>
Tabulated cylinder	Creating a surface by moving a line along a curve [Ralph <i>et al.</i> 2006].	 <p>[AutoCAD 2007]</p>
Extrusion	Creating a surface by moving a curve in a specific direction [Ralph <i>et al.</i> 2006].	 <p>[AutoCAD 2007]</p>

3.4.2 Synthetic Surfaces

Synthetic surfaces are formed from a given set of data points or curves and include the bicubic, Bezier, B-spline and Coons patches (4-Boundary curves) [Hsu 1998]. More details about synthetic surfaces are given in Table 3.2.

Table 3.2: Synthetic surfaces

Fitting models	Required data	Figure
Bezier surface	The surface that approximates given input data [Hsu 1998].	 <p>[Hsu 1998]</p>
<i>B-spline surface</i>	Similar to Bezier surface the difference is it permit local control of the surface [Hsu 1998].	 <p>(a) Data points (b) B-spline</p> <p>[Hsu 1998]</p>
Coons patch	4-curves to form a closed boundary [Ralph <i>et al.</i> 2006].	 <p>(a) Closed boundary (b) Coons patch</p> <p>[Hsu 1998]</p>

A variety of surface fitting techniques exist and the selection of appropriate technique depends on the application and data collection scheme. The data representation (gridded or scattered) is the organization of the data which will be used for construction. Grid fitted data is ideal for fitting synthetic surfaces while randomly collected data can be fitted using analytic surfaces. Surface fitting can be classified into interpolation and approximation. Interpolation result in a surface fitted to data points that are known to high precision. While approximation finds some kind of best fit to data [Chivate & Jablokow 1995].

3.5 SOLID RECONSTRUCTION FROM SURFACES

For a solid there should be a boundary which encloses volume fully with no gaps exist in the surface [Lee & Requicha 1982]. Solid reconstruction involves constructing a whole model from partial representations. Reconstructing a solid from surfaces is the first step in computing volume from incomplete boundary representation models. Different applications for solid reconstruction are: surface blending, hole filling, compression and model simplification [Kazhdan, 2005]

The results of solid reconstruction can be either a model with complete boundary representation or a volumetric model consisting of several shapes composing the final solid. Solid reconstruction method, which produce boundary representation model, is stitching several scans covering different side of the object [Stroud 2006]. Moreover, the methods that can produce a volumetric model are surface projection [Pflipsen 2006; Ohanian 2003] and convex hull reconstruction (Delaunay tetrahedralization).

3.5.1 Building Solid/Model from Surface Patches

In order to reconstruct a solid from surface patches, different side of the object should be scanned and their surface collectively will create the complete solid after merging the scans [KONICA 2004]. The method does not only work for surface scan but it also include surfaces reconstructed using any method. Figure 3.12 displays the several surfaces being blended to construct model.

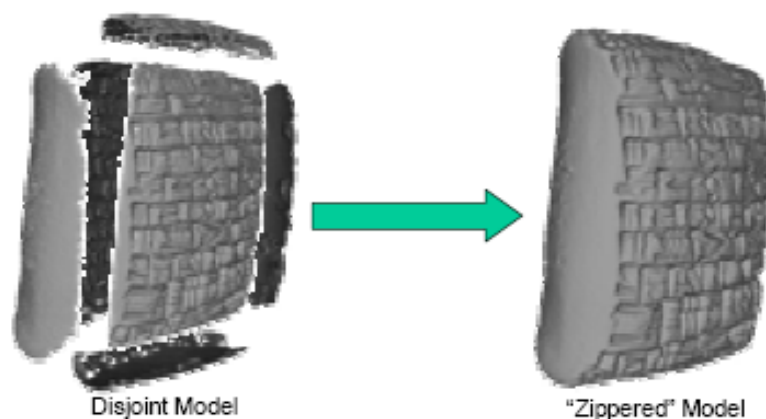


Figure 3.12: Stitching surfaces [Kazhdan, 2005]

The steps needed to create a complete model from surface patches are:

1. Obtain surface scans covering all the sides of the desired object. Use reference points for the matching process or rotate it with exact angle for automatic merging.
2. Sew together the surface scans.
3. Handle problems.
4. Throw unwanted object created as a side effect.

The expected problems are: (a) no coincidence between the boundary curves of two adjacent surfaces and (b) non consistent surface orientations. Creating the object involves a process of modifying the topology and geometry to match. When sewing together partial object scans, the difficult task is to match the topology of the separate partial models in order to merge them [Stroud 2006].

3.5.2 Projection

In some cases it is impossible to obtain different surface scans which collectively cover the whole object (e.g. scanning a pile of sand for surveying). To determine the height and the volume, the ground level surface has to be estimated [Pflipsen 2006]. Another case is when to scan a wound the wound model can not be obtained using several sides scanning.

3.5.2.1 *Projecting surface to a plane*

A solid can be constructed by projecting surface faces to a plane. By projecting triangular faces to a plane a solid consisting of prisms is created. The volume for the constructed solid can be computed by adding up the volume of all the prisms in the solid [Pflipsen 2006]. Figure 3.13 displays the prism constructed by projecting face 1 to the origin XY plane in which $Z=0$ i.e. face 2.

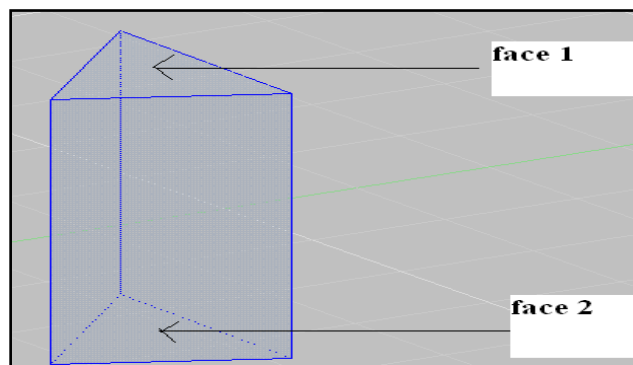


Figure 3.13: Projecting a triangular face to the origin

Figure 3.14(a) display a surface scan and Figure 3.14(b) shows the corresponding solid resulting from projecting the triangular faces to a reference plane. The solid is composed of several prisms.

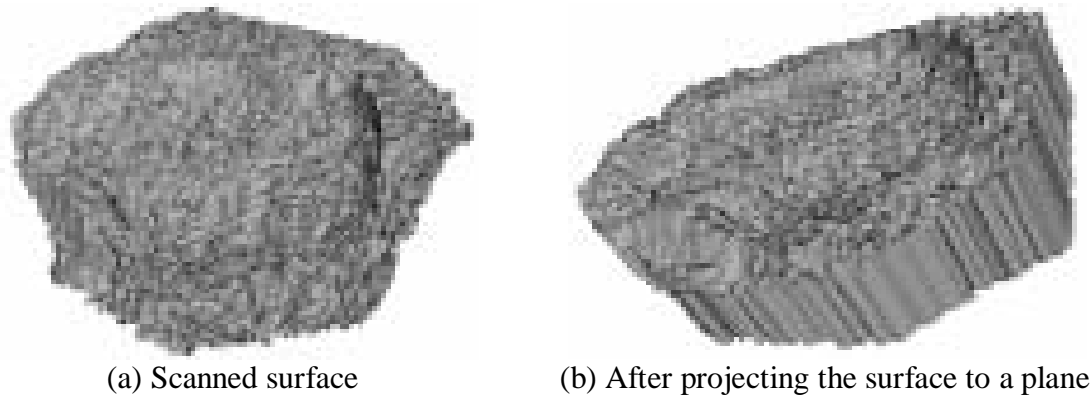


Figure 3.14: Projecting scanned surface faces to a plane

For regular objects, calculating the volume is relatively easier than non-regular surface with high curvature. This is because the depth can easily be obtained given a reference plane [Zhang *et al.* 2005]. An example of regular object (Figure 3.15(a)) with targets calibrated (Figure 3.15(b)) for testing scanner accuracy is given in Figure 3.15.

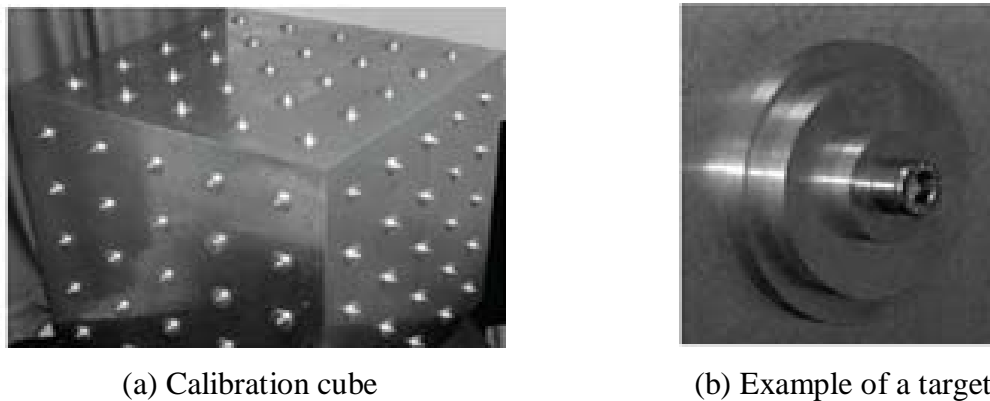


Figure 3.15: Calibration cube for scanner measurement validation [Zhang *et al.* 2005]

Triangular meshed surface is one of the popular schemes for representing surfaces because of the simplicity of the calculations. When projecting this triangular mesh to a surface, a model consisting of several prisms is created. Volume of the solid constructed by using the projection method can be calculated by adding all the volumes (trapezoidal prisms) formed by connecting each triangle to its projection onto the $z = 0$ plane [Pflipsen 2006; Zhang *et al.* 2005]. If the vertices of a face are not having the same heights (z

value), the resulting shape of projection is not exactly a prism. This can be solved by assigning the average height to all the vertices.

3.5.2.2 *Projecting surface faces to origin point /reference point*

Based on the target shape the surface faces can also be projected to any reference point of choice e.g. origin point. Figure 3.16 shows the tetrahedron constructed from projecting one triangular face to the origin point.

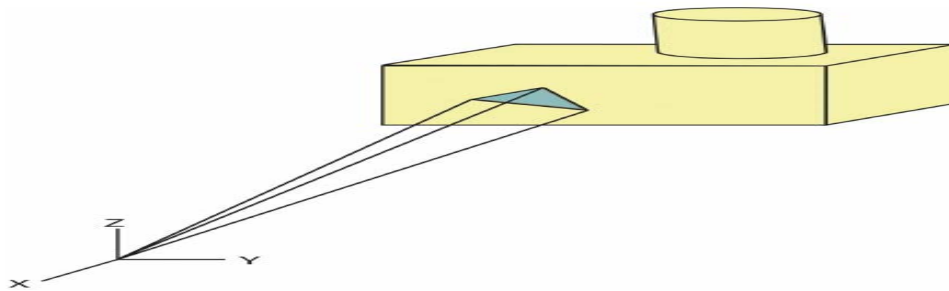


Figure 3.16: Projecting faces to origin point [Ohanian 2003]

3.5.3 Convex Hull Approximation

The convex hull created by applying Delaunay tetrahedralization is frequently used for "piecewise-linear" interpolation of scattered data. Enclosing surface/solid by the minimum bounding polyhedron can approximately identify mass properties of the surface/solid in less time. The convex hull is created by connecting the farthest vertices around the surface. The resulting shapes will not include all the vertices of the original shapes [Shewchuck 1999; Berg *et al.* 2008]. Figure 3.17 displays a 3D model enclosed inside the smallest convex shape; this can give estimation of the model mass properties.

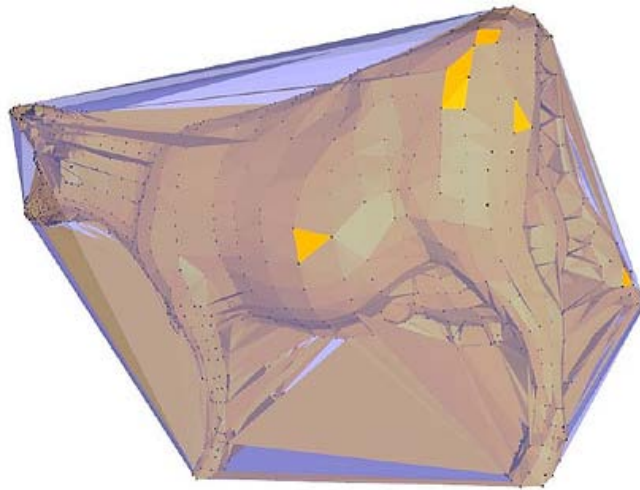


Figure 3.17: Enclosing a model in convex polyhedron

Decomposing a shape into a number of convex pieces will give a better approximation of the model compared to convex hull without decomposition. Two types of decomposition exist namely exact and approximated. For many applications, an approximate convex decomposition (ACD) can represent the important structural features of the model more accurately. ACD provides a mechanism for ignoring less significant features, such as surface texture [Lien & Amato 2008]. Figure 3.18(a) display a 3D model and Figure 3.18(b) shows the corresponding simplified model using ACD.

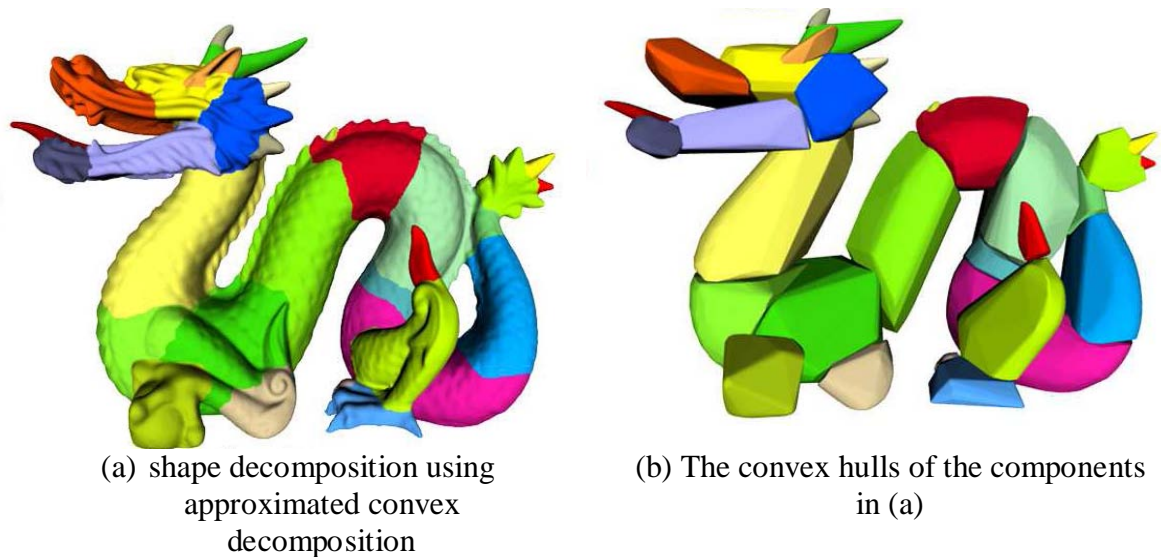


Figure 3.18: Convex decomposition [Lien & Amato 2008]

3.6 VOLUME COMPUTATION

For solids, data related to their geometric properties and to their mass properties can be obtained. The properties for rectangular regions and box shaped solids are relatively easy to compute. If some arcs, curves, spheres and few holes are introduced the calculations becomes more complicated [Hoffmann 1989].

Objects are represented in computer modeling using one of the representation schemes, this include constructive solid geometry (CSG), boundary representation, primitive instancing, quasisdisjoint decomposition and sweep representation. Some geometric properties can easily be computed from one representation while it might be difficult to obtain them from others [Lee & Requicha 1982]. It is important to note that the representation of geometric models is the main factor in choosing the appropriate volume computation method [Pflipsen 2006].

Boundary representation is a popular scheme in computer graphics and 3D modelling. In boundary representation, the boundary of a solid must determine unambiguously what is inside and hence comprises the solid. Boundary representation is mostly used to represent surfaces scans in the computer [Requicha & Rossignac 1992].

For calculating solids volume, some primitive shapes (e.g. box, cylinder, prism, etc.) are having formulas that can be used to directly obtain the volume. For non primitive types, the representation scheme must be investigated and consequently the appropriate method for volume calculation is chosen.

3.6.1 Morphological Approach to Volume Calculation – Cross sectioning

One approach for volume calculation of 3D reconstructed objects is to use cross sectional area. The method is based on the concept that states the volume of an object can be computed as the limit of the sum of the area of infinite number of sections, which cut the 3D object. This approach can be used for different sets of data including medical data (e.g. MRI) where several cross sectional images are obtained and later used to create volumetric models [Sirakov *et al.* 2003]. Having cross sections with known distance (displacement), the volume of the model can be calculated as summation of all the area of the cross section multiplied by the displacement between the different slices. Figure 3.19

displays several cross sectional 2D sections which can be used to reconstruct volumetric model.

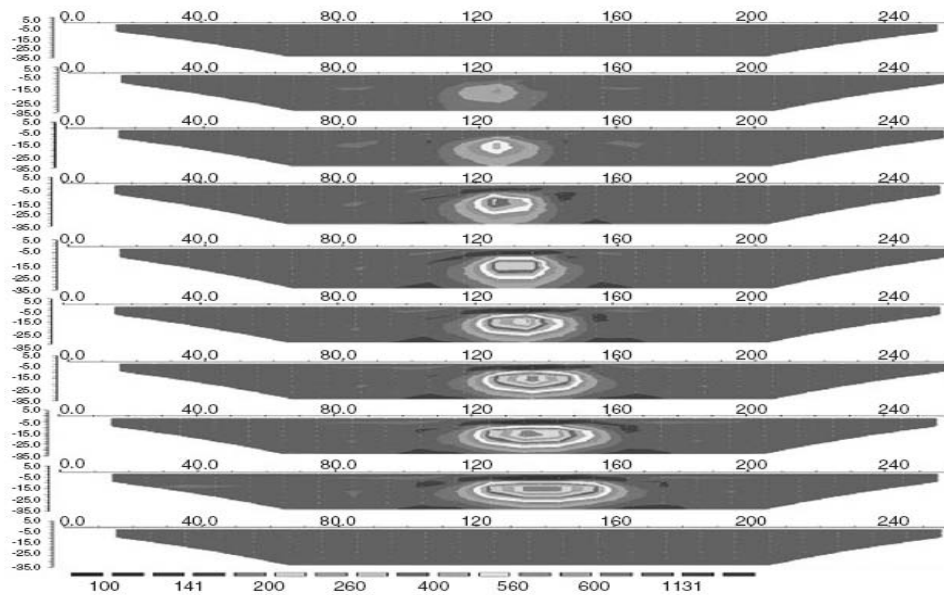


Figure 3.19: Ten generated vertical 2D electrical resistivity sections [Sirakov *et al.* 2003]

This method is also suitable for computing volume of models generated using sweep and revolution operation, the models are created by moving a 2D area over a path or curve. The Minkowski sum of two solids A and B is the result of sweeping one solid over the other. Mathematically, it is defined by $\{a + b, a \in A, b \in B\}$, where point $a+b$ corresponds to the translation of point a by the vector from the origin to point b [Requicha & Rossignac 1992].

3.6.2 Integration and Divergence Theorem

For computing the volume of solids represented using complete boundary representation, divergence theorem methods and direct integration methods can be used. These methods have the advantage that they do not need to decompose the model into standard geometric forms, but only need the surface of the model on which to operate [Lee & Requicha 1982; Requicha & Rossignac 1992].

For example, the integral of a function $f(x, y, z)$ over the polyhedral solid depicted in Figure 3.20 may be evaluated by adding the appropriately signed contributions of the prisms defined by the faces and their XY projections. The contribution of face F_i in Figure 3.20 is the integral

$$- \int_{F'_i} \int dx dy \int_0^{z_i(x,y)} f(x, y, z) dz \quad \text{Eq. 3.1}$$

Where F'_i is the XY projection of face F_i and $z_i(x, y)$ is obtained by solving for z the equation of the plane in which F_i lies.

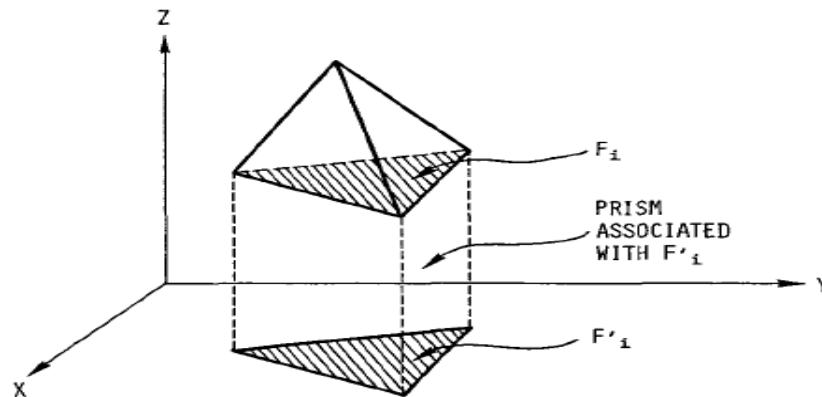


Figure 3.20: Illustration of the Method of Direct Integration [Lee & Requicha 1982]

In [Jon 2009] an algorithm for computing the volume using surface integration is presented. Given a closed surface represented by triangles, each triangle is coded counter clockwise with the normal vector to the triangle pointing out of the volume. The algorithm for computing the volume is as follow:

Algorithm: *Volume computation using surface integration*

Input: *triangular mesh surface*

Output: *The contribution of each face to the volume*

Make all z coordinates positive.

Compute the average z for a triangle, "height".

Compute the area for a triangle, "base".

Compute the z component of the normal vector, z_{norm} .

The volume of this piece of the surface is $height \times base \times z_{norm}$

If z_{norm} is positive, the face (triangle) is on top and contributes positive volume.

If z_{norm} is negative, this face (triangle) is on the bottom and contributes negative volume.

The area in the x - y plane is the area of the triangle $\times z_{norm}$.

A vertical triangle has $z_{norm} = 0$.

A horizontal triangle has $z_{norm} = 1$ on top and -1 on bottom.

A triangle tipped 45 degrees has a $z_{norm} = \cos(45 \text{ degrees}) = 0.7071$.

3.6.3 Projecting Surface Boundaries to Centre Point / Origin Point, Tertahedralization

If the boundary representation (e.g. triangular mesh) got projected to a point inside the solid, this will create a volumetric solid composed of many tetrahedra. Instead of converting the volume integral to surface integral, volume can be obtained by working directly on the volumetric representation. The surface faces can be projected to a point inside the volume constructing a volumetric representation of the solid. The projection method can be used to construct volumetric element from the surface faces [Lee & Requicha 1982]. Figure 3.21 display the process of projecting solid faces to a point inside the solid (centre point).

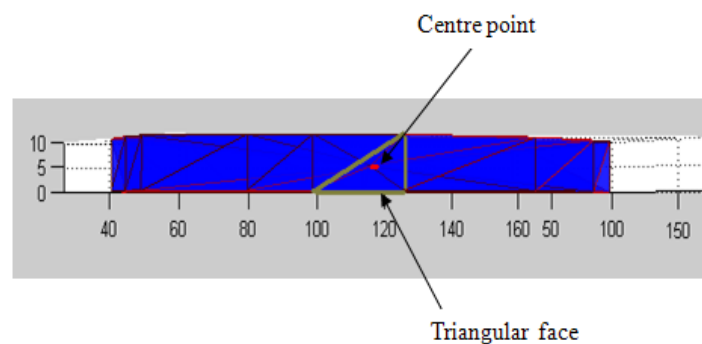


Figure 3.21: Projecting faces to centre point

The vertices representing the boundaries of any surface can be connected in a process called meshing using 2-D simplex triangles or 3-D simplex tetrahedra. When the 3-D simplex is used the process is called tetrahedralization. The resulting model will be constructed of several tetrahedra which do not intersect each other and their volume collectively is the volume of the 3D shape [Shewchuck 1999]. Figure 3.22 displays a model reconstructed using a set of tetrahedra shapes.

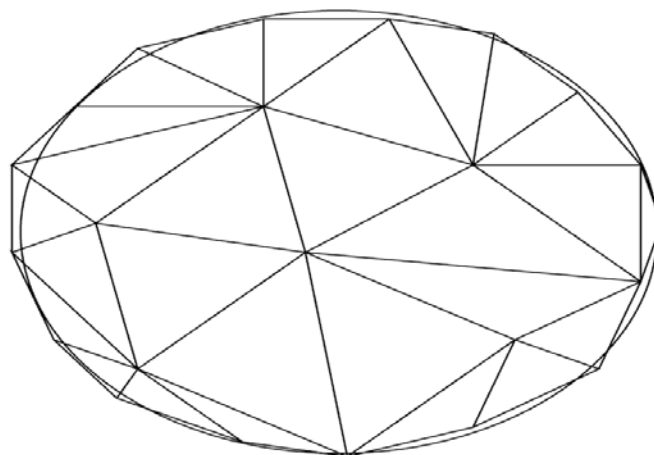


Figure 3.22: Subdivision of a model into tetrahedra [Hoffmann 1989]

3.6.4 Dividing the Solid to Equal Size Elements

The idea behind most of the mathematical techniques for computing property data is to divide the area (for regions) or the volume (for solids), into extremely small element. The final area or volume will be calculated by totalling the results of the small element. One approach for volume computation is to assume that the body is enclosed in a box. Subdivide the intervals up to a given precision ($\epsilon > 0$) and then count how many of the obtained cubes have non-empty intersection with the object [Simonovits 2003]. Decomposing the solid to small symmetric elements is applicable for CSG representation. The volumes of these small elements are easy to calculate (e.g. boxes) and their volumes collectively give the volume of the solid [Wilson 2001; Hoffmann 1989]. Figure 3.23 shows solids divided to small elements.

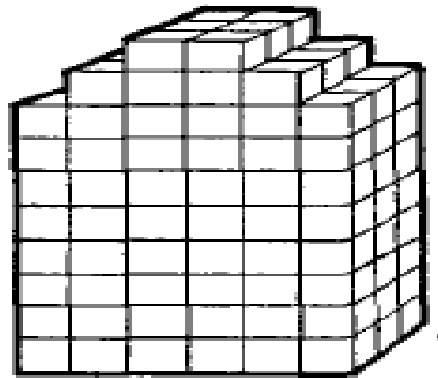


Figure 3.23: Dividing an object into identical cubes [Lee & Requicha 1982]

Division of the model into small volumetric elements result in decomposition of the shape into small entities with a volume that can be easily calculated. Their volume collectively gives the volume of the whole shape. When using smaller shapes the volume result will be more accurate volume approximation but this will increase the computation time.

In general obtaining solid properties is easier in some solid representations compared to others. A conversion between certain representations is possible and it can be considered for calculating volume [Lee & Requicha 1982].

3.7 SUMMARY

With the availability of techniques that provide accurate depth measurement and surface profile, it is important to develop algorithms that can construct solids out of the cavity at skin surfaces in order to compute volume.

Since the wound does not represent a complete solid model (3D model) its volume cannot be computed before completing the wound solid by fitting a surface in place of the original missing healthy skin surface.

The reported methods for wound volume computation are for pressure ulcers or ulcers that can be captured from one view [Callieri *et al.* 2003; Albouy & Treuillet 2007]. These wounds are deep and do not span over a high curvature area. For the leg ulcer case, the wound is not as deep as pressure ulcers [Shai & Maibach 2005] but the curvature of the leg poses a challenge in determining the ulcer volume. Leg ulcer can span the circumference of the leg which makes it difficult to reconstruct the missing top surface. Difficulties can arise when dealing with leg ulcers, as: (a) irregularities at skin (swelling and existence of scales) surrounding the wound surface that will affect surface construction and (b) the high curvature of the leg. Wounds located on different sites of the body should be treated differently based on the limb characteristics.

Options for modelling and surface fitting should be selected based on the required solid shape need to be reconstructed. Different parts at the body have different shape and thus require different surface fitting method. Analytic surfaces do not necessarily require data that are fitted to a grid unlike synthetic surfaces that require data which is fitted to a grid. When fitting scattered data to a grid a sample of the point will be taken to create the grid. Converting surface consisting of scattered data to grid fitted data is useful for reducing the amount of data by taking a sample of points.

To create a solid out of surfaces, different methods can be used. If it is possible to have a complete set of surfaces covering all sides of object; stitching multiple surfaces can be used. If some parts of the object cannot be scanned, either projection to a plane/any reference point or convex hull approximation can be used.

Normally volume computation of irregular shapes is performed by dividing solids into a number of elements that their volume is easier to be obtained and collectively their volume gives the volume of the irregular shapes.

CHAPTER 4: ALGORITHM DEVELOPMENT AND WOUND MODELING FOR NONINVASIVE WOUND ASSESSMENT

This chapter discusses the several steps required for obtaining wound measurements. Section 4.1 discusses the algorithm design considerations. Section 4.2 covers the scanning setup and surface registration. Section 4.3 shows the surface enhancement by removing unwanted data points namely small clusters and spikes at the surface. Wound modelling is presented in section 4.5; the wound shape attributes are presented in addition to the model development using AutoCAD. Calculating wound top area and true surface area is explained in section 4.6. Creating wound solid models using midpoint projection and convex hull approximation is presented in section 4.7 and 4.8. Modelling leg curvature using surface division prior to convex hull approximation is shown in section 4.9. Volume computation is discussed in section 4.10.

4.1 ALGORITHM DESIGN CONSIDERATIONS

In this work, 3D laser scanner is used to obtain 3D wound surface scans. Wound top area and true surface area can be obtained from the surface scan. Wound depth can be obtained from ultrasound and OCT as discussed in chapter 3 however; wound depth varies along the wound. It is more meaningful to measure average depth for wound assessment. One of the ways for obtaining average depth of the wound is by dividing wound volume by wound area.

Reconstruction of wound model out of surface scans using different algorithms is called solid reconstruction. Wound volume can only be obtained after reconstructing a solid out of surface scans. When using surface interpolation to fill the wound gap from the healthy skin data around the wound, irregularities (swelling and existence of scales) on the skin surface might affect the accuracy of the interpolation. The proposed method should be able to reconstruct the missing skin surface of the wound and minimize the effect of the irregularities.

Converting 3D surface consisting of scattered data to 2D gridded data is useful for reducing the amount of data by taking a sample of points. This conversion can be effective if the surface can be represented as $z=f(x, y)$ meaning that for each grid cell

there is one z value. In the case of ulcer wounds, there might be some of the surface parts which are occluded (depressed edges, undermined wounds). To overcome this problem, 3D volumetric grid can be used. However this will require large memory space and many of the grid cells will have no data since the shape of the wounds surfaces is not regular. Thus, scattered data will be used in the algorithm development. Since analytic surface models are used in this work, this data representation is useful. This data representation will not work for synthetic surface models as discussed in chapter 3.

Different options exist to reconstruct wound model from surface scan. Based on the above discussion, the following criteria are used for the development of the algorithm:-

1. The algorithm should work on scattered data.
2. Irregularities on the surrounding wound surface due to swelling and presence of scales should not affect the algorithm. The proposed method should reconstruct solid models of wounds located at the leg using only wound base, edges and top boundary. The skin around the wound will not be used for surface reconstruction.
3. The reconstructed shape should be able to model leg curvature for wounds located at the leg.

According to the criteria given above, two methods for solid reconstruction from surface scans will be considered in this work; namely midpoint projection and convex hull approximation. Convex hull approximation method is improved by applying surface division prior to the convex hull approximation to model the leg curvature. Creating a solid model by stitching several surfaces will not be considered since the missing surface interpolation is affected by the irregularities surrounding the wound surface.

Pre-processing steps are done using Rapidform software and the code for the different algorithms is developed in Matlab. The wound models are created using AutoCAD.

This chapter describes the several steps that need to be taken to calculate the wound top surface, true surface area, average depth and volume of ulcer wounds from 3D surface scans. The steps are:-

- (a) Acquiring 3D images of ulcer wound surface

(b) Removing unwanted data points from the surface. There are two types of unwanted data points namely small clusters due to cropping and spikes at the surface. Detailed description is given in section 4.3.

(c) Wound top area and true surface area are obtained from the triangular mesh. The top area is calculated from the surface boundary projected to *XY* plane. While true surface area is obtained by totalling the area for all the triangles representing the 3D surface.

(d) Applying solid reconstruction and volume computation methods on the surface. Two methods have been considered for solid reconstruction namely, midpoint projection and convex hull approximation (Delaunay tetrahedralization). Those methods do not require surface interpolation based on wide area around the wound. Therefore they are not affected by the irregularities (swelling and scales) in the surrounding skin surface.

4.2 3D LASER SCANNING

Accurate data acquisition methods are essential in the success of any measurement and inspection applications (e.g. volume computation). The suitability of scanners for a particular application has to be assured [Zhang *et al.* 2005; Halim 2004]. In this research, 3D laser scanner capable of providing dense points on the surface representing depth measurement at different surface locations is used. The point cloud from the scan is equally distributed along the surface with difference between the data points as small as 0.1 mm.

Konica Minolta 3D Laser scanner (VI-910) is used to obtain skin and ulcer surfaces. A scan area from 11x8 cm at a subject distance of 60 cm up to 120x90 cm at a subject distance of 2.5 m can be covered with each scan. Measuring time in fine mode (307000 points) can be reached in 2.5 seconds and in fast mode (76800 points) in 0.3 seconds. The system achieves accuracy of Z , $\pm 0.10\text{mm}$ to the Z reference plane. The Konica Minolta non-contact 3D Digitizer is based on the principle of laser triangulation. Objects are scanned using a laser light strip. Figure 4.1 (top) shows the scanner used in this work Konica Minolta during a scanning session of ulcer wound from a patient at HKL (Hospital Kuala Lumpur). Figure 4.1 (bottom) displays the different parts of the scanner.



Figure 4.1: Obtaining wound surface scan using 3D laser scanner

One scan takes 2.5 seconds, several scans are normally needed to cover the whole wound surface and to ensure complete coverage. Typically, three scans are sufficient to ensure good coverage of the wound surface. However for wounds that span a large area and surround the leg, more scans are needed to cover the wound area. For complete follow up for patients' lesions, several scanning sessions with regular intervals should be performed with quantitative assessment throughout the treatment to estimate the progression or regression of the lesion.

Accurate measurements for the locations of multiple points located at a surface are obtained using the laser scanner. These dense measured points are collectively called

point clouds refer to Figure 3.8 (a). From this raw data certain information can be obtained, for example point to point distance. For surface area computation, a process called meshing is required.

The Rapidform2006 software is used for controlling the scanner when performing the scan, registering surfaces covering several views of a wound surface, meshing the surface, tracing wound boundary (segmenting wound surface), removing scattered points from the wound surface (enhancement) and exporting the wound surface to 'stl' file format. STL file is a triangular representation of a 3D surface geometry. The surface is represented using a number of triangles. Each facet is described by the unit outward normal and three points listed in counterclockwise order representing the vertices of the triangle. For a detail description on using the Rapidform [INUS 2005] is referred.

In this study, 9 with patients from Hospital Kuala Lumpur have been involved in providing 22 3D laser scanned surface images of ulcers at the legs. A list of the captured wounds surfaces images is given in Appendix A. Prior to applying the appropriate volume computation of leg ulcer wounds, leg ulcer wounds images of patients are analyzed. Parameters that describe the wounds are developed based on real ulcer wound surface images for wound modelling. Wound models representing possible ulcer wounds developed using AutoCAD software are used to investigate the performance of volume computation techniques.

4.2.1 Surface Scanning Setup

Prior to performing a 3D surface scan of an ulcer wound, several conditions must be ensured:

1. For capturing 2D colored image, sufficient light is required (minimum 300 lx and maximum 500 lx). The colored image will be aligned to the 3D surface scan. For scanning 3D surfaces, no light is needed since the laser light is used.
2. White balance calibration is performed, for colors correction for each scan session.
3. The body part of the patient should not move during the scan.
4. If any contact is needed with the patients, gloves and general hygiene procedures should be followed since the wound is open and can easily catch infections.

5. It is preferable to perform the wound scan after cleaning the wound because ulcer wound frequently produces some liquid (Figure 4.2). This might create artifacts when performing the scanning [Wendelken *et al.* 2003]. Shiny object affects the scanning process and causes the laser rays to refract as shown in Figure 4.3 [LEVOY 1999]. To solve this problem wound scanning should be scheduled with wound dressing changed.
6. Reference points should be marked in the target surface for the registration process as shown in Figure 4.2.



Figure 4.2: Liquids at wound surface (date: 4-12-08; patient: P-9; hospital: HKL)

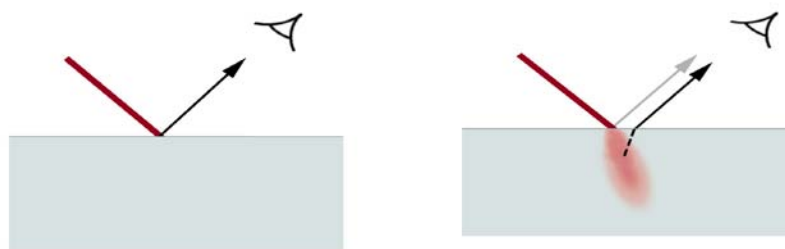


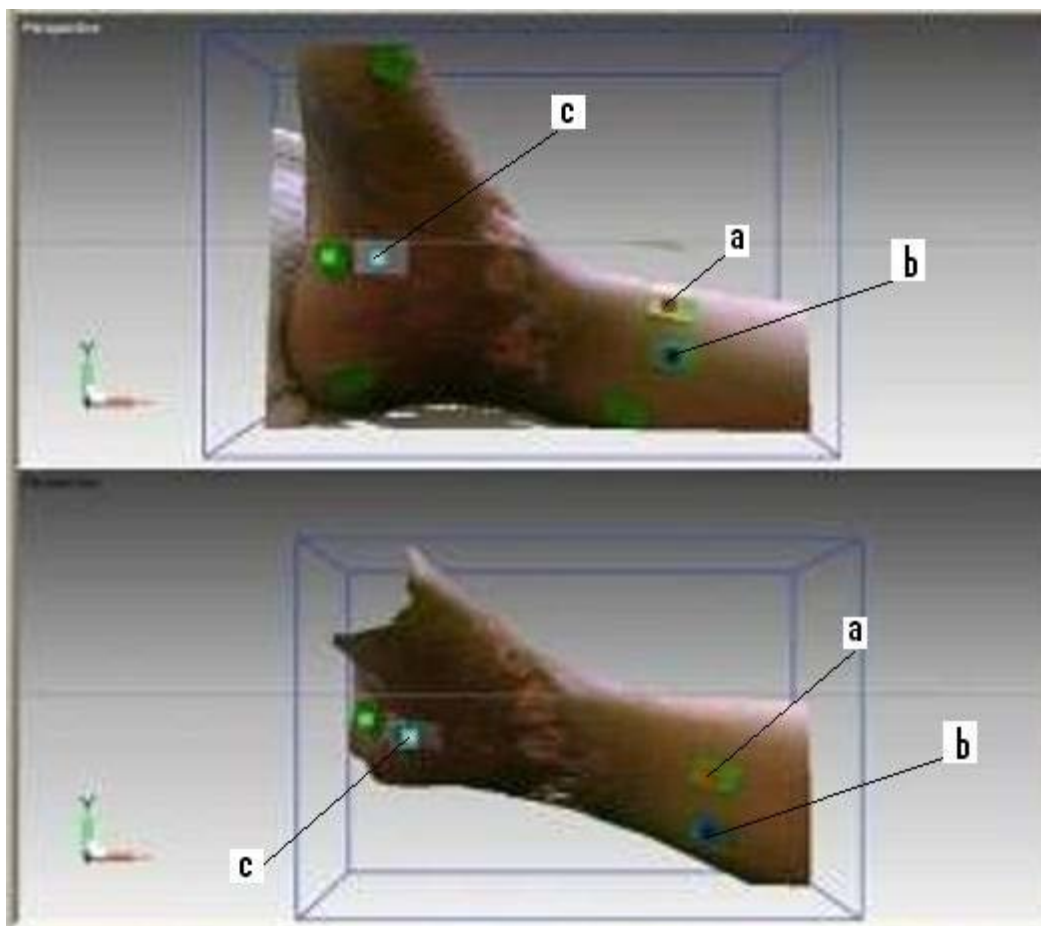
Figure 4.3: Ray refraction due to shiny surface [LEVOY 1999]

The scanned surface should cover the wound surface and the area surrounding it. This is done in order to have reference points in the surrounding skin and to store this data for surface reconstruction if needed.

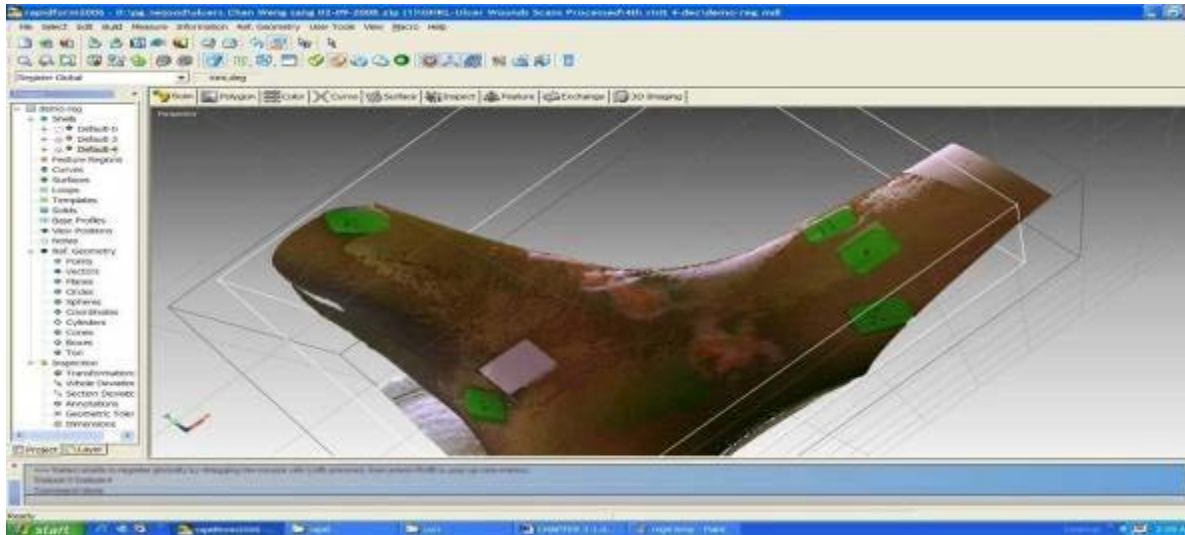
4.2.2 Registering Multiple Scans

When registering several surface scans, a surface that covers different views can be reconstructed. The resulting surface will cover large area not obtainable from one view.

Holes or gaps due to occlusion will be filled by the registration process [Unten & Ikeuchi 2004]. To register 2 surfaces using reference points, a minimum of 3 matching points between the surfaces are required. There should be a difference between the angles for the scans of at least 45° . If small angle is used between the scans, holes might get introduced to the surface. The holes are due to failure in matching very large overlapping in the surface [INUS 2005]. Figure 4.4(a) displays two scans of ulcer wounds with three matching reference points at the surface; Figure 4.4(b) shows the resulting surface after registering the scans in Figure 4.4(a).



(a) Two views of a specific wound surface, with three corresponding reference points.



(b) The result of registering the surfaces in (a).

Figure 4.4: Surface registration using two surface scans

4.2.3 Segmenting Wound Area

After scanning the wound and performing the surface registration, wound surface should be cropped for the purpose of volume computation. The volume computation algorithms are coded in Matlab and the input surface is in *stl* file format. Wound boundary is selected using the mouse by selecting a polygon consisting of several points around the wound as in Figure 4.5. The selected wound surface is then exported as an *stl* file.

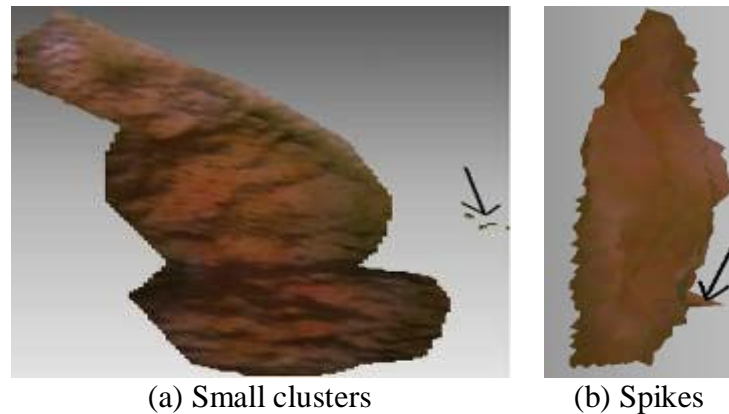


Figure 4.5: Wound surface selection

4.3 ENHANCEMENT

Frequently, unwanted data points are present in surface scan [Sun *et al.* 2008]. Unwanted points at the surface will affect volume computation significantly. Two types of unwanted points have the potential to introduce large error to volume computation. These are small clusters of vertices (Figure 4.6(a)) and spikes at the surface (Figure 4.6(b)). Small clusters happen due to segmentation (cropping the wound area). Noise is reduced by removing small clusters of points having point count less than 50. Selecting the value of the 1.5 for edges to represent spikes is suitable for most of the tested scans. However,

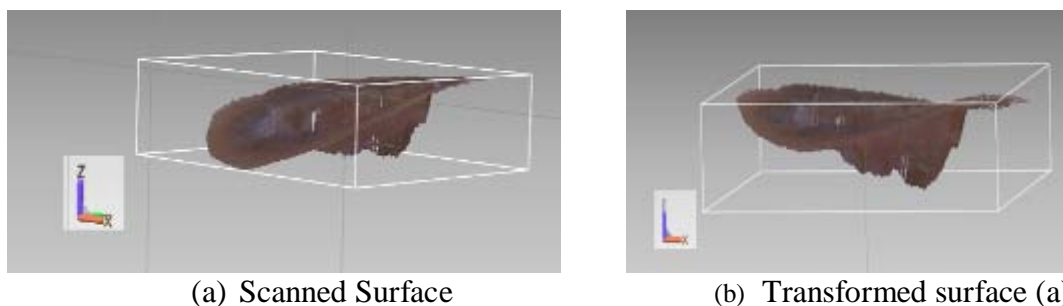
visual inspection (highlighted edges) might be used before deleting the selected edges. In some cases, especially wounds which are deep with occlusion, faces with edges greater than 1.5 is not necessarily noise.



(a) Small clusters (b) Spikes
Figure 4.6: Wound surface with noise

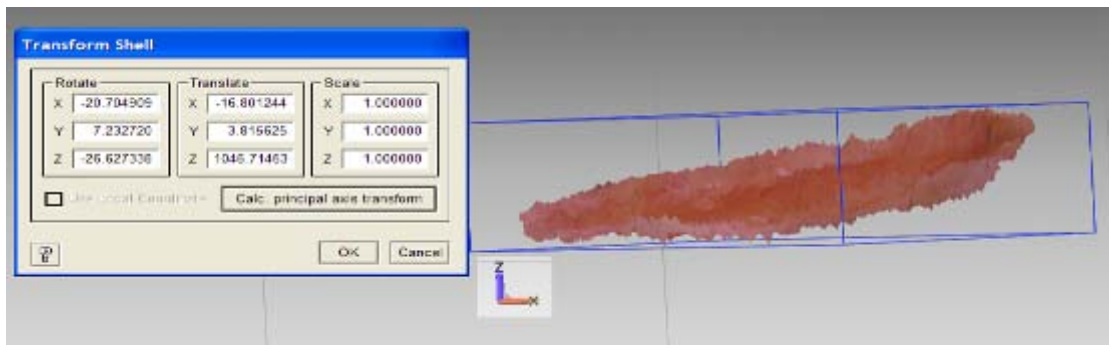
4.4 ALIGNMENT AND COORDINATE SYSTEM

Ideally when scanning a wound surface, the z -axis should correspond to the wound depth. However this is not the case when registering scans from multiple views which cover big wound surfaces or when the scanner cannot be placed perpendicular to the wound. To overcome this problem, an option in the Rapidform software called ‘Calc Principal Axis Transform’ is used to ignore all the previous input and transform the object with respect to its principal axis. This causes the object’s centroid to move to the zero point. If the scanned surface is skewed to principal axes the surface will be rotated until it is parallel to the XY plane [INUS 2005]. Figure 4.7 provides an example of 2 scanned surfaces (a), (c) and their transformed surfaces (b), (d) respectively.

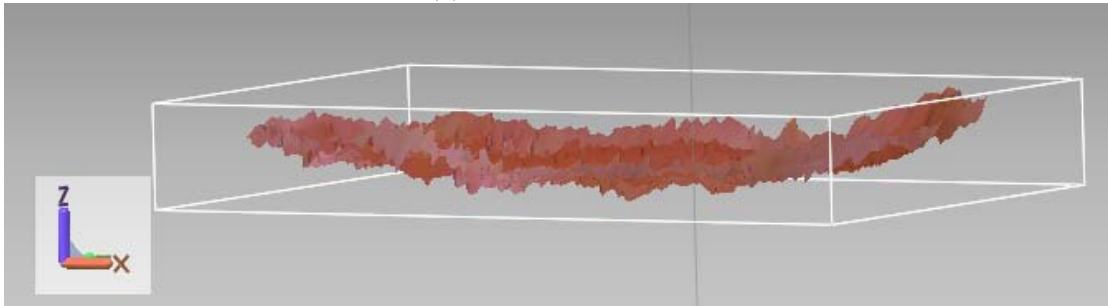


(a) Scanned Surface

(b) Transformed surface (a)



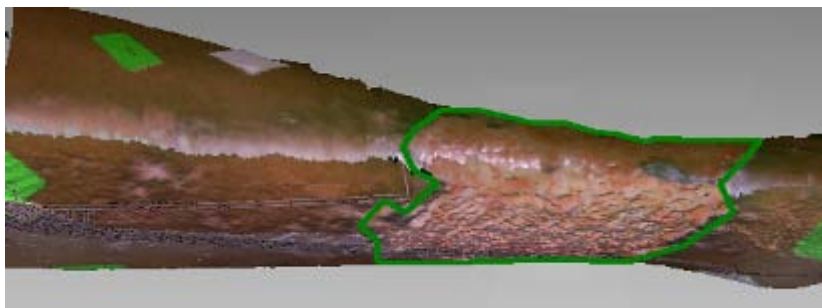
(c) Scanned Surface



(d) Transformed surface (c)

Figure 4.7: Surface translation and aligning

The correct z orientation could be obtained using this option. Yet, for very large wound that span more than half of the leg circumference it is not possible to have one correct z alignment for the whole surface. In this case the wound surface is divided into 2 surfaces along the y -axis and the new surfaces are aligned using the previous option. Figure 4.8 illustrates this process: 4.8(a) shows the scan of a large wound, 4.8(b) the wound surface after cropping it, 4.8(c) and 4.8(d) surface divisions after transformation (rotate, translate).



(a) Scan of leg ulcer spanning more than half of the leg circumference

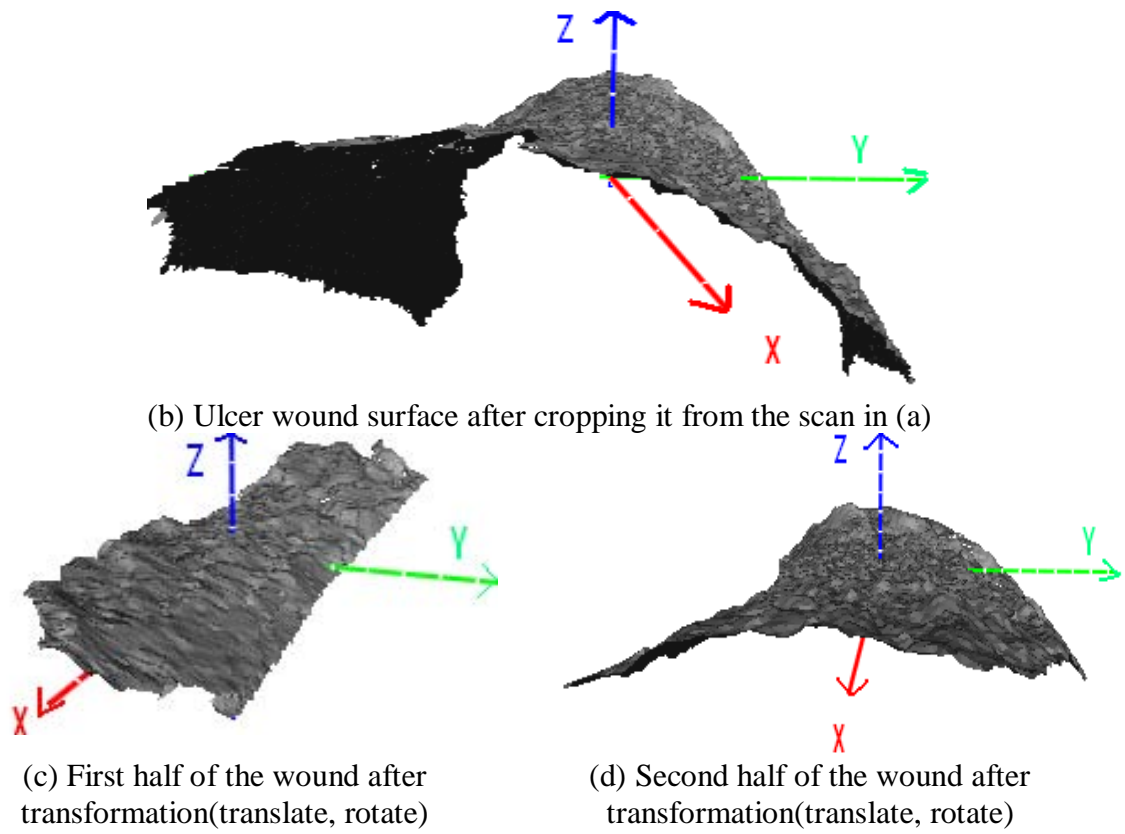


Figure 4.8: Wound surface with different coordinates

The steps described in sections 4.2, 4.3 and 4.4 are summarized in Figure 4.9.

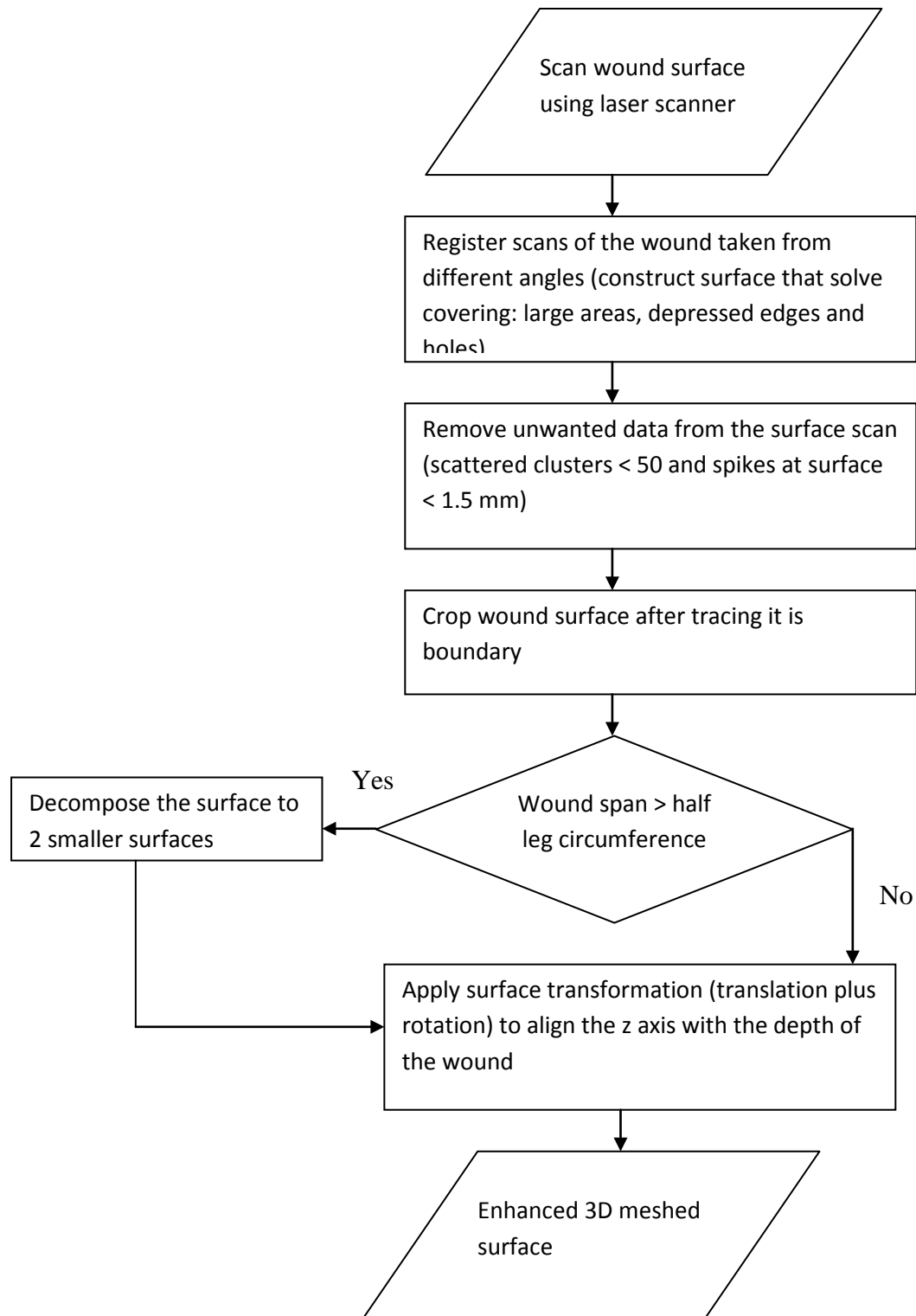


Figure 4.9: Surface acquisition and pre-processing steps

4.5 WOUND MODELING

4.5.1 Wound Shape Attributes

The shape of the wound is described based on its appearance. Shape descriptors can identify the cause behind the wound. To identify the Attributes which control the shape of wounds, medical classification, doctors' descriptions and images of wounds have been investigated. After careful examination of leg ulcer wounds it is found that real wounds can be modelled by three attributes with descriptors for the shape of wounds edge, wound boundary and for the curvature of wound base as depicted in Figure 4.10.

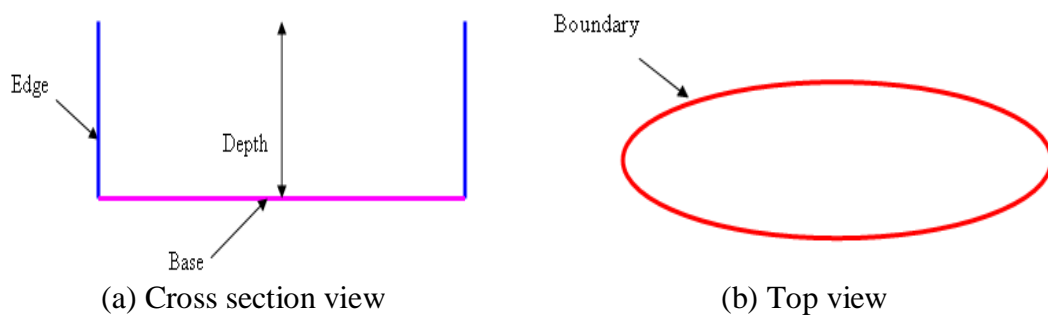






Figure 4. 10: Illustrations of the geometrical attributes of ulcer wounds

Table 4.1 lists the descriptors of each wound attribute that describe wound shape based on the analysis of real ulcer wounds. Several solid models are simulated based on different combinations of these attributes.

Table 4.1: Wound attributes and their descriptors

Attribute	Descriptors	Schematic	Similar wounds
Wound edge - raised sides of the wound	Slope shape		
	Chopped		


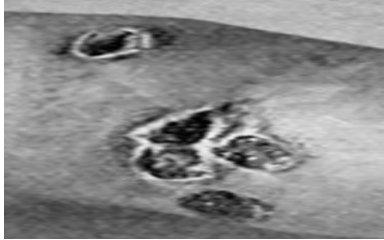



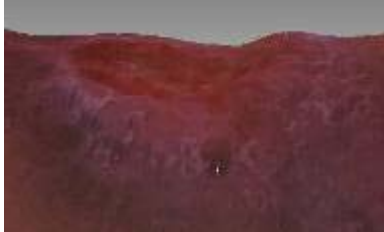


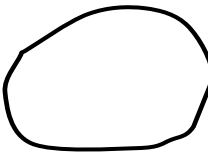

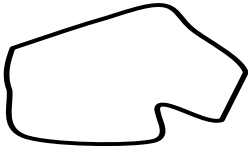

	Rolled over / Punched out		 [Thomson & Miles 2006]
Wound base - bottom part of the wound	Homogeneous depth		
	Depressed		
	Elevated base		
Boundary - shape obtained by tracing around the wound surface	Regular (Oval, ...)		
	Irregular (zig-zag)		

Table 4.2 lists the different wound models generated based on different combinations of descriptors for the wound attributes.

Table 4.2: Wound Models

#	Model	Wound Edge	Wound Boundary	Wound Base
1	M1h	Chopped	Regular	Homogeneous depth
2	M1a	Chopped	Regular	Depressed
3	M1b	Chopped	Regular	Elevated Base
4	M2h	Chopped	Irregular	Homogeneous depth
5	M2a	Chopped	Irregular	Depressed
6	M2b	Chopped	Irregular	Elevated Base
7	M3h	Slope Shape	Regular	Homogeneous depth
8	M3a	Slope Shape	Regular	Depressed
9	M3b	Slope Shape	Regular	Elevated Base
10	M4h	Slope Shape	Irregular	Homogeneous depth
11	M4a	Slope Shape	Irregular	Depressed
12	M4b	Slope Shape	Irregular	Elevated Base
13	M5h	Punched Out	Regular	Homogeneous depth
14	M5a	Punched Out	Regular	Depressed
15	M5b	Punched Out	Regular	Elevated Base
16	M6h	Punched Out	Irregular	Homogeneous depth
17	M6a	Punched Out	Irregular	Depressed
18	M6b	Punched Out	Irregular	Elevated Base

4.5.2 Developing Wound Models

The models are developed using AutoCAD software. The process involves a series of set operation on primitive solids in addition to extruding some surfaces with variant angles. Creating elevated and depressed base shape was possible using set operations on models (union, subtraction) [Finkelstein 2006]. Union and subtraction of solids are shown in Figure 4.11.

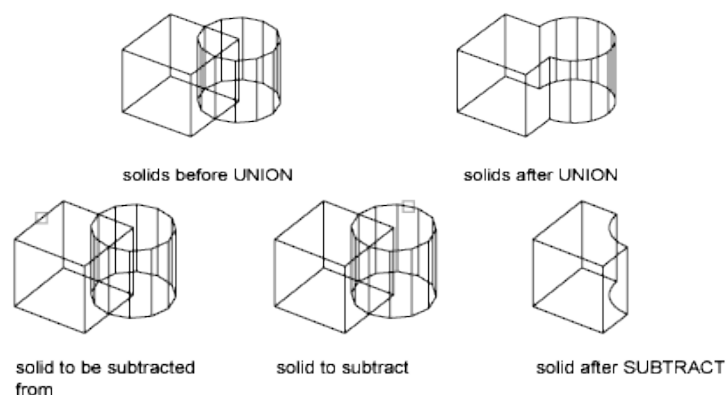


Figure 4.11: Union and subtraction commands [AutoCAD 2007]

Extruding a polygonal shape and using angles inwards and outwards is a useful tool especially for the edge simulation. The 'EXTRUDE' command can result in creating a solid object from circles, polygons and objects, in addition to polylines (free form

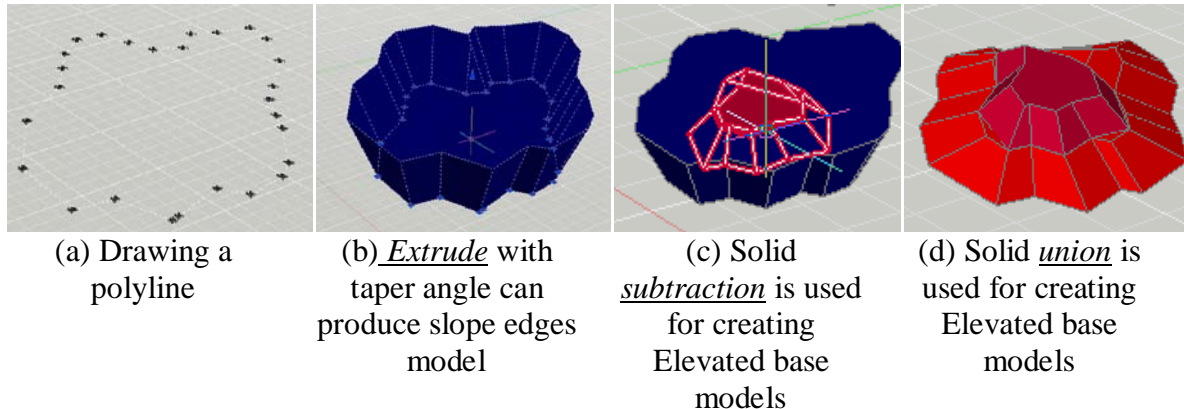
shapes), that have ‘closed’ paths. Two of the parameters that are used with the command are the height and taper angle. When using angle=0 and a particular height this will result in creating a solid with a thickness equal to the height value as shown in figure 4.12 (a). When a value different from zero is given to the taper angle this will result in extrusion taper in or out from the base object as displayed in figure 4.12 (b) [AutoCAD 2007].



(a) Extrude with a height and 0 angle (b) Extrude with negative angle – taper in

Figure 4.12: Extrude command [AutoCAD 2007]

The following Figure 4.13 displays the construction of solids using the operations mentioned above. Figure 4.13(a) displays the first step in modeling that is drawing a 2D polygon; Figure 4.13(b) displays the solid created by performing extrusion on the 2D polygon. Figure 4.13(c) and 4.13(d) shows set operations (subtraction and union) on solids.



(a) Drawing a polyline

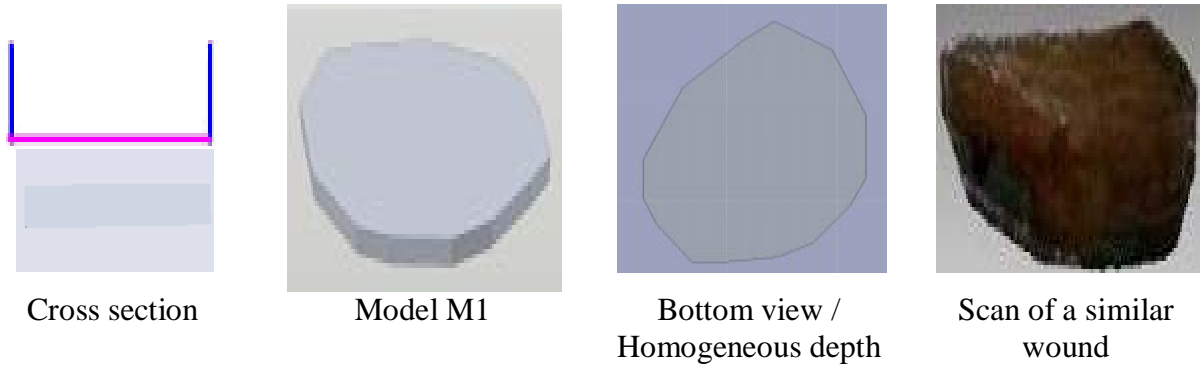
(b) Extrude with taper angle can produce slope edges model

(c) Solid subtraction is used for creating Elevated base models

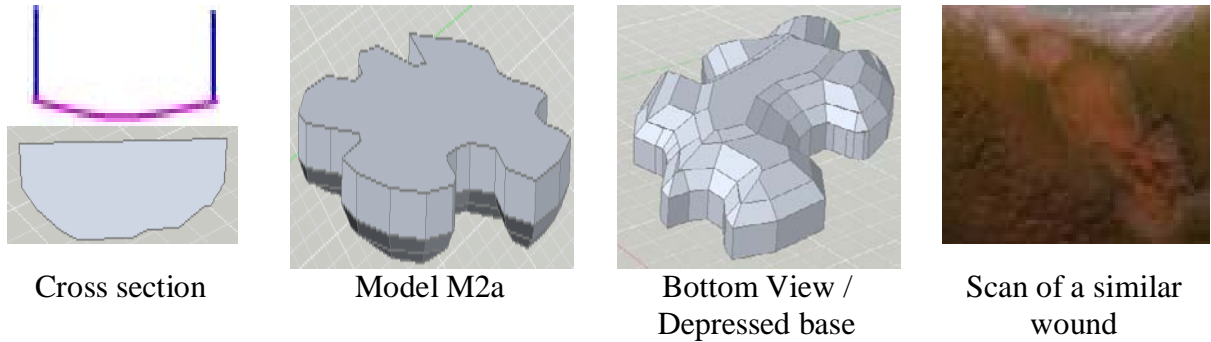
(d) Solid union is used for creating Elevated base models

Figure 4.13: Creating solid models using AutoCAD

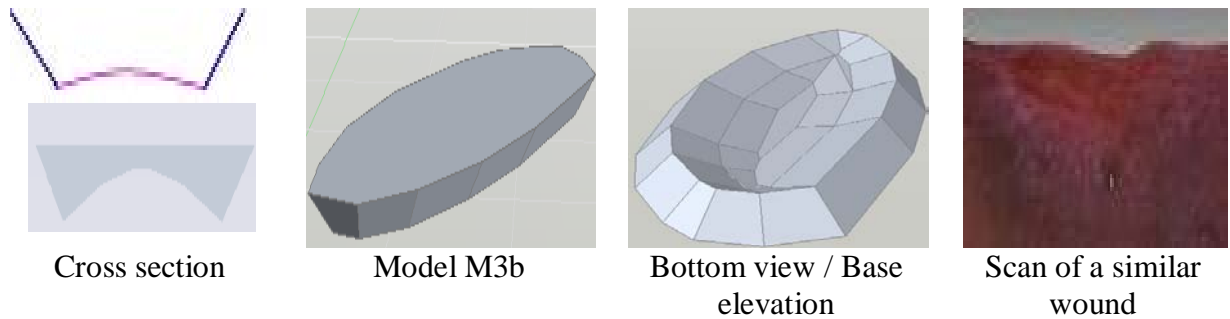
The wound models described in Table 4.1 and Table 4.2, which can be obtained from filling a wound surface by any molding material, have been modeled using AutoCAD and their volumes were obtained from the software. A complete list of the models is given in Appendix B. The reference volume of the wound models was calculated using AutoCAD function named ‘*massprop*’. This function calculates several mass properties of the solid models including the volume. Figure 4.14 shows four ulcer models representing real and common leg ulcers found in patients.



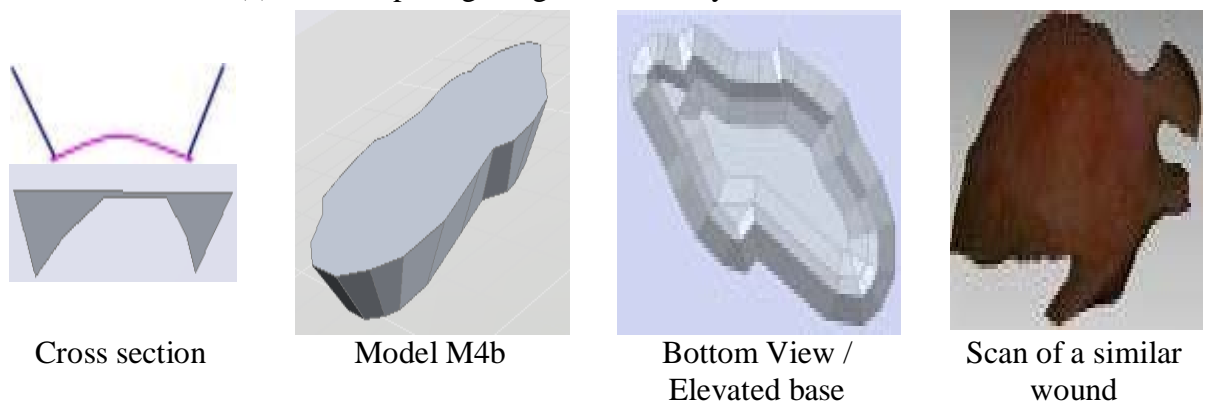
(a) M1, chopped edge, regular boundary and Homogeneous depth



(b) M2a, chopped edge, zig-zag boundary and depressed base



(c) M3b, slope edge, regular boundary and elevated base



(d) M4b, slope edges, zig-zag boundary and Elevated base

Figure 4.14: Models M1, M2a, M3b and M4b

4.6 CALCULATING WOUND TOP AREA AND TRUE SURFACE AREA

The following Figure 4.15 displays a system block diagram that give an overview of the algorithms developed and investigated to obtain wound parameters such as top area, true surface area, average depth, and volume.

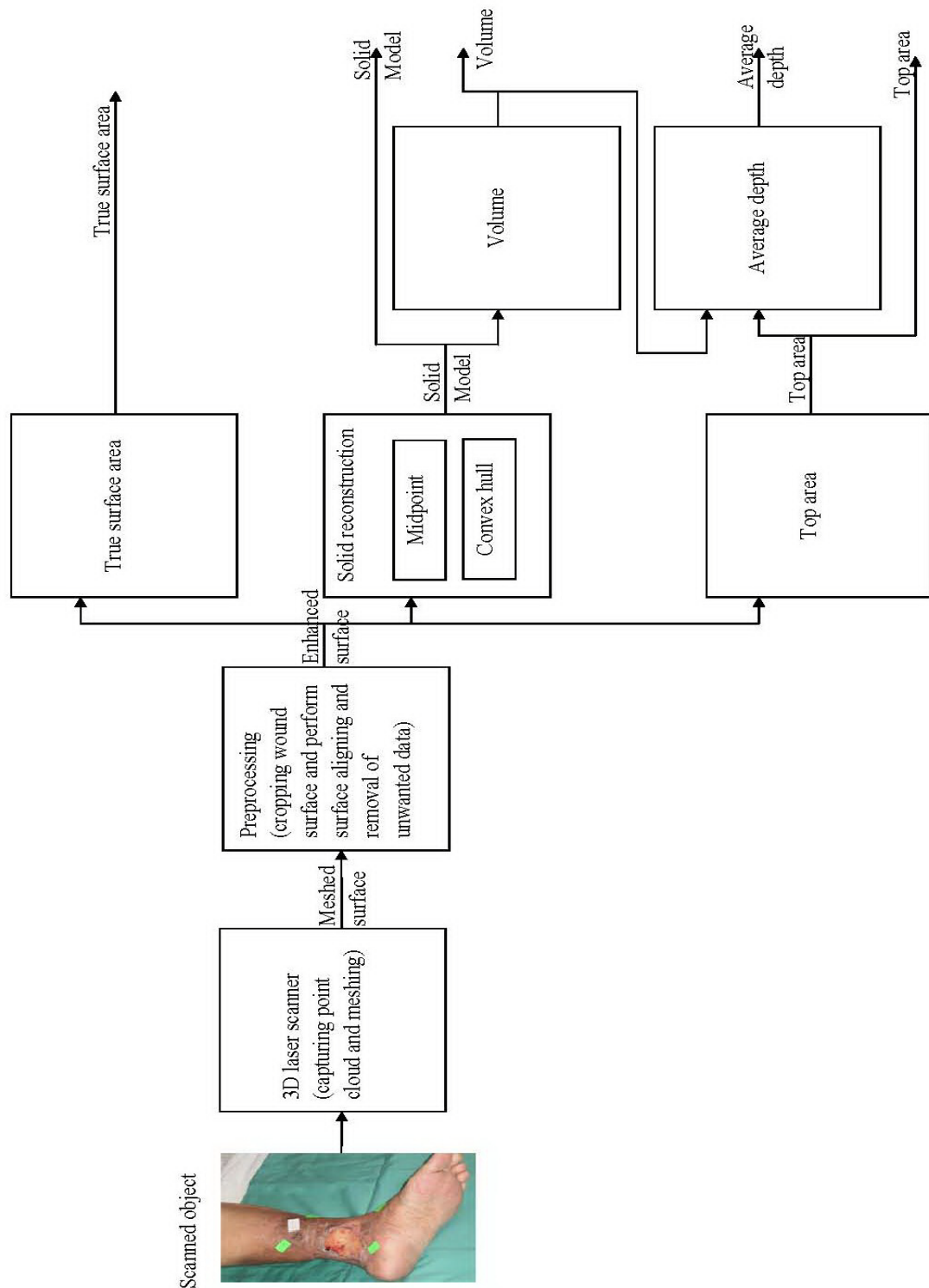
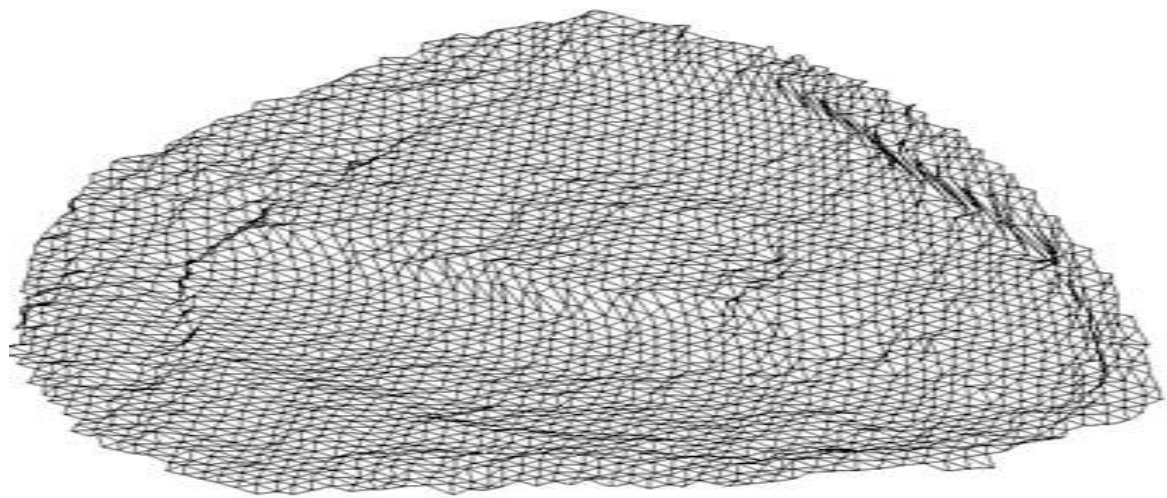


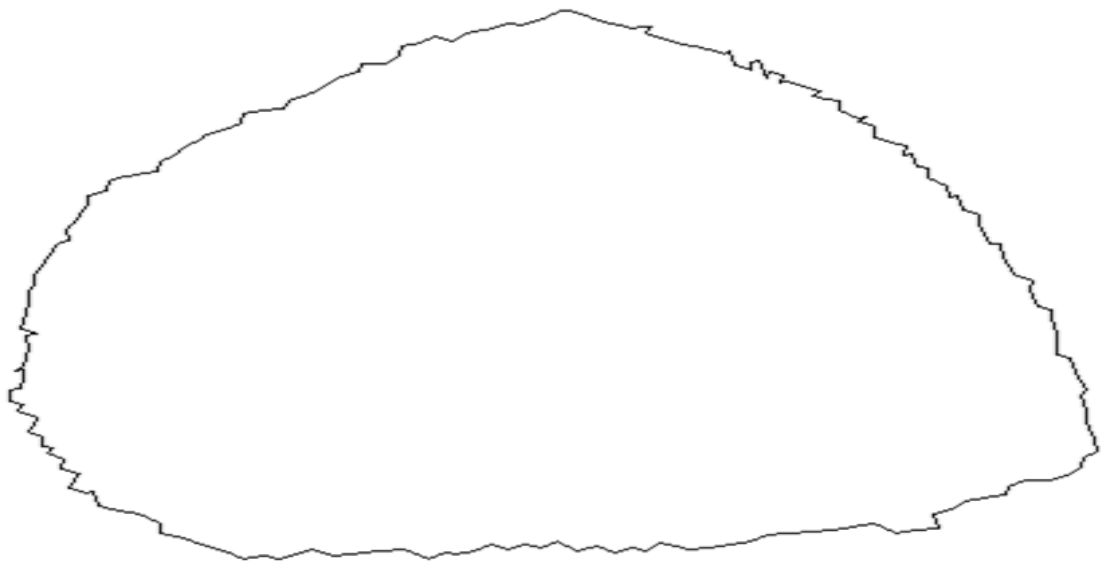
Figure 4.15: Overview of the system diagram

4.6.1 Top Area

Figure 4.16 displays a surface (Figure 4.16(a)) and its corresponding boundary polygon (Figure 4.16(b)). From the figure, the outer boundary of the wound can be obtained from the triangular mesh and it is defined as all the edges that belong to only one triangle [Persson & Strang 2004]. All the internal edges are shared by exactly two triangles. The top area of the wound is calculated as the area of the polygon created by extracting the wound boundary and projecting this outer boundary to the XY plane ($z=0$). The projected outer boundary is then divided to small triangles impeded in 2D space and the top area is computed as the totaling of all the triangles area.



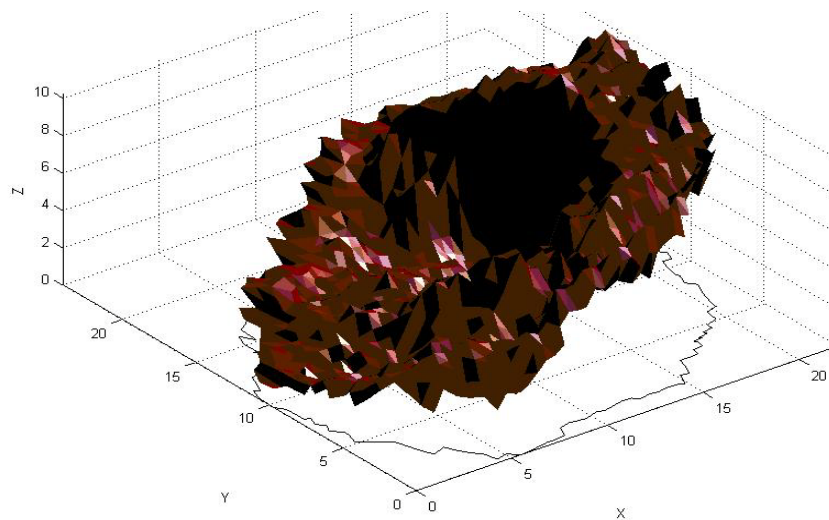
(a) Meshed surface



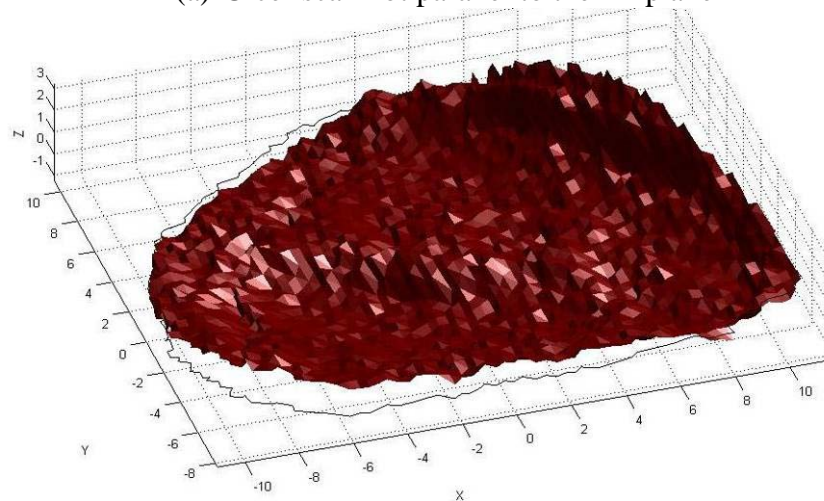
(b) Boundary edges

Figure 4.16: Extracting surface boundary

As described in Section 4.3 the surface has to be aligned parallel to the XY plane with no skewness in the surface alignment. When the surface is not parallel to the XY plane (Figure 4.17(a)) the projected area will be smaller than the actual area calculated by tracing the top boundary of the wound and this will affect average depth calculations. The required projected area here is the maximum projected area with no skewness in the surface with respect to the XY plane as shown in Figure 4.17(b).



(a) Ulcer scan not parallel to the XY plane



(b) Ulcer scan aligned parallel to the XY plane

Figure 4.17: Surface alignment

4.6.2 True Surface Area

As the surface is constructed of triangular mesh, the area of the surface is obtained by calculating the area of the individual triangles in the mesh. In meshed models three vertices represent each triangle. If a triangle is embedded in 3D space with the

coordinates of the vertices given by $V_j = (x_j, y_j, z_j)$ the area is given by Equation 4.1 [Weisstein, E.W].

$$\Delta = \sqrt{\begin{vmatrix} x_1 & z_1 & 1 \\ x_2 & z_2 & 1 \\ x_3 & z_3 & 1 \end{vmatrix}^2 + \begin{vmatrix} z_1 & x_1 & 1 \\ z_2 & x_2 & 1 \\ z_3 & x_3 & 1 \end{vmatrix}^2 + \begin{vmatrix} x_1 & y_1 & 1 \\ x_2 & y_2 & 1 \\ x_3 & y_3 & 1 \end{vmatrix}^2} \quad \text{Eq. 4.1}$$

To measure the whole surface area, the area of all the triangles in the triangular mesh is totalled as stated in Equation 4.2.

$$Area = \sum_{j=1}^N \Delta_j, \text{ where } N \text{ is the number of triangles. } \rightarrow \text{Eq. 4.2}$$

The average depth can be computed by dividing the wound volume by the top area. Volume computation will be described in the following sections.

4.7 SURFACE RECONSTRUCTION: CREATING SOLID BY PROJECTING SURFACE FACES TO MIDPOINT

Before computing wound volume, a solid must be reconstructed out of wound surface scan. Here, a solid is reconstructed by connecting all the triangular faces to a midpoint creating many tetrahedra. The midpoint is calculated from a number of points selected at the edges of the wound/ model. Figure 4.18 show midpoint calculated from a number of edges at the boundary.

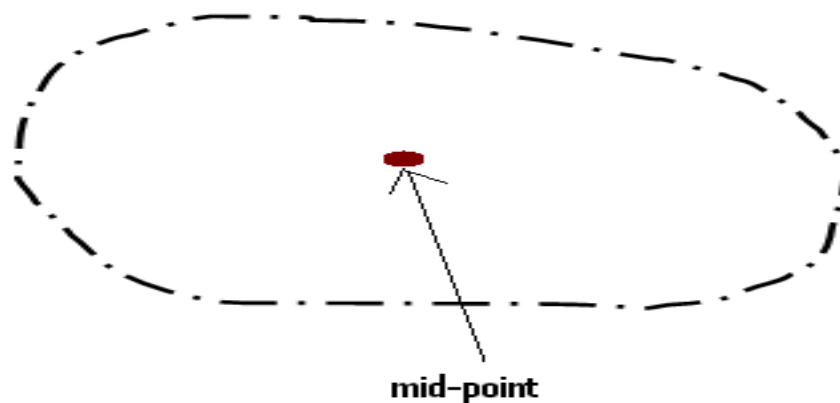
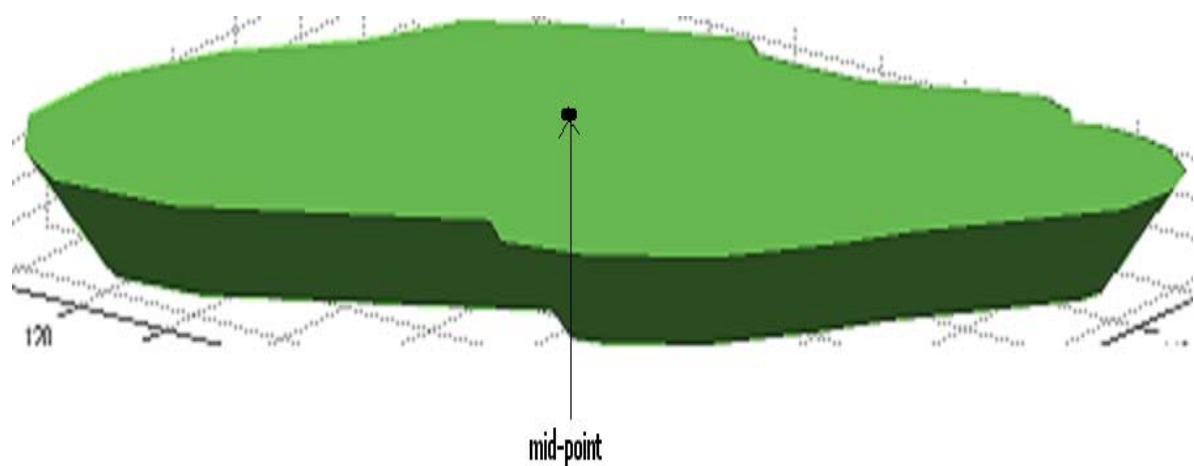


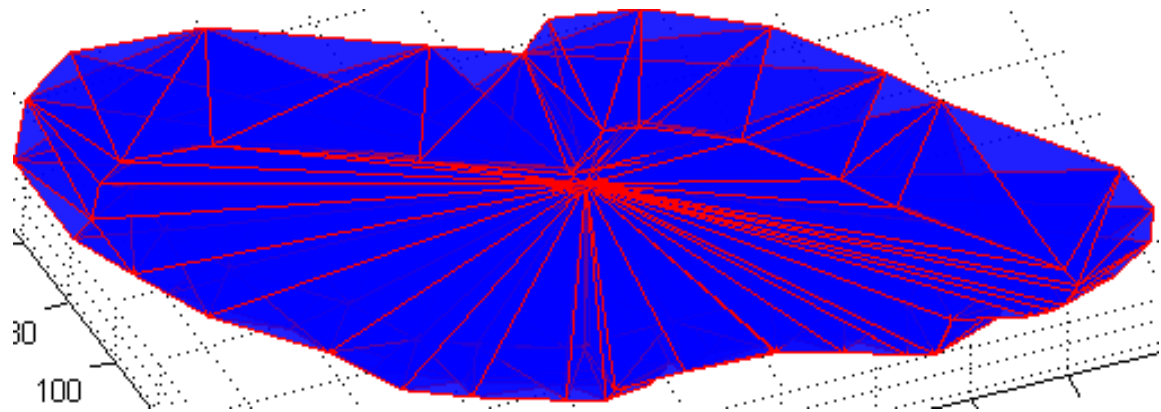
Figure 4.18: Midpoint calculation

The volume of the cavity or wound is computed by summing up the volume of all the tetrahedra. Projecting surfaces to a plane or reference point is useful for volume reconstruction. The shape of the models under construction is the key in selecting the appropriate projection method. In the case of wound models, the reconstruction of a projected wound surface to an edge point, reference plane or to a point interpolated at the top surface will lead to an approximation of wound volume. However, one of the issues in developing the algorithm is to obtain reproducible results of the wound volume. If a point at the boundary is used as a reference point for solid reconstruction, it is not possible to have land mark in the wound boundary and measure the wound using the same point in each assessment. Projecting the surface faces to one edge point, which is difficult to identify in each assessment (landmark), might lead to irreproducible results. Calculating a midpoint from several points at the wound boundary will produce more reproducible results.

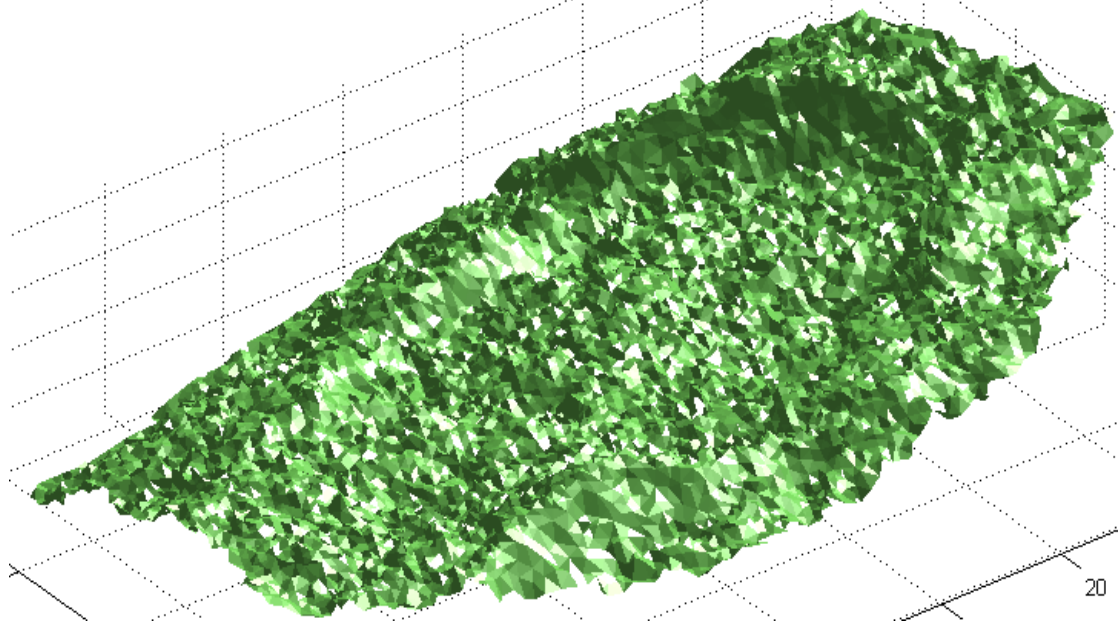
Midpoint is obtained from a set of points selected at the wound boundary. Selecting points is not a straightforward process. The selection is having some complications since the display is 2D and we need to select 3D points. Thus, SELECT3D tool is used [Conti n.d.]; it determines the selected point P in 3D data space. P is a point on the first patch or surface face intersected along the selection ray. It returns the closest face vertex. Figure 4.19 shows the results of constructing solids from a model and a real scan using midpoint solid reconstruction. Figure 4.19(a) shows a wound model and Figure 4.19(b) shows its reconstructed solid using midpoint projection. Figure 4.19(c) shows wound surface scan and Figure 4.19(d) shows its solid model created using midpoint projection.



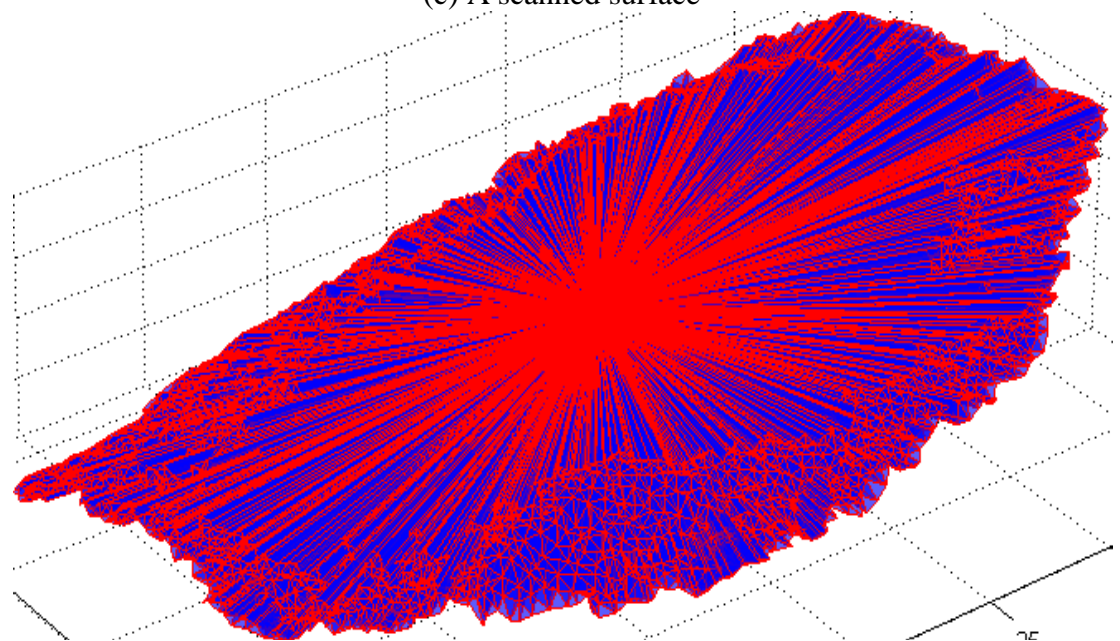
(a) A wound model



(b) After connecting all the faces to midpoint (bottom view)



(c) A scanned surface



(d) After connecting all the faces to midpoint

Figure 4.19: Midpoint solid reconstruction for a model and a skin surface

In some unusual wound (e.g. L-shape wound) in which the midpoint might lie outside the surface as shown in Figure 4.20, recalculation of the midpoint is required. The same z -value can be used for the new midpoint and the location of XY coordinates should be altered.

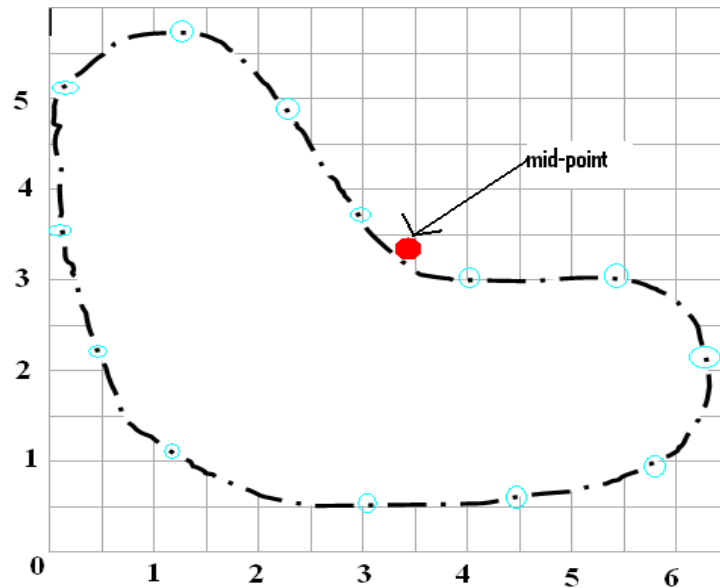


Figure 4.20: L shaped wound

Modification in midpoint or recalculating midpoint is by allowing the user to select a point inside the surface. The x and y coordinates will be obtained from the user selection while the z value from midpoint calculation is still valid.

This algorithm is sensitive to the existence of holes at the surface because all the faces of surface in the triangular mesh is used in volume computation. Even though surface registration eliminates gaps at the surface scan, some holes at the surface may be left unfilled. In order to use this algorithm for volume computation, all holes at the surface must be filled. This can be performed as a pre-processing step using Rapidform software.

When using this method for solid reconstruction and volume computation, points around the surface do not need to be dense. In case of the surface scan, the number of vertices in the surface can be reduced using the decimation process that will lead to reduction in the algorithm execution time. Decimation refers to the process of reducing the number of triangles, while preserving the original surface shape.

The flow chart of reconstructing wound models using midpoint projection is as follows:

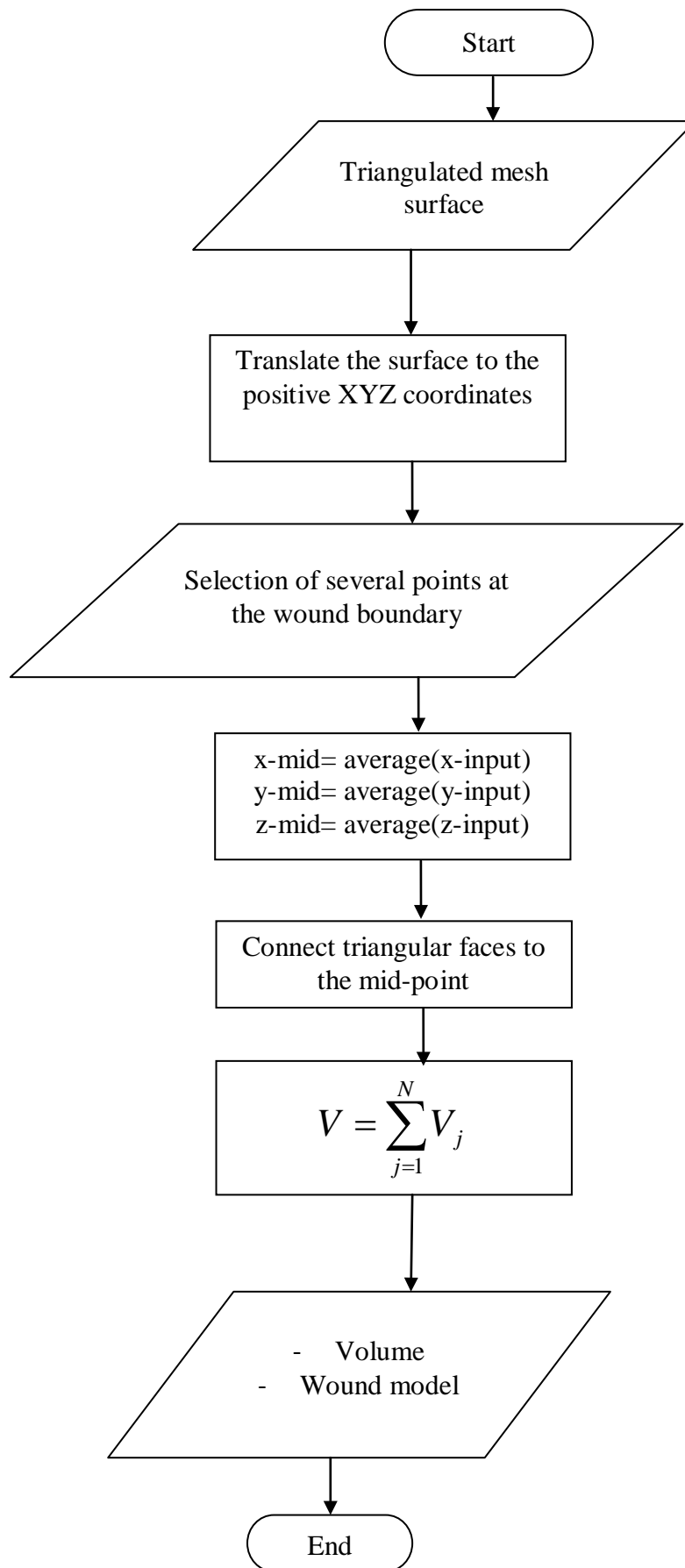


Figure 4.21: Flow chart diagram of mid-point projection algorithm

The algorithm from the flow chart in Figure 4.21 is outline as follows:

ALGORITHM: Creating wound models using midpoint projection

Input: triangulated surface

Output: wound volume and the wound model

- 1- Translate the surface to the positive XYZ coordinates.
- 2- Ask the user to select several points on the wound outer boundaries.
- 3- Average all the points to obtain midpoint XYZ values.
- 4- Connect all the triangular to faces to the midpoint creating collection of tetrahedra (the midpoint will represent the fourth vertex in all the tetrahedra in the model).
- 5- Compute the volume of the wound model by adding the volumes of all the tetrahedra on the surface.

4.8 SURFACE RECONSTRUCTION: CREATING SOLID USING CONVEX HULL APPROXIMATION (Delaunay Tetrahedralization)

Another method of constructing solids out of surfaces is by using convex hull approximation (Delaunay tetrahedralization). A tetrahedralization of V is a set T of tetrahedra in 3D whose vertices collectively are V , whose interiors do not intersect each other and whose union is the convex hull of V . A convex hull, $CH(V)$ is the smallest polyhedron in which all elements of V on or in its interior. The convex hull approximation encloses all the vertices representing the surfaces in the smallest polyhedron. The *Quickhull* algorithm for convex hulls [Barber *et al.* 1996] has been used to create the convex hull approximation. The construction of convex hull out of 3-simplexes (tetrahedra) is performed by growing tetrahedra vertex by vertex, thus constructing more tetrahedra shapes. A convex hull is constructed by:

- Firstly, building a tetrahedron using 4 points (Delaunay 3-simplex); which is used as a seed upon which the remaining Delaunay tetrahedra crystallize one by one.

- Secondly, when adding the next point its visible faces have to be found. For any integer $r \geq 1$, let $\mathbf{Pr} := \{ \mathbf{p}_1, \mathbf{p}_2, \dots, \mathbf{p}_r \}$. If the new point to be added is inside the current convex hull it will be ignored. If the new point is outside the current hull the visible facets form a connected region on surface of $\mathbf{CH}(\mathbf{P}_{r-1})$, called visible region or \mathbf{p}_r on $\mathbf{CH}(\mathbf{P}_{r-1})$, which is enclosed by a closed curve consisting of edges of $\mathbf{CH}(\mathbf{P}_{r-1})$. This curve is called the horizon of \mathbf{p}_r on $\mathbf{CH}(\mathbf{P}_{r-1})$, the horizon of a point \mathbf{p}_r is shown in Figure 4.22. The horizon of \mathbf{p}_r plays a crucial role when transforming $\mathbf{CH}(\mathbf{P}_{r-1})$ to $\mathbf{CH}(\mathbf{P}_r)$.

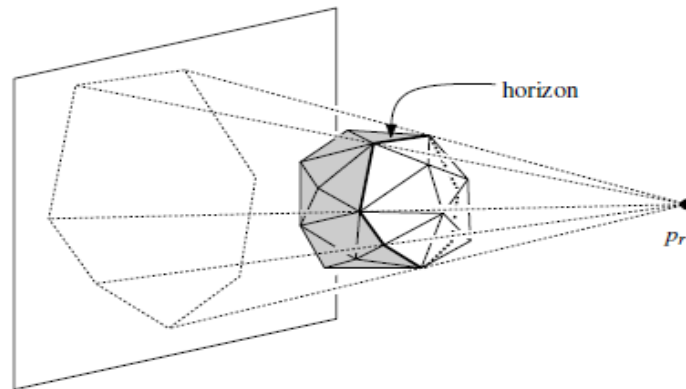


Figure 4.22: The horizon of a polytope [Berg *et al.* 2008]

- Finally, the new point \mathbf{p}_r will act as an apex for all the visible faces in its horizon adding several tetrahedra to the convex hull. While growing the convex hull a point \mathbf{p}_r will be added to the convex hull of \mathbf{P}_{r-1} , that is, transforming $\mathbf{CH}(\mathbf{P}_{r-1})$ into $\mathbf{CH}(\mathbf{P}_r)$ as shown in Figure 4.23 [Shewchuck 1999; Berg *et al.* 2008].

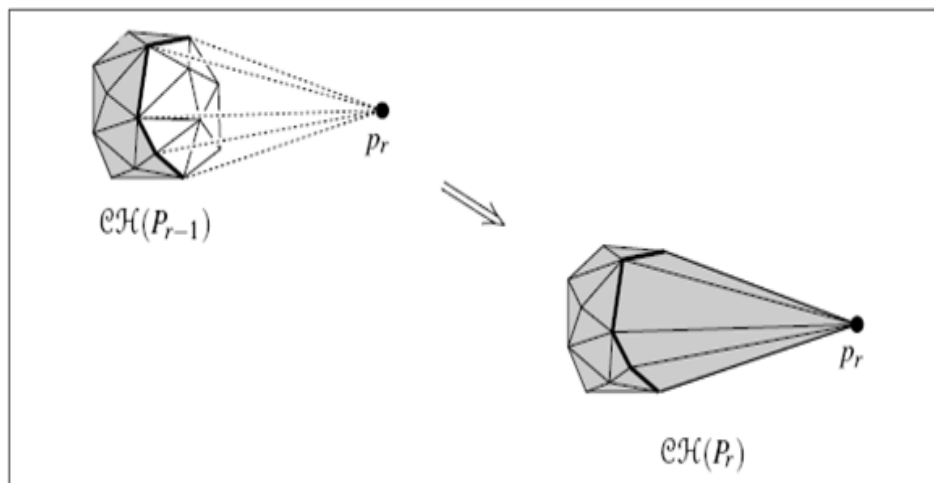


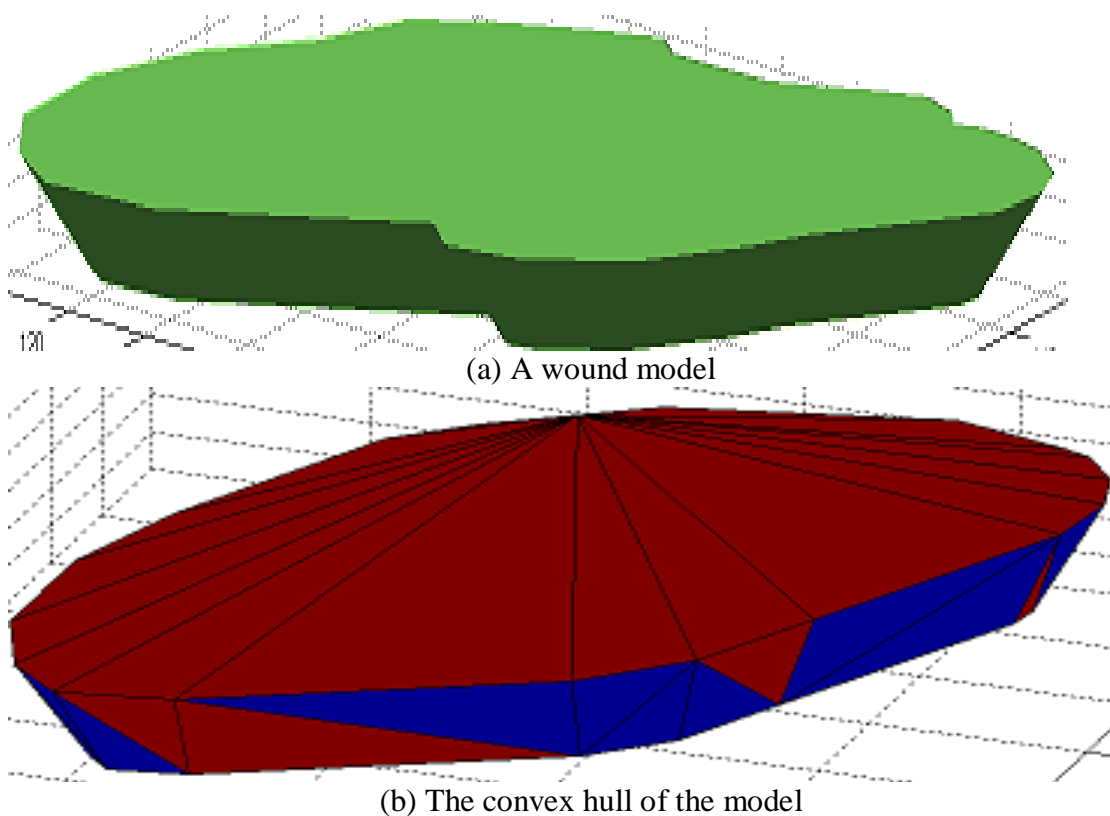
Figure 4.23: Adding a point to the convex hull [Berg *et al.* 2008]

There are 4 main algorithms for constructing the convex hull of a set of vertices. The results are identical with difference in algorithm execution time. The algorithms are incremental with complexity of $O(n \log n)$, gift wrapping with complexity $O(n^2)$, divide & conquer with complexity of $O(n \log n)$ and quickhull with complexity of $O(n \log n)$.

Convex hull in 3-Dimensional space are used in various application:

- (a) Speeding up collision detection in computer animation [Kumar & Yıldırım 2008].
- (b) Dividing huge models into smaller parts for the purpose of modification and processing results in pieces that are easy to process and aid in avoiding memory overflow [Lien & Amato 2008].
- (c) Other problems can be reduced to the convex hull. Examples are halfspace intersection, Delaunay triangulation and Voronoi diagrams [Barber *et al.* 1996].

Figure 4.24 shows the results of constructing solids from a model and a real scan using convex hull approximation. Figure 4.24(a) shows a wound model and Figure 4.24(b) shows its reconstructed solid using convex hull approximation. Figure 4.24(c) shows wound surface scan and Figure 4.24(d) shows its solid model created using convex hull approximation.



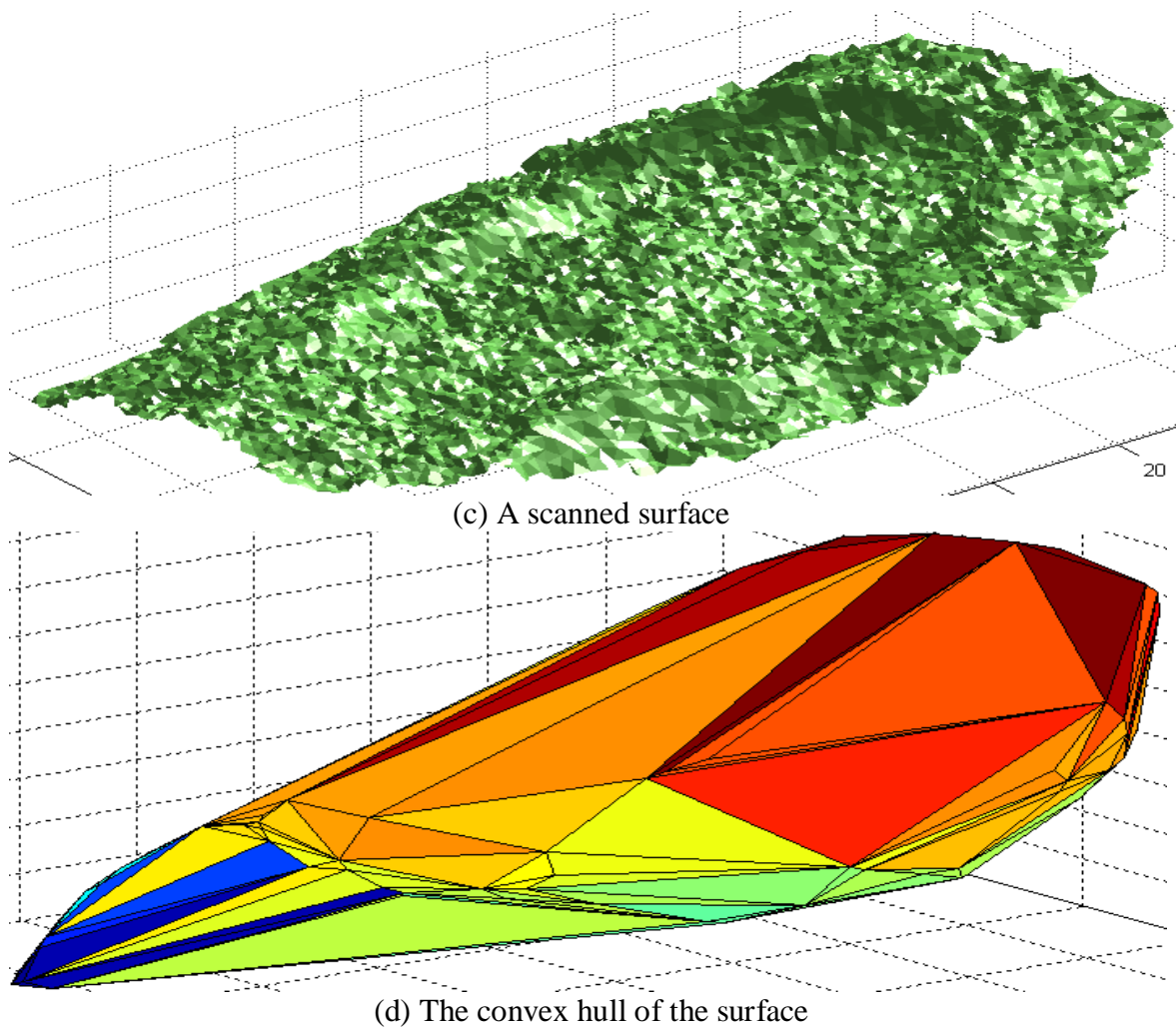


Figure 4.24: Convex hull solid reconstruction for a model and a skin surface

The solid reconstructed will be composed of set of tetrahedra as described which enclose all the vertices on the surface. The volume of the solid is equal to the summation of the volumes of all the tetrahedra composing the solid.

4.9 SURFACE DIVISION FOR MODELLING LEG CURVATURE

Based on the models shape, a specific surface fitting approach should be selected. Generation of surfaces always is starting from points and curves. Curves are generated from points and surfaces can be generated from curves [Hachenberger 2007]. There are several alternatives for creating a particular surface, surface can generated by using: (a) 4 corner points, (b) 2 or 3 boundary curves, (c) 4 boundary curves [Ralph *et al.* 2006].

Here, 2 boundary curves were found to be sufficient for representing approximately cylindrical shape body parts; specifically leg models. Dividing complicated shapes to a

number of convex pieces is a common practice when dealing with 3D objects [Hachenberger 2007]. Decomposition is a technique used to partition complex models into simpler components [Lien & Amato 2008]. The shape of the leg can be mimicked by a tabulated surface as seen in figure 4.25.

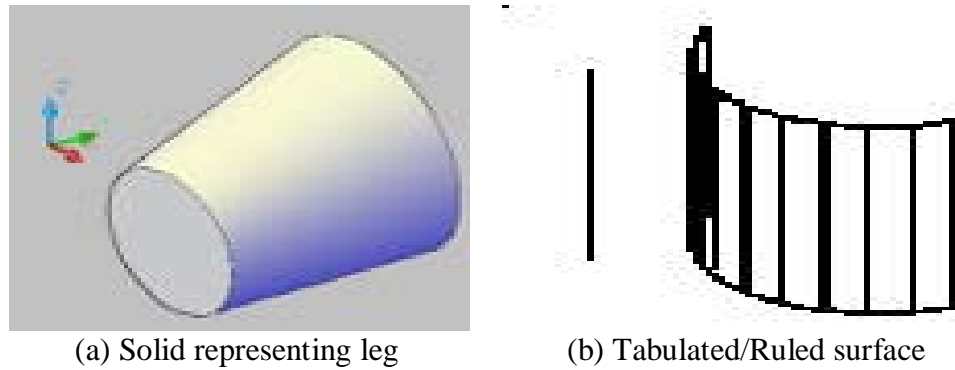


Figure 4.25: Tabulated surface reconstruction

Dividing wound surface along the leg length (creating equal distance parts) and constructing convex hull shapes (Delaunay tetrahedralization) from the divisions has been used for solid reconstruction. After reconstructing the convex pieces the complete model is reconstructed by applying union of the individual pieces as shown in Figure 4.26.

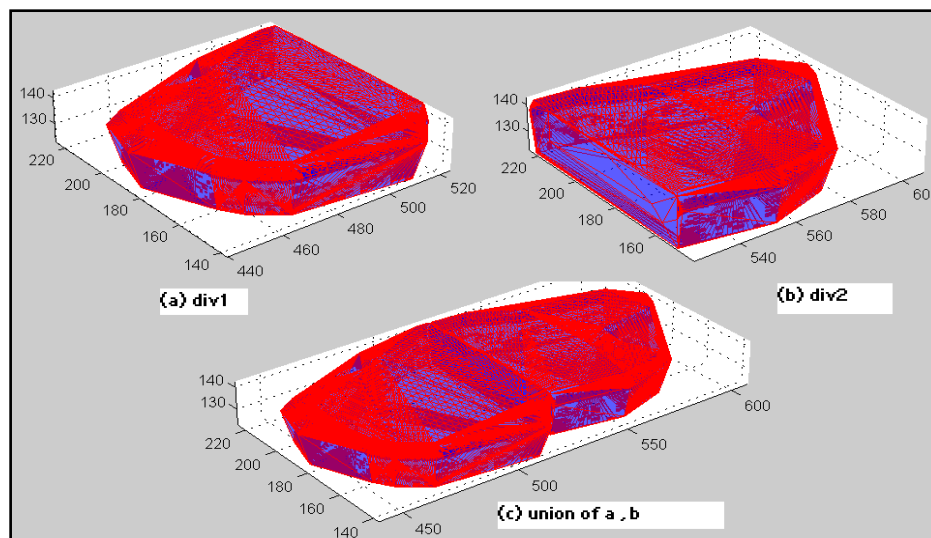


Figure 4.26: Constructing the model by performing division union

In order to reconstruct the wound model using surface division prior to convex hull approximation the Y-axis is aligned to the leg width. Surface division is performed by dividing the surface along the Y-axis into equal distance surfaces.

Applying surface division to ulcer scan for wound located at the leg prior to convex hull approximation can simulate the high curvature of the leg. Figure 4.27 shows the process of constructing wound solid from surface scan. Figure 4.27 (a) displays two views of a wound surface scan. In order to construct solid model the Y-axis is aligned to the direction of the leg width. Convex hull approximation preceded by surface division along the Y-axis to equal distance surfaces is shown in Figure 4.27(c). If the division is performed along the width, the result will not simulate the leg curvature as can be seen in Figure 4.27(b).

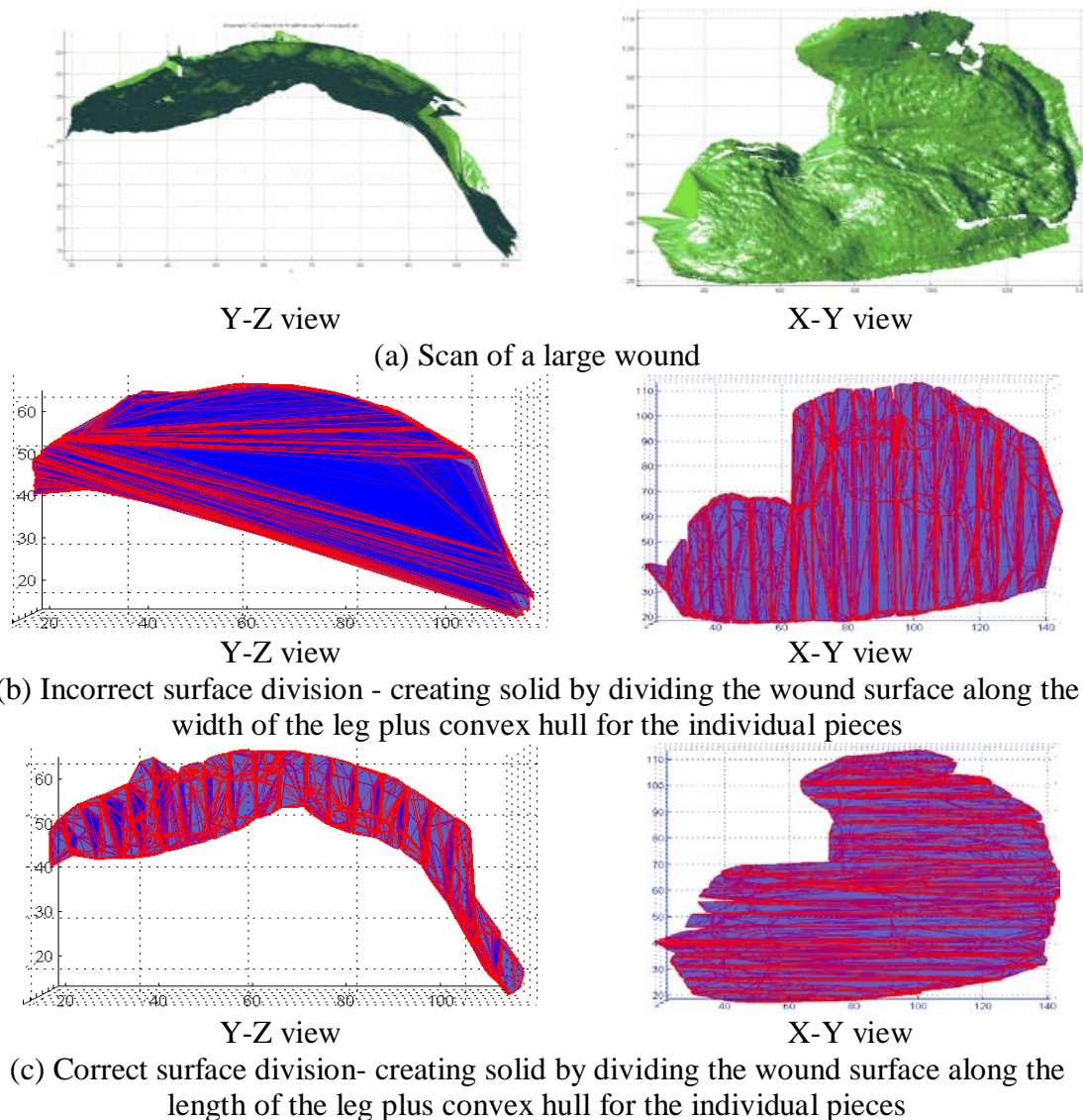


Figure 4.27: Constructing solids out of surfaces using surface division prior to convex hull approximation (Delaunay tetrahedralization)

The models are developed using AutoCAD. For 3D modelling, minimum number of vertices that can accurately represent the model is normally used. Large flat surfaces contain few vertices compared to areas with curvature in which larger number of vertices is used. For real surface scans, dense vertices will cover the surface with a distance between the points of about 0.1 mm [KONICA 2004]. The vertices are distributed equally throughout the surface regardless of the curvature.

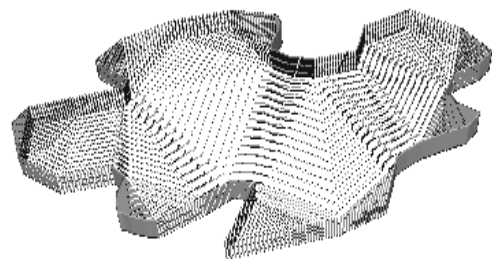
In order to perform surface division prior to convex hull approximation algorithm, the wound models should have dense vertices distributed equally around the surface to avoid gaps which will occur when using few number of vertices.

An option called subdivision surface in Rapidform is used to add more points to the surface. The subdivide operation improves the surface of the polygonal model by adding new vertices and adjust the existing vertices coordinates. Here no adjustment of the vertices coordinates is made because adjusting the vertices location will change the model volume. The operation produces three or four triangles for every original triangle resulting in a greater number of triangles in the surface [INUS 2005].

Two terms that sound similar but different in functionality are used in this work that is, subdivision surface and surface division/subdivision. Subdivision surface is a standard procedure used to generate more points for each triangle in the triangular mesh as shown in Figure 4.28. While surface division is used to describe the process of dividing the surface to a number of equal distances surfaces.



(a) Model m2a represented using
Vertices=2776
Faces=5548



(b) Model m2a represented
Vertices=19783
Faces=39562

Figure 4.28: Representing models using different point density

The flow chart of reconstructing wound models using surface division and convex hull approximation is as follows:

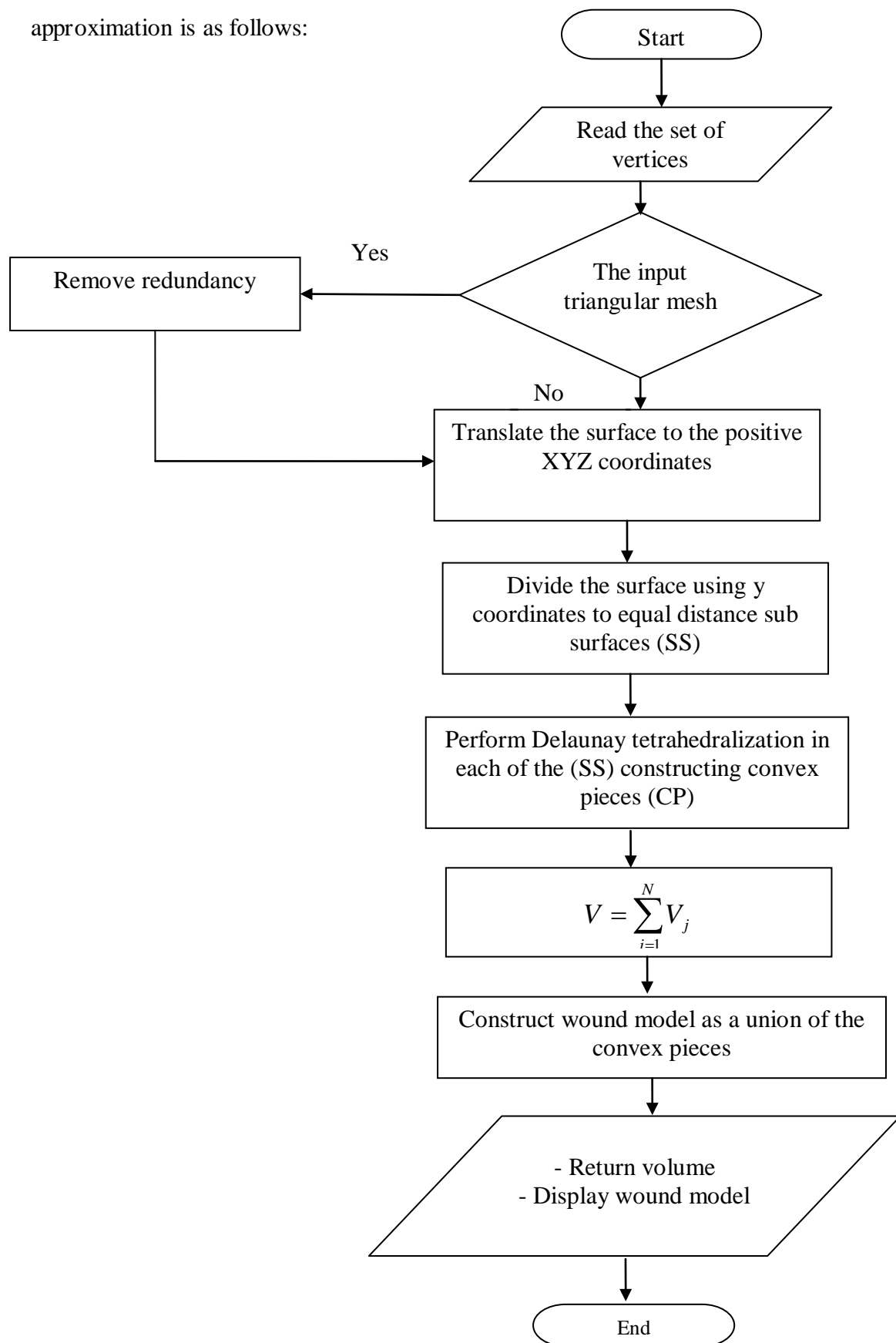


Figure 4.29: Flow diagram of convex hull reconstruction with surface division

The algorithm from the flow chart in Figure 4.29 is outlined as follows:

ALGORITHM: Modelling wound using convex hull approximation preceded by surface division

Input: dense point cloud covering the wound surface

Output: wound volume and the wound model

- 1- Translate the surface to the positive XYZ coordinates.
- 2- Find the range for Y axis values.
- 3- Use Y range to divide the surface to equal distance sections (sub surfaces **SS**).
- 4- Construct the convex hull (Delaunay tetrahedralization) for each of the SS. (Convex Pieces **CP**).
- 5- Compute the volume for each of the CPs as the summation of the tetrahedra volume, which compose the convex hull.
- 6- Concatenate the convex pieces together to obtain the complete wound model – CPs union (adding all the tetrahedra composing the CPs to one list and change the allocation table for the vertices).

4.10 VOLUME COMPUTATION FROM RECONSTRUCTED SOLIDS

When computing volume for solids, the shape is divided into extremely small elements (e.g. boxes, tetrahedra) and then their volumes are totalled to obtain the volume of the whole shape [Wilson 2001; Hoffmann 1989]. The result of solid reconstruction step using any of the two methods mentioned above yields a solid consisting of multiple tetrahedra. This way the volume of the wound can be easily computed.

In case of solids which consist of several tetrahedra, the volume of the model can be obtained by computing the volume for each tetrahedron and the volume of the complete model is computed by totalling the volume for all the tetrahedra in the model. This way the volume of the wound could be easily computed. A tetrahedron is a polyhedron composed of four triangular faces, three of which meet at each vertex. For a tetrahedron with vertices $P_1 = (x_1, y_1, z_1)$, $P_2 = (x_2, y_2, z_2)$, $P_3 = (x_3, y_3, z_3)$ and $P_4 = (x_4, y_4, z_4)$, the volume is given in Equation 4.3.

$$V_j = \left(\frac{1}{3!} \right) \begin{vmatrix} x_1 & y_1 & z_1 & 1 \\ x_2 & y_2 & z_2 & 1 \\ x_3 & y_3 & z_3 & 1 \\ x_4 & y_4 & z_4 & 1 \end{vmatrix} \quad \text{Eq. 4.3}$$

To compute the volume of the solid, the volumes for all the tetrahedra in the solid are summed as shown in Equation 4.4.

$$V = \sum_{j=1}^N V_j \quad , \text{ where } N \text{ is the number of tetrahedra.} \quad \text{Eq. 4.4}$$

4.11 VALIDATING THE PERFORMANCE OF SOLID RECONSTRUCTION ALGORITHMS USING SOLID MODELS

To validate the performance of solid reconstruction algorithm either visual inspection or numerical values can be used. The shape of the output can be visualized to investigate the correctness of the algorithm. However numerical values that can be obtained by comparing the reference volume obtained from the solid models and the volume of the reconstructed models is more objective. Reference volume can be obtained if only the input is a solid model, while for solid reconstruction algorithms the expected input is a surface.

The two algorithms for solid reconstruction must produce solid models given base, edge and top boundary information (wound surface scan).

The models described in section 4.4.2 are represented using complete boundary representation. The models' volumes are computed using AutoCAD software (reference volume). The reference volumes are used to validate the performance of the solid reconstruction algorithms.

The models represent different wounds shape by changing 3 parameters (wound boundary, wound edge and wound base). The top of the model is enclosed by a flat surface (coplanar) that:

1. Will not affect the solid reconstruction algorithm.
2. Make it possible to compute the reference volume accurately due to the complete boundary representation.

Having a coplanar top surface will not affect the performance of solid reconstruction and the reconstructed shape will be equivalent to creating a solid out of a surface similar to the model without top part. The two algorithms construct top surface as follows:

1. When constructing a convex hull out of a set of points, there is always a path between any pair of points (e.g. A & B) in the set which is contained in the convex hull. This process is shown in figure 4.30.



Figure 4.30: Solid reconstruction using convex hull approximation algorithm

2. When using midpoint projection, all the faces will be connected to the midpoint which is calculated or determined from a number of edge points resulting in a group of tetrahedra. If there is a face at the same level as the midpoint, no tetrahedron will be created. This process is shown in Figure 4.31.

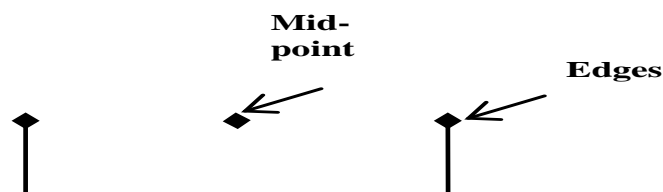


Figure 4.31: Solid reconstruction using midpoint algorithm

4.12 SUMMARY

In this chapter noninvasive algorithms for computing wound parameters (top area, true surface area, volume and average depth) are presented. The algorithms are based on 3D surface scans and the scanner used in this work is 3D laser scanner Konica Minolta. The scanner uses the triangulation concept in which the depth of large number of points located at the scanned surface is accurately obtained.

Wound attributes that describe the wounds are modelled based on real ulcer wound surface images. Wound models described in section 4.5 representing possible ulcer wounds are created using AutoCAD software, are used to investigate the performance of solid reconstruction methods.

The top area of the wound is calculated as the area of the polygon created by extracting the wound boundary and projecting it to the XY plane ($z=0$). In large wounds top area will not be accurate, thus the wound surface is divided to smaller surfaces and the top surface is measured for each section. This is overcome by decomposing the surface into 2 smaller surfaces so that the surface does not go beyond half of the leg circumference. In addition, surface transformation is required if the wound surface is not parallel to the XY plane.

True surface area is obtained directly from the meshed surface. The area of all the triangles constructing the surface that is impeded in 3D space is computed and totalled to obtain the true surface area as such computing true surface area is not affected by surface alignment and the size of the wound.

In this work a method called midpoint projection has been developed to reconstruct solids from surfaces. In addition the convex hull approximation is investigated. These methods do not require large area around the wound for surface interpolation. Thus these methods are not affected by the irregularities (swelling and scales) in the surrounding skin surface. The volume is computed from scattered data to handle depressed edges.

In the developed midpoint projection method, a solid is reconstructed from surface scans in which a point at the top missing surface is calculated by averaging several points selected at the wound boundary and then all the triangles composing the surface is projected to the midpoint composing several tetrahedra shapes. In the convex hull

approximation (Delaunay tetrahedralization) all the vertices composing the wound surface is enclosed inside the nearest convex shape. In this work, the convex hull method is improved by performing surface division along the length prior to convex hull approximation to handle large leg curvature. Both algorithms produce solid shape composed of several tetrahedra; the volume of the solid shape is computed by totalling the volume of all the tetrahedra in the shape.

The average depth of a wound is computed by dividing wound volume by top area.

CHAPTER 5: RESULTS AND ANALYSIS

Volume computation results on the wound models using midpoint projection and convex hull approximation are discussed in section 5.1. Enhancement on the performance of convex hull approximation by applying surface division prior to approximation is presented in section 5.2. Sections 5.3 and 5.4 present the volume computation results on real wound scans. The performance of the algorithms in assessing wound parameters (top area, true surface area and volume) is compared against measurements obtained using invasive methods for two moulded wound surfaces.

5.1 SIMULATION RESULTS OF VOLUME COMPUTATION

This section demonstrates the results of volume computation using midpoint projection (refer to Section 4.7) and convex hull approximation (Delaunay tetrahedralization, refer to Section 4.8) methods for solid reconstruction on wound models. Table 5.1 lists the simulation results for volume computation using the two algorithms on the 18 wound models described in Section 4.5 in table 4.2. The error in volume computation is measured against the reference volume (calculated using AutoCAD).

The percentage error is computed as

$$\%Error = \frac{CalculatedVolume - V_{ref}}{V_{ref}} \times 100\% \quad \text{Eq. 5.1}$$

, where *CalculatedVolume* is the volume obtained using midpoint projection and convex hull approximation method for solid reconstruction and volume computation, *V_{ref}* is the reference volume obtained using AutoCAD.

Table 5.1: The results of volume computation using midpoint projection and convex hull approximation

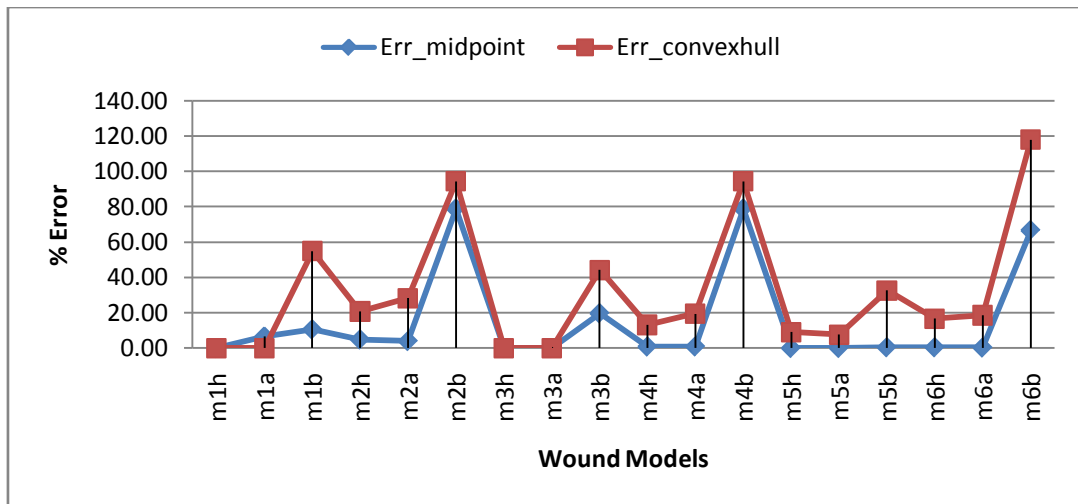
N o	Edge Descri- ptor	Wound Models *	V_{ref} The volume calculated using AutoCAD (mm³)	$V_{midpoint}$ The volume computed using midpoint projection (mm³)	$V_{convexhull}$ The volume computed using convex hull approximation (mm³)	<u>Err_{midpoi}</u> The percentage error using midpoint (%)	<u>Err_{convex}</u> The percentage error using convex hull (%)
1	Chopped	m1h	131054	131054	131054	0.00	0.00
2		m1a	177545	189135	177737	6.53	0.11
3		m1b	84564	93468	131054	10.53	54.98
4		m2h	142757	149621	172477	4.81	20.82
5		m2a	251651	261515	322806	3.92	28.28
6		m2b	112818	201835	219449	78.90	94.52
7	Sloped	m3h	208306	208306	208306	0.00	0.00
8		m3a	130308	130308	130436	0.00	0.10
9		m3b	69079	82683	99671	19.69	44.29
10		m4h	147426	148604	166881	0.80	13.20
11		m4a	268561	270867	320833	0.86	19.46
12		m4b	112818	201835	219450	78.90	94.52
13	Punched	m5h	59108	59108	64458	0.00	9.05
14		m5a	70867	70867	76291	0.00	7.65
15		m5b	48591	48778	64459	0.38	32.66
16		m6h	181506	182171	211754	0.37	16.67
17		m6a	262002	262580	310845	0.22	18.64
18		m6b	97109	161835	211754	66.65	118.06

* Model m#h/a/b:

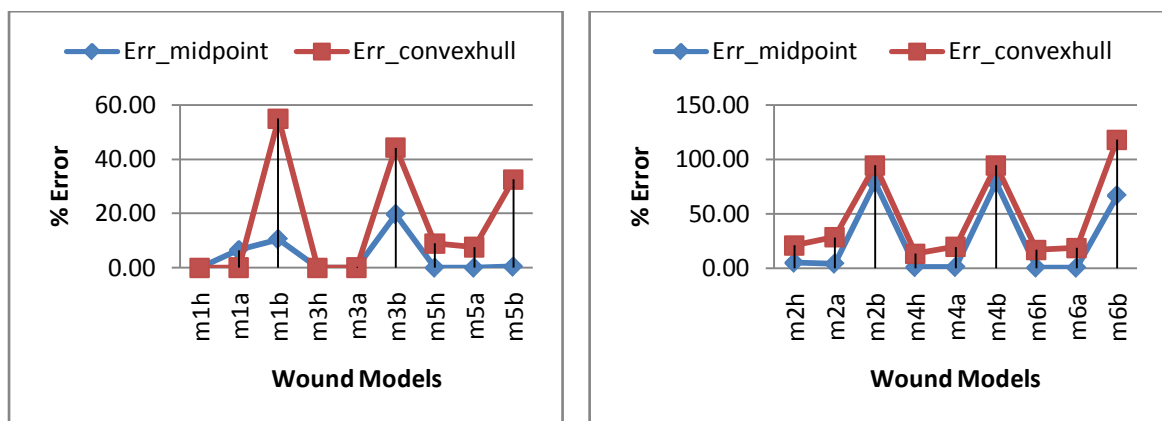
Odd number models - regular boundary models, even number - irregular boundary models.

'h' - homogeneous base models, 'a' - depressed base models and 'b' - elevated base models.

Figure 5.1 shows the percentage errors when using midpoint and convex hull approximation (Delaunay tetrahedralization) for volume computation for all wound models. Figure 5.1 (b) lists the percentage errors for regular boundary errors and Figure 5.1 (c) shows irregular boundary models.



(a) Percentage errors of volume computation



(b) Regular boundary wound models

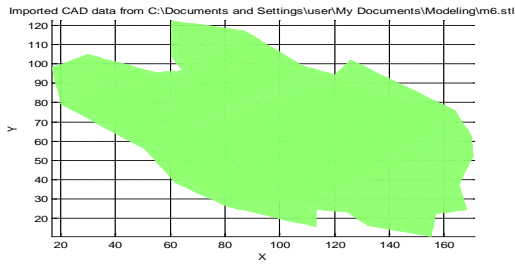
(c) Irregular wound boundary models

Figure 5.1: Percentage errors of volume computation using midpoint projection and convex hull approximation

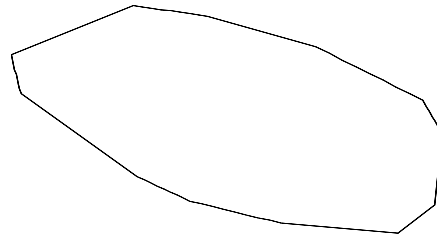
From Figure 5.1 (a), the error for midpoint method 0.0% - 78.9% and for convex hull 0.0% - 118.1%. From Figure 5.1(b) regular boundary models error for midpoint method 0.0% - 19.7%, and convex hull 0.0% - 55.0%. From Figure 5.1 (c) irregular boundary models error for midpoint method 0.2% - 78.9%, and using convex hull the error ranges 13.2% - 118.1%.

From the results it can be seen that:

- a. For convex hull approximation, regular boundary models produce less error compared to irregular boundary models. In the method, a solid model (whether a convex hull or not) as shown in Figure 5.2 (a) is made a convex hull by enclosing the vertices within a regular shape, cancelling any irregularity in the shape as shown in Figure 5.2 (b). This larger approximation of the shape produces an overestimation in volume.



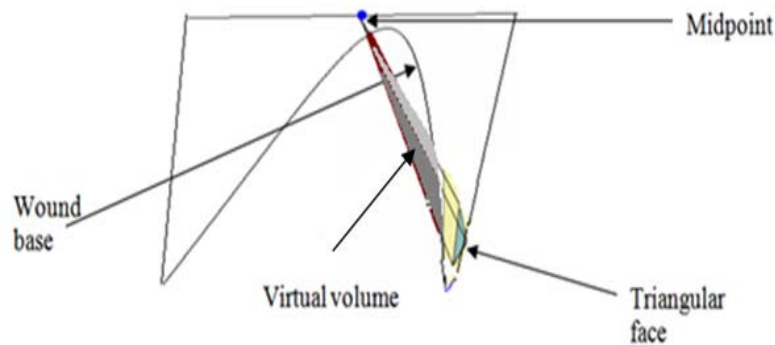
(a) Example of a 2D shape



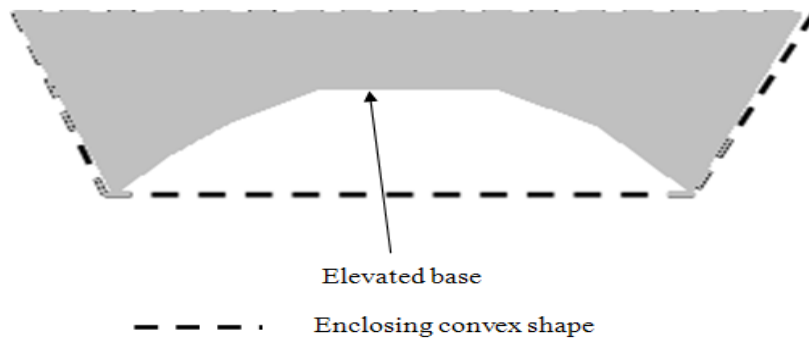
(b) The convex hull of (a) wrapping the irregularities into nearest convex polygon shape

Figure 5.2: The top view of a model and its convex hull approximation

- b. For regular and irregular boundary models, models with elevated base produce larger errors for both algorithms. From Figure 5.1(a), both algorithms produce overestimation in the case of elevated base models. In midpoint projection method, the inclusion of virtual volume from faces those are not visible to the midpoint as shown in Figure 5.3 (a), results in overestimation. In the case of convex hull approximation, any elevation at the base will be enclosed in a regular shape as shown in Figure 5.3 (b) resulting in overestimation.



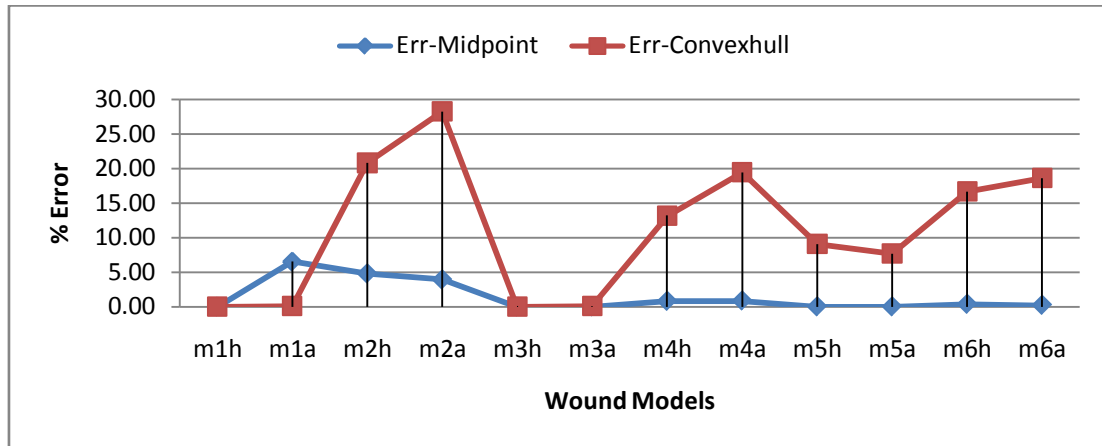
(a) Invisible faces to midpoint resulting in inclusion of virtual volumes



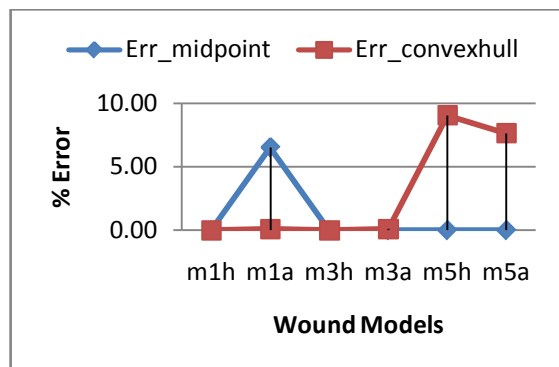
(b) A cross section of a model and its convex hull shape

Figure 5.3: The effect of base elevation on solid reconstruction algorithms

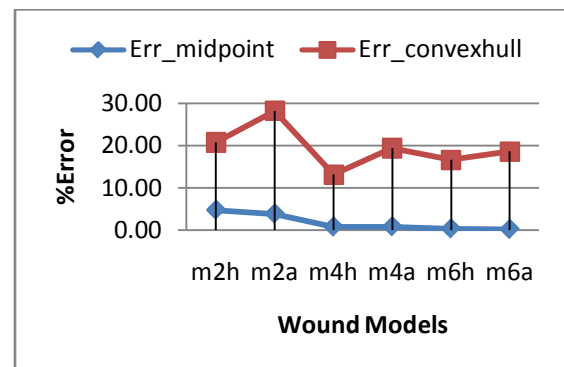
Figure 5.4 (a) shows the percentage errors when using midpoint and convex hull approximation (Delaunay tetrahedralization) for volume computation for all wound models excluding elevated base wound models. Figure 5.4 (b) lists the percentage errors for regular boundary errors and Figure 5.4 (c) shows the percentage error for irregular boundary models.



(a) Percentage errors of volume computation



(b) Regular boundary wound models



(c) Irregular wound boundary models

Figure 5.4: Percentage errors of volume computation excluding elevated base wound models




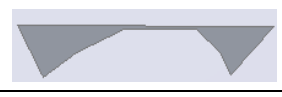
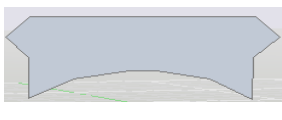

From Figure 5.4 (a), the error for midpoint method ranges from 0.0% - 6.5% and for convex hull from 0.0% - 28.2%. From Figure 5.4(b), the error for regular boundary models in the case of midpoint method ranges from 0% - 6.5%, and in the case of convex hull from 0% - 7.7%. From Figure 5.4 (c), the error for irregular boundary models in the case of midpoint method ranges from 0.2% - 4.8%, and in the case of convex hull the error ranges 13.2% - 28.2%.

As expected, convex hull approximation gives less error in case of regular boundary models compared to irregular boundary models. The reasons are the same, as discussed above in case (a).

Generally, midpoint projection method outperforms convex hull approximation (Delaunay tetrahedralization) method for volume computation. The reason is that irregular boundary does not affect the performance of midpoint projection method.

Table 5.2 displays the cross sections of the elevated base models with the percentage errors, Err_midpoint and Err_convexhull, due to midpoint and convexhull methods respectively.

Table 5.2: The effect of base elevation on volume computation

Model #	Model Cross Section	Err_midpoint	Err_convexhull
m1b		10.5	51.1
m2b		78.9	81.3
m3b		19.7	39.8
m4b		78.9	81.1
m5b		0.4	24.8
m6b		66.7	99.9

From Table 5.2, for midpoint method it can be seen that the error increases if the distance between the base and the midpoint decreases. For example, smaller error is obtained for m5b representing deep wound while higher error is introduced for m4b representing shallow wounds. Similarly for convex hull method but the error is higher for irregular boundary models due to vertices being enclosed in a regular shape. In the case of midpoint, the elevated base will cause occlusion of faces at the edges resulting in the inclusion of virtual volume as shown in figure 5.3(a).

From observations, base elevation in the wound is due to curvature in the limb (called global curvature) or irregularity at the wound bed (called local curvature).

For the local curvature case, irregularities at the wound bed do not affect the wound edge location. The base elevation from the models shown in Table 5.2 represents only the local curvature case. In the global curvature case, base elevation is also accompanied by changes in the wound edge location.

‘Global’ curvature here refers to limb curvature. For the leg case, the leg is having high curvature along the leg width. The ‘local’ curvature refers to sudden changes at the wound base can be seen when a cross section along the leg length is taken. Figure 5.5 display the two types of curvatures. The dashed line shows a cross section across the length representing local curvature and the cross section across the leg width shows global curvature.

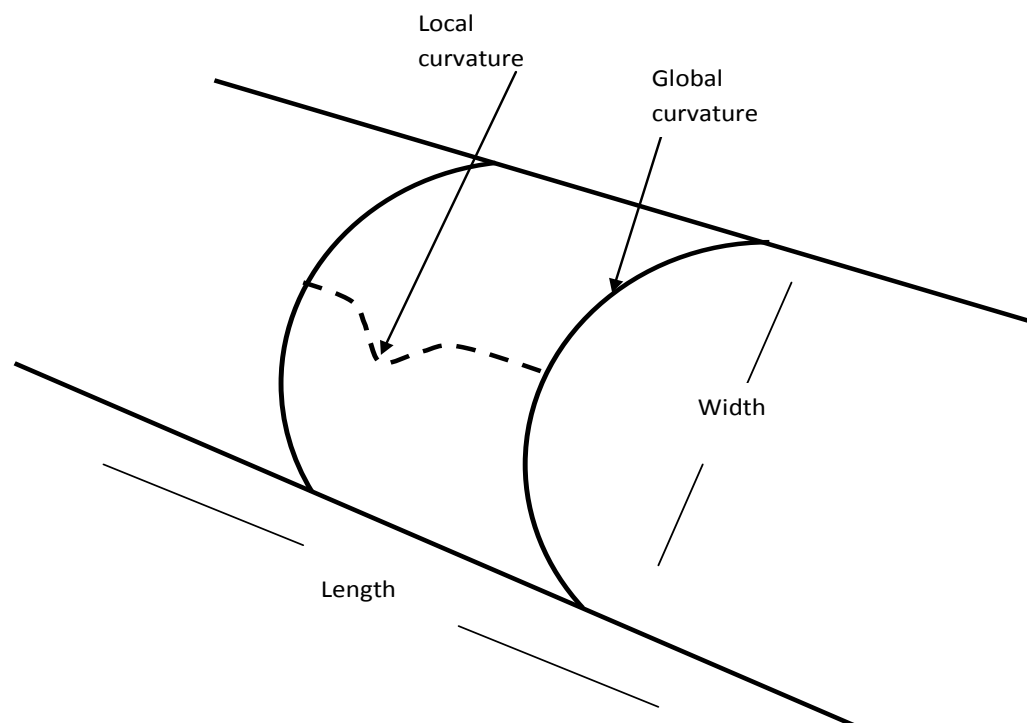


Figure 5.5: Elevation at the wound base

For the midpoint method both types of elevations produce errors with the increase in the degree of elevation. The midpoint projection produces a smaller error if the elevation is not high compared to the midpoint. In general, local curvature does not produce high error compared to global curvature due to the elevation size compared to the wound size. The effect is more prominent in the case of global curvature because the global curvature

is accompanied by changes in the edges locations which will affect the position of midpoint itself. As such, solids reconstructed using midpoint projection method will not be able to model wounds that span over a large area with high curvature.

5.2 SURFACE DIVISION PRIOR TO CONVEX HULL APPROXIMATION (Delaunay tetrahedralization)

From the previous section, it is clear that when using convex hull method two parameters affect the performance (overestimation in volume) of the algorithm namely irregular boundary and elevation at the base. The elevation at the base is normally due to limb curvature (global) and/or irregularity at the base (local).

In order to overcome the above problems, the surface is divided into equal distance surfaces. This is done so that the high curvature of the leg and irregularity at the boundary can be represented using a number of linear segments. Convex hull approximation (Delaunay tetrahedralization) is then applied for the vertices within the sub surfaces.

Figure 5.6 gives the simulation results of volume computation using convex hull and convex hull with surface divisions of 2, 5, 10 and 20 sections.

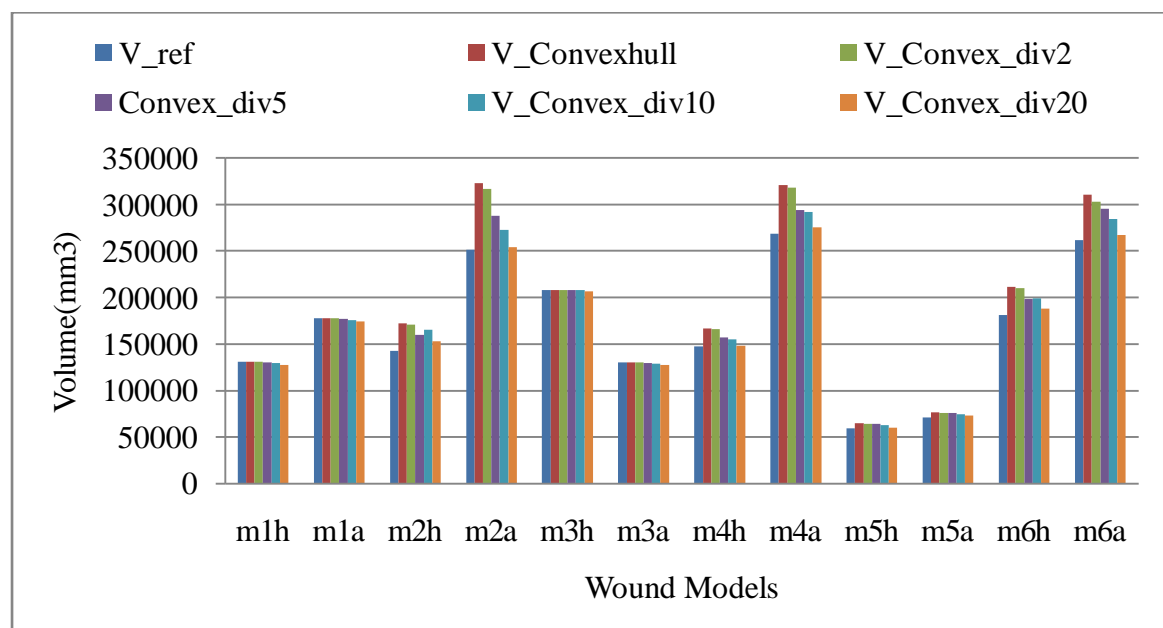


Figure 5.6: Results of volume computation using convex hull and convex hull with 2,5,10 and 20 divisions

Figure 5.7 shows the percentage error in volume computation using midpoint, convex hull, convex hull with 2, 5, 10 and 20 surface divisions in the wound models.

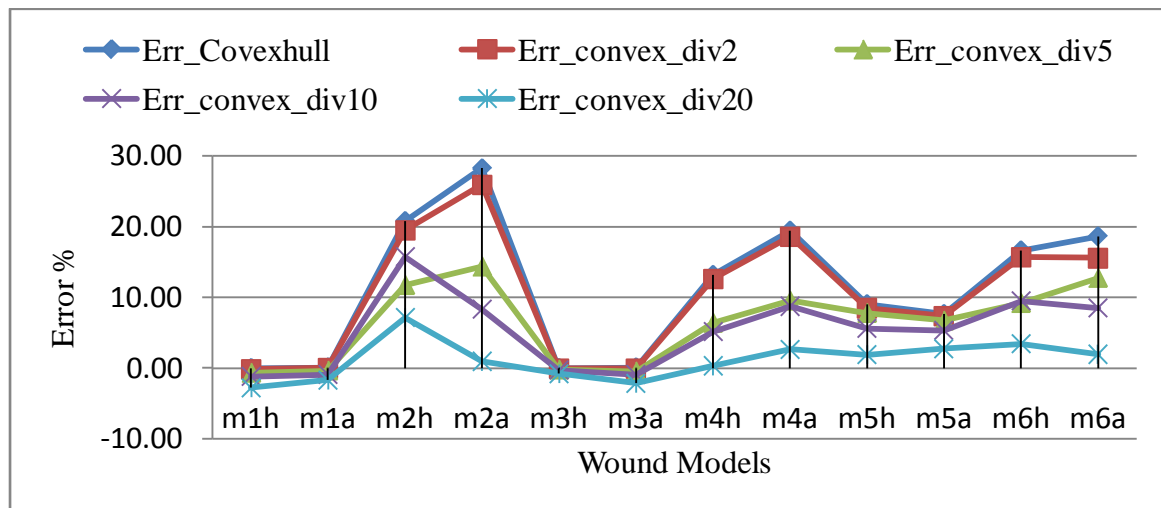


Figure 5.7: Percentage error in volume computation using convex hull, convex hull with 2,5,10 and 20 divisions

From Figure 5.7 (a), the percentage error in volume computation when using convex hull approximation in all the models excluding models with elevated base ranges (0- 28.2) and when using surface division of 20 sections prior to convex hull approximation the error ranges (-2.7 – 7.2).

It is clearly seen that errors in volume computation are reduced with the increase in surface divisions.

The following Figures 5.8 - 5.11 displays the top-view of four models and the reconstructed models using convex hull and convex hull preceded by 20 divisions. Figure 5.8 displays a regular boundary model. Figures 5.9-5.11 provide three irregular boundary models and their reconstructed solids.

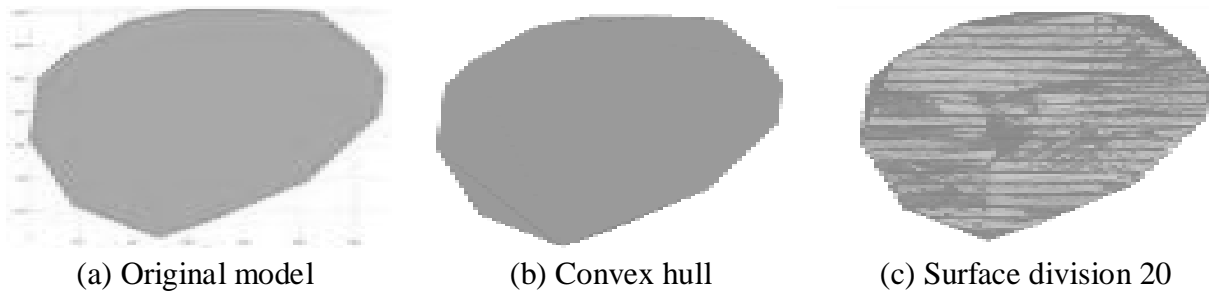


Figure 5.8: Solid Reconstructionf for regular boundary model(m1h)

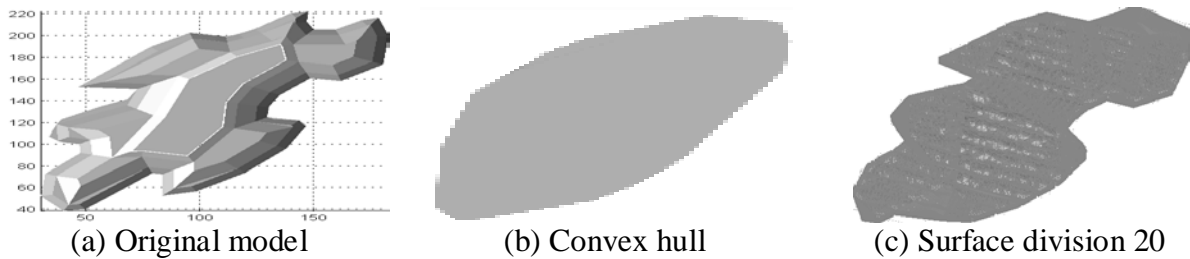


Figure 5.9: Solid Reconstruction for irregular boundary model (m2h)

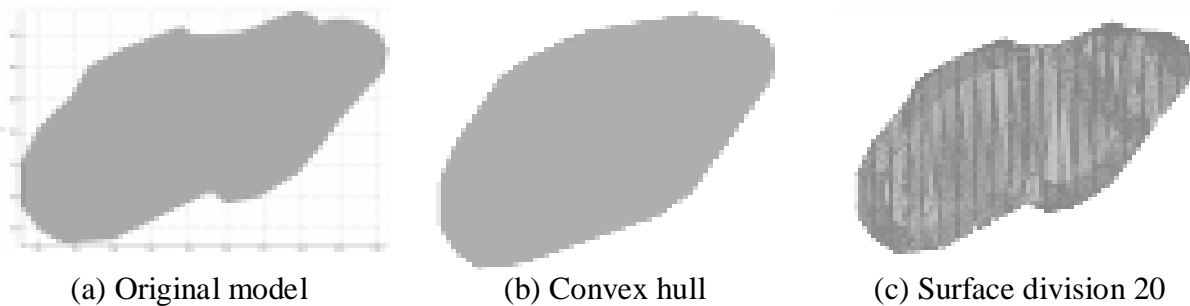


Figure 5.10: Solid Reconstruction for irregular boundary model (m4h)

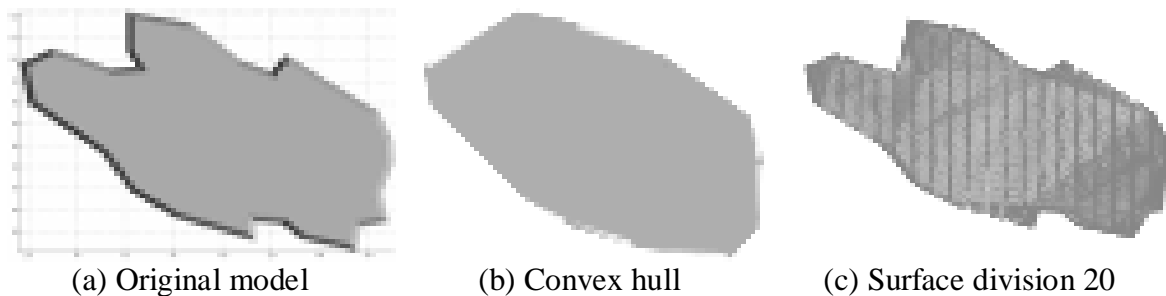


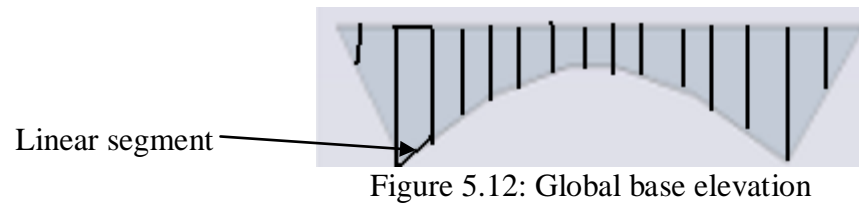
Figure 5.11: Solid Reconstruction for irregular boundary model (m6h)

With the increase in surface division, the shape of the reconstructed irregular boundary models will be closer to the original model as can be seen from Figure 5.9, Figure 5.10 and Figure 5.11. There is no effect of surface division in the performance of solid reconstruction on regular boundary models as can be seen in Figure 5.8.

Surface division prior to convex hull approximation can simulate wound shapes with ‘*global*’ curvature while for wounds with ‘*local*’ curvature there will still be overestimation. In cases of wounds that span large area with high curvature, the effect of global curvature on the calculation is high compared to local curvature since it does not extend through the whole wound base. While the effect of local curvature in volume computation could be significant in cases of small wounds.

Global curvature of the leg can be mimicked by applying surface division on the scanned surface in the direction of the leg width prior to convex hull approximation. When using

surface division prior to convex hull approximation the base shape will not be as dents that is wrapped to construct the convex hull shape. The small sections representing the elevation appear as small linear segments as shown in Figure 5.12. Division is only applicable if there is parallel edge size on top of the wound.



As shown in section 4.9 convex hull preceded by surface division can better estimate volume of cylindrical shape models. Thus, it can produce shapes that are having curvature along the width and no curvature along the length. For this reason, the convex hull with division can handle global curvature. The effectiveness of the reconstruction algorithm on wounds with global curvature is evaluated visually. Figure 5.13 shows the results of solid reconstruction with 20 divisions prior to convex hull approximation in real wound surface scans.

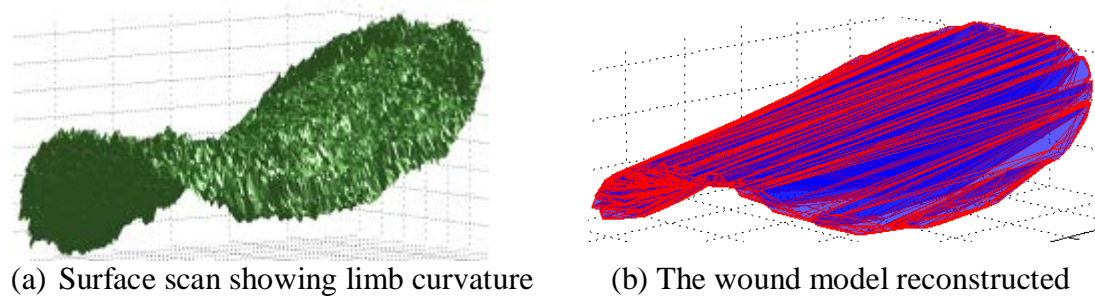


Figure 5.13: The results of solid reconstruction for a large wound

Surface division gives results that are more accurate in volume computation and reduces errors that occur due to irregular boundaries and global curvature. Underestimation of volume can happen with the increase of the division since the vertices covering the models might not be dense enough. Thus, the number of divisions should be selected according to the size and point density of the model.

5.3 MEASUREMENTS on REAL WOUNDS SCANS

In this section, the 22 wounds scans obtained from HKL are measured using the algorithms for calculating top are, true surface area, average depth and volume using both algorithms (midpoint and convex hull preceded by surface division).

Table 5.3 lists the different ulcer wound scans taken from 9 patients in four visits.

Table 5.3: The measurement of the DB wounds scans

Ulcer #	Patient # - (visit-patient-ulcer)	X-range mm	Y-range Mm	Z-range mm
1	Patient1 (Visit1-patient1)	140	110	50
2	Patient 2 (Visit1-patient2)	40	35	30
3	Patient 3(Visit1-patient3- ulcer1)	45	20	20
4	Patient 3(Visit1-patient3-ulcer2)	10	15	8
5	Patient 1 (Visit2-patient1)	120	110	50
6	Patient 4(Visit3- patient1-ulcer1)	30	20	3
7	Patient 4(Visit3- patient1-ulcer 2)	25	10	5
8	Patient 5(Visit3-patient2)	23	20	7
9	Patient 6(Visit3- patient3-ulcer1)	40	43	6
10	Patient 6(Visit3- patient3-ulcer2)	12	18	2
11	Patient 6(Visit3- patient3-ulcer3)	23	23	3
12	Patient 6(Visit3- patient3-ulcer4)	40	30	2
13	Patient 6(Visit3- patient3-ulcer6)	17	9	1
14	Patient 7(Visit3-patient4)	50	65	15
15	Patient 8(Visit4-patient1-ulcer1)	35	25	4
16	Patient 8(Visit4-patient1-ulcer2)	25	65	10
17	Patient 8(Visit4-patient1-ulcer3)	17	17	4
18	Patient 9(visit 4-patient2-rightleglarge)	100	60	35
19	Patient 9 (visit4-patient2-heel)	25	25	10
20	Patient 9 (visit4-patient2-left_foot)	50	85	53
21	Patient 9(visit 4-patient2-left_leg)	50	85	25
22	Patient 9(visit4-patient2-right_foot)	70	60	20

The wound scans has a range of sizes. In the table *X*, *Y* and *Z-range*, represent the range of each of the coordinates. For example, *X-range* is the difference between the minimum and maximum *X* coordinate values of the vertices at the surface.

According to classification by NHS [1997], large wound are described as the wounds having area $> 10\text{cm}^2$ and small wounds are having area $< 10\text{cm}^2$. When approximating the area as $X\text{-range} \times Y\text{-range}$, 11 of the ulcer scans can be considered large wounds while the other 11 represent small wounds.

Another way of sorting the ulcer wounds listed in Tables 5.3 is as follows:

- a. Large wound that spans more than half the leg circumference (ulcer 18).
- b. Large and deep (ulcers 1 and 5).
- c. Large and shallow wounds (ulcers 14,16, 20, 21 and 22).
- d. Ulcer wounds that is having Y-range (20-50) mm (ulcers 2, 3, 6, 8, 9, 11, 12, 15 and 19).
- e. Small ulcers with Y-range less than 20 mm (ulcers 4, 7, 10, 13 and 17).

To evaluate the effectiveness of the model reconstruction algorithms, both visual and numerical comparisons are used. For real wounds surface scans, however, most of the time visual comparisons can be done. This is because the reference volume required for evaluation is difficult to obtain. Invasive methods for computing wound volume can cause pain and infections. Table 5.4 lists the volume computation results on real wound scans.

In Table 5.4 Depth_{mid} is computed by dividing V_{midpoint}/top area and Depth_{convex} is computed by dividing V_{convexhull}/top area. The percentage difference between the two methods is obtained using the equation:

$$\% Diff = \frac{|V_{midpoint} - V_{convexhull}|}{|(V_{midpoint} + V_{convexhull}) / 2|} \times 100\% \quad \text{Eq. 5.2}$$

Table 5.4: The top are, true surface area, average depth and volume results obtained by applying the algorithms on real wound scans

Ulcer #	Y-range (mm)	Top Area (mm ²)	True Surface area (mm ²)	Depth-mid (mm)	Depth-convex (mm)	V-Midpoint (mm ³)	V-Convexhull (mm ³)	% diff
1	110	3908	9330	13.5	16.8	52524	65838	22
2	35	824	973	6.8	2.1	5623	1768	104
3	20	169	834	14	11.6	2354	1964	18
4	15	266	526	2	2	527	534	1
5	110	2614	12830	33.2	40.5	86791	105990	20
6	20	314	632	3	3	929	927	0
7	10	347	388	1.6	1.2	552	426	26
8	20	272	406	6.2	5.4	1675	1478	12
9	43	966	1393	1.7	3.0	1675	2939	55
10	18	116	194	0.8	1.7	97	198	68
11	23	326	474	1.6	2.4	527	769	37
12	30	585	794	1.4	1.5	847	877	3
13	9	272	406	2.9	2.5	795	678	16
14	65	1795	3144	5.5	5.1	9803	9227	6

Ulcer #	Y-range (mm)	Top Area (mm ²)	True Surface area (mm ²)	Depth-mid (mm)	Depth-convex (mm)	V-Midpoint (mm ³)	V-Convexhull (mm ³)	% diff
15	25	597	736	1.8	1.9	1051	1126	7
16	65	793	1290	3.1	1.6	2535	1264	67
17	17	118	168	1.5	1.5	176	171	3
18	60	946	8318	-	24.7	Not-applicable	23394	
		5774	8318	-	3.4		19538	
19	25	263	581	3.9	4	1034	1060	2
20	85	1140	3744	18.7	6.9	21403	7878	92
21	85	2514	3994	5.2	4.3	12996	10744	19
22	60	1522	3486	5.6	4.5	8505	6907	21

(a) In ulcer 18, the wound spans more than half of the patient's leg. Midpoint projection for solid reconstruction is not suitable because the midpoint will lie below some of the scanned surface faces. As discussed in section 4.3, it is not possible to have one correct z alignment for the whole surface when obtaining the volume for very large wound that span more than half of the leg circumference. In this case, the wound surface is divided into 2 surfaces along the y-axis as in Figure 5.14 (a) and the new surfaces are aligned. The results of calculating the wound volume as one surface and dividing it into 2 surfaces are given in Table 5.4 (ulcer 18).

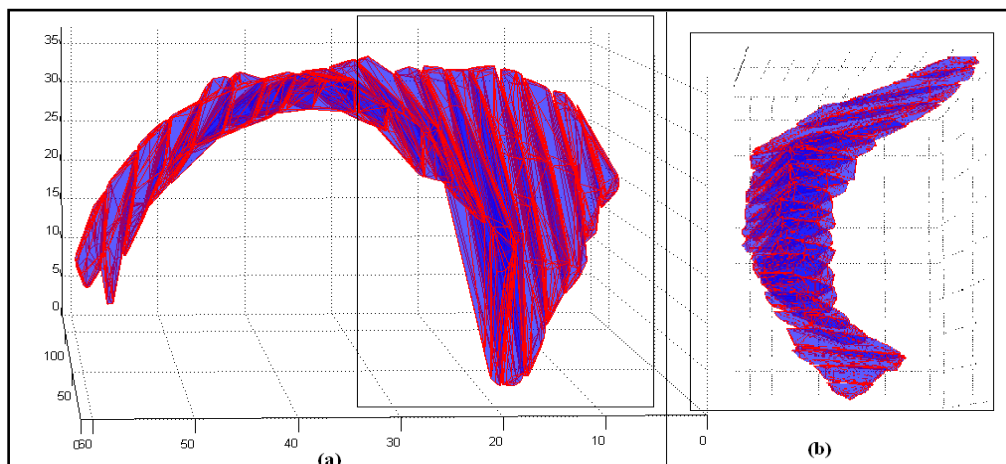


Figure 5.14: Large wound model reconstruction (Ulcer 18)

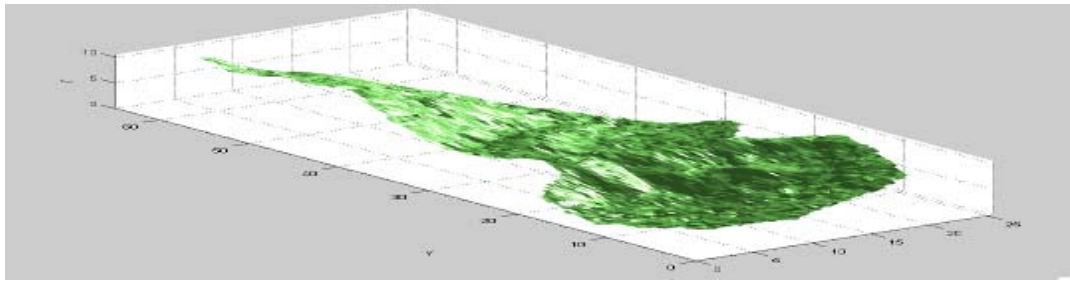
From the top area results of ulcer 18 it is seen that the high curvature of the surface will reduce the projected area. Dividing the surface and applying the transformation on the surface will solve the problem. The results show that volume computation for the complete surface without dividing the surface to two parts and aligning those parts produces overestimation. The overestimation in

large wounds happens because of the orientation of the surface vertices. The convex hull with division might include sub surfaces in different locations of the leg up and down.

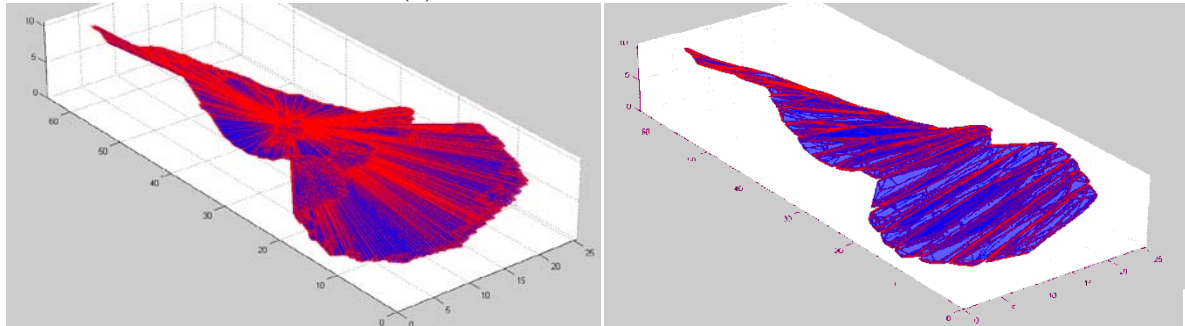
- (b) From Table 5.4, ‘ulcer 1’ and ‘ulcer 5’ represent two scans of the same large wound in two assessment sessions. There was a three weeks interval between the first and second scan. The doctor’s observation on the wound is that regression had happened and the wound is growing larger. Using the midpoint the difference between the volumes of the two surfaces recorded at the two sessions was 13314 mm^3 and when using the convex hull with division algorithm the difference was 19199 mm^3 . Both algorithms show that there was an increase in the wound size (regression). The parameters measured showed that there is an increment in surface area and wound volume using both methods. For top area, there was a decrement in the area size because the wound covers high curvature area that made the wound boundary to project smaller boundary as explained in section 5.2.1.
- (c) In case of shallow wounds that extend a large area, midpoint projection produces overestimation because in case of shallow wounds, inclusion of large volume occurs when projecting the farthest faces at the surface to the midpoint. Figure 5.15(a) displays a picture of two ulcer wounds located at the leg, Figure 5.15(b) shows the surface scan of the wound labeled 1 on Figure 5.15(a). Figure 5.15(c) and 5.15(d) displays the reconstructed wound models out of the surface scans in Figure 5.15(b) using both algorithms. The model reconstructed in Figure 5.15(c) yield overestimation. From the table, the case in which the ulcer wound spans a wide area along the width of the leg and having a shallow depth is found in Ulcers (14, 16, 20, 21 and 22).



(a) Irregular boundary and shallow wounds



(b) Surface scan of wound 1



(c) Reconstruction using midpoint; volume= 2535 mm³ (d) Reconstruction using convex hull; volume= 1264 mm³

Figure 5.15: Wound model reconstructed from wound surface (Ulcer 16)

(d) Both methods can be used for the ulcer cases that are having a Y -range between 20 - 50 mm and depth ≥ 3 mm; this can be seen in ulcers 6, 8 and 19, results which have a percentage difference of 0, 12 and 2 respectively. For ulcers with the same Y -range and having depth < 3 mm (shallow), convex hull preceded by surface division is preferable. These are ulcers 2, 3, 11, 12 and 16. The percentage difference was (55 %) in case of 'ulcer 9'; convex hull was not suitable since the wound is having overgranulation (in which the tissue at the wound bed grow above the level of the missing top healthy skin) is shown in Figure 5.15.



Figure 5.16: Foot ulcers (Ulcer 9)

(e) When using convex hull method, surface division is not necessary for wounds with a Y -range less than 20mm. As discussed in section 4.8, it is expected that

convex hull with 5 surface divisions produces under estimation while midpoint projection gives more accurate results in this case (ulcers 4, 7, 10,13 and 17).

The following are observations on the performance of the algorithms on different wound surfaces located at the leg.

1. Generally, there is a difference in the volume results obtained by the two algorithms.
2. If a wound has large area it does not necessarily means that it spans high curvature side. Y -range that determines the width of the wound has a bigger effect compared to the X -range that determines the length of the wound as shown in Figure 5.17. Figure 5.17 (a) displays schematic figure of a wound having large area due to large X -range. Figure 5.17 (b) displays a wound having large area due to large Y -range. If the large area is due to the large Y -range this might indicate that midpoint is not suitable for the calculation. If the large area is due to big X -range this might indicate that both algorithm might be suitable.

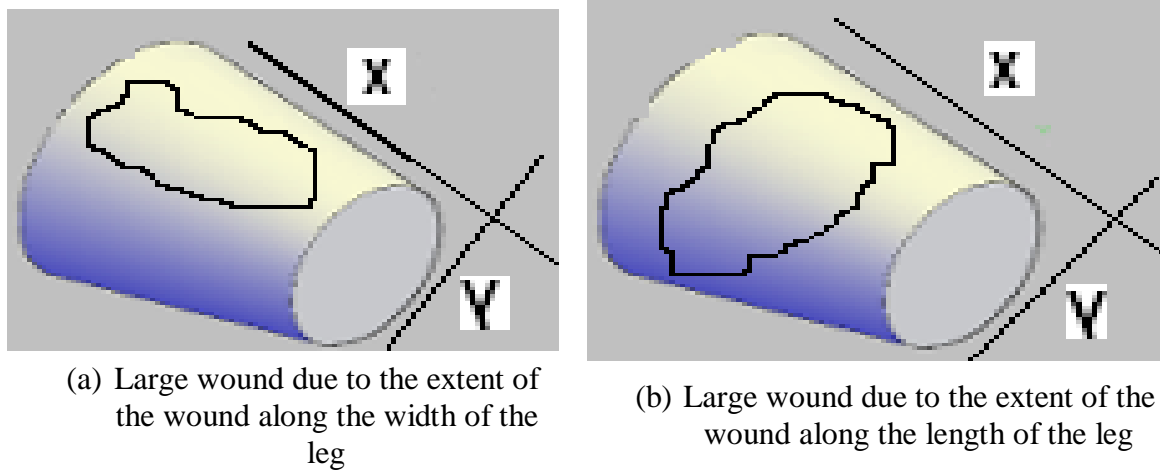
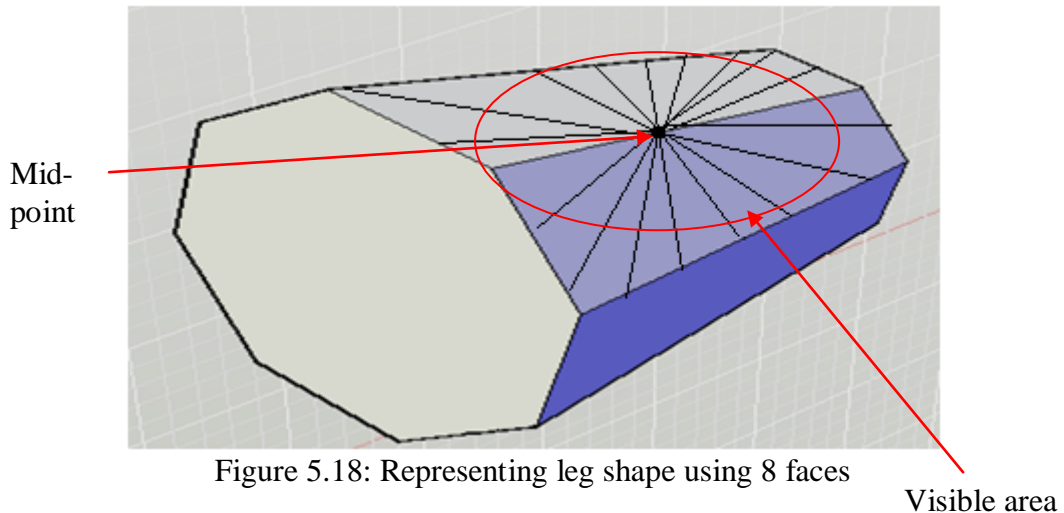


Figure 5.17: Wounds with large area

3. Midpoint projection has limitation in modeling leg curvature (cylindrical shape). A number of linear segments can represent cylindrical shape models. The accuracy of the shape representation improve with the increase in the number of linear segments (faces numbers) used. An estimation of cylindrical shape can be obtained by using 8 faces as shown in Figure 5.18. This indicates that 4 midpoints are needed to cover the whole leg. Thus, midpoint can only cover $\frac{1}{4}$ of the leg circumference.



4. The surface division plus convex hull approximation suits cylindrical shape limb. This method can be used for legs or arms in addition to sites that can be covered by a flat surface. For midpoint projection, in case of wounds that span large area the midpoint location may fall below the edge vertices due to the curvature. For ulcer wounds that are located at the foot, reconstructing the wound models using these algorithms will only work for small wounds at the leg. However, for rapidly changing curvature parts the reconstruction will yield overestimation. Midpoint is not suitable for very shallow wounds. However, it can give more flexibility for surfaces that is not having a cylindrical shape. For ulcer wounds that are located at the foot, as shown in Figure 5.19, the foot consists of parts with different pattern of curvature that must be considered when selecting appropriate model reconstruction method.

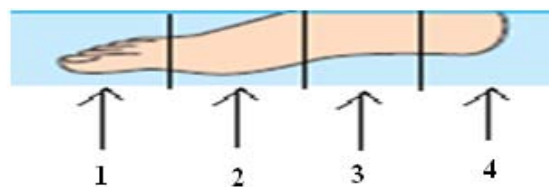


Figure 5.19: Foot ulcers

Considering the suitability of solid reconstruction method for the different curvature pattern in Figure 5.19:

- For the foot part labelled 1 midpoint is preferable to convex hull

- For the foot part labelled 2 convex can work even for shallow wounds in this part
- For the foot part labelled 3 either methods can work
- For the last part midpoint is more suitable.
- If the wound extends more than one of the areas, convex hull is not suitable. Midpoint can work for wounds that are deep at the foot even if it extends more than one part.

5.4 RESULTS of REAL SCANS COMPARED to MOLDED SURFACES

3D representations that can be touched and physically manipulated by the observer convey information not obtainable from 2D projections. Rapid Prototyping (RP) is capable of moulding 3D models and surface with the actual size. A three dimensional object is created by layering and connecting successive cross sections of thin layers of a material[Séquin 2005; Unimatic 2006]. In order for a 3D surface to be moulded, a supporting structure is needed. The 3D surface needs to be projected to a reference plane prior to printing the model [Unimatic 2006].

RP technique is used to compare the algorithms performance compared to the measurements obtained using the invasive method. The type used for moulding the wound surface models uses layers of wax fused together and builds up a solid model.

Two wounds surfaces were moulded (shown in Figure 5.20(a) and Figure 5.20(c)) with their measurements obtained using invasive methods are used to validate the algorithms performances. For volume, filling the cavity in the moulded surface with a liquid was applicable for the mould 'ulcer 6' since the surface scan does not span area with high curvature. Aligning a flexible material to fill the gap in the surface created by the wound and use this wound cast to measure the volume of the wound using water displacement method was applicable for both moulded wound surfaces. The flexible material aligned over the wound surface of the two moulded wounds is shown in Figure 5.20(b) and Figure 5.20(d). The cast is placed on a graded cylinder having measured level water as shown in Figure 5.20(e).

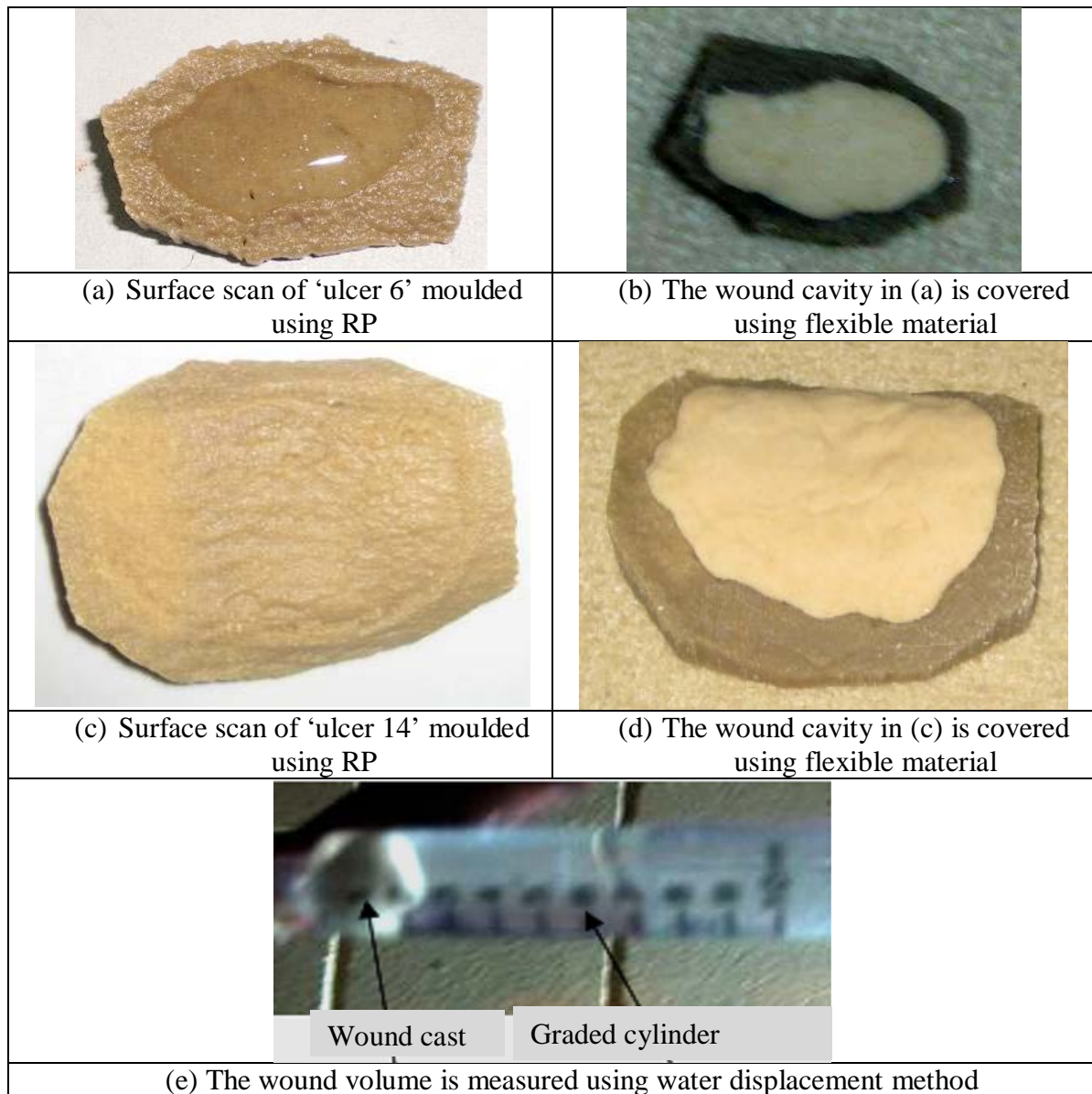
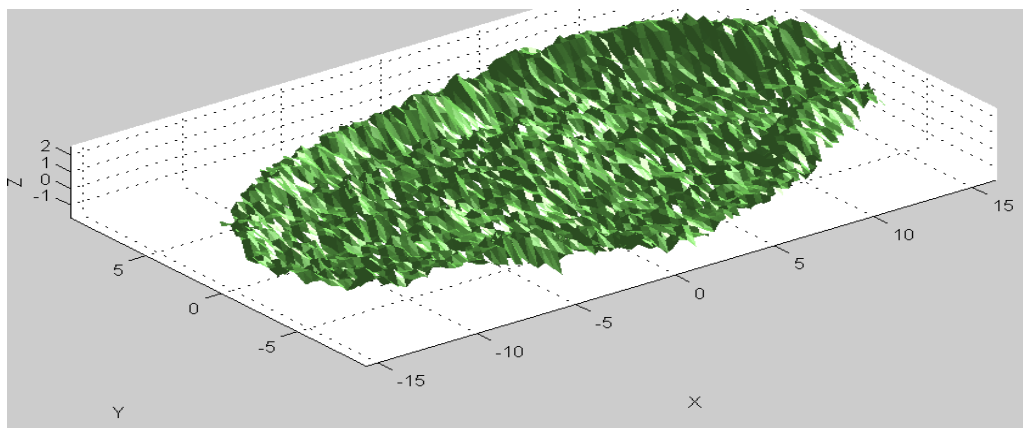
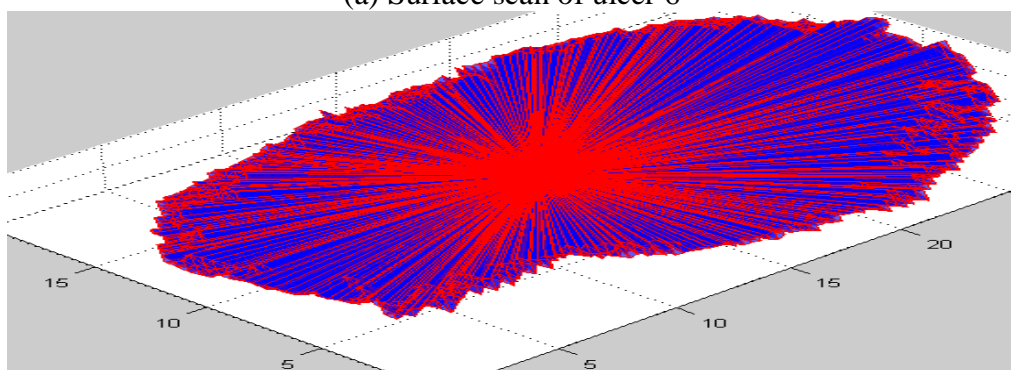


Figure 5.20: Steps for measuring wound volume using flexible material

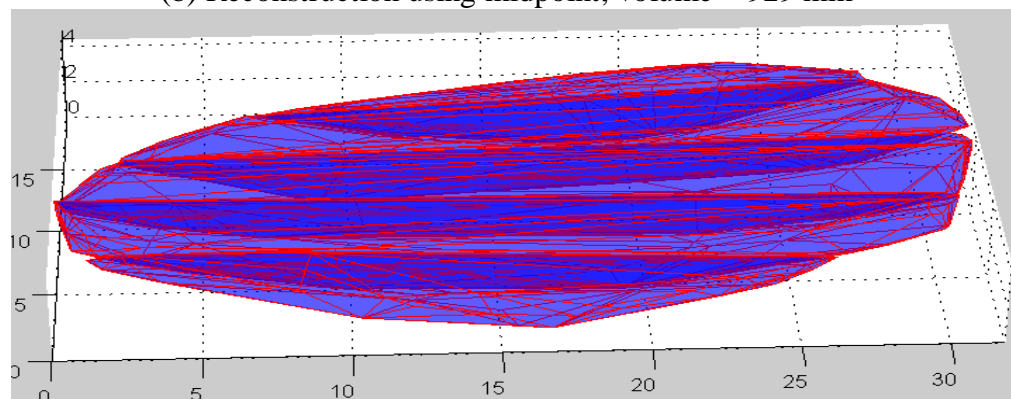
Figure 5.21 and Figure 5.22 shows the results of solid reconstruction and volume computation using the two algorithms for the two moulded surface scans. Figure 5.21 (a) displays the scanned surface of 'Ulcer 6' and 5.22(a) shows the scan of 'Ulcer 14'. Figure 5.21 (b) and Figure 5.22 (b) shows the reconstructed models using midpoint projection method. Figure 5.21 (c) shows the reconstructed model using convex hull preceded by surface division (5 divisions) method. Figure 5.22 (c) shows the reconstructed model using convex hull preceded by surface division (20 divisions) method.



(a) Surface scan of ulcer 6

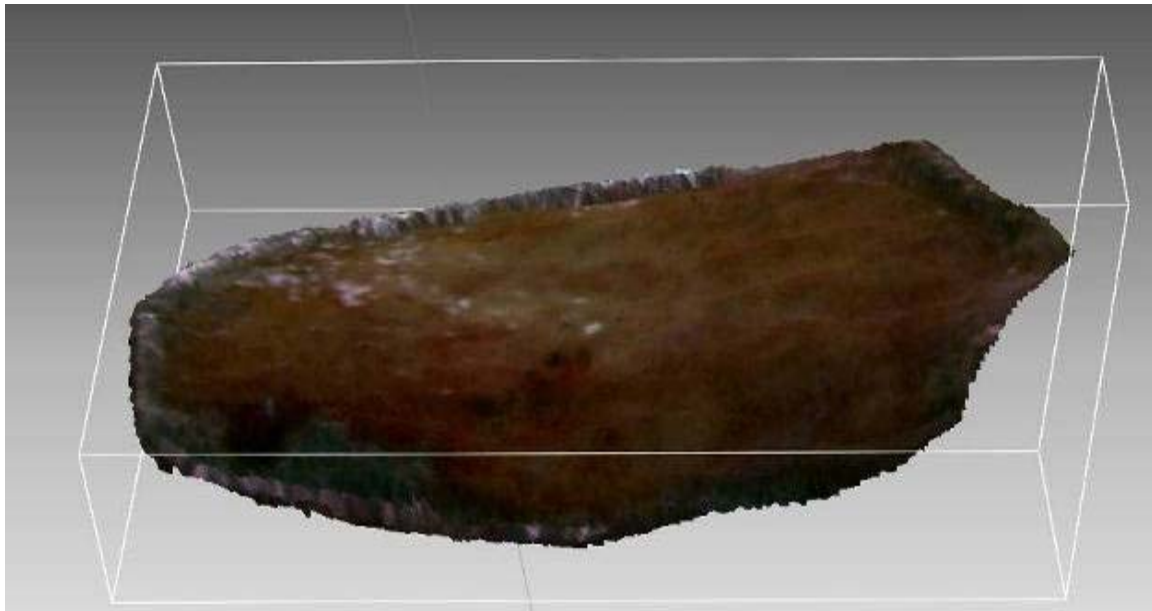


(b) Reconstruction using midpoint; volume = 929 mm^3

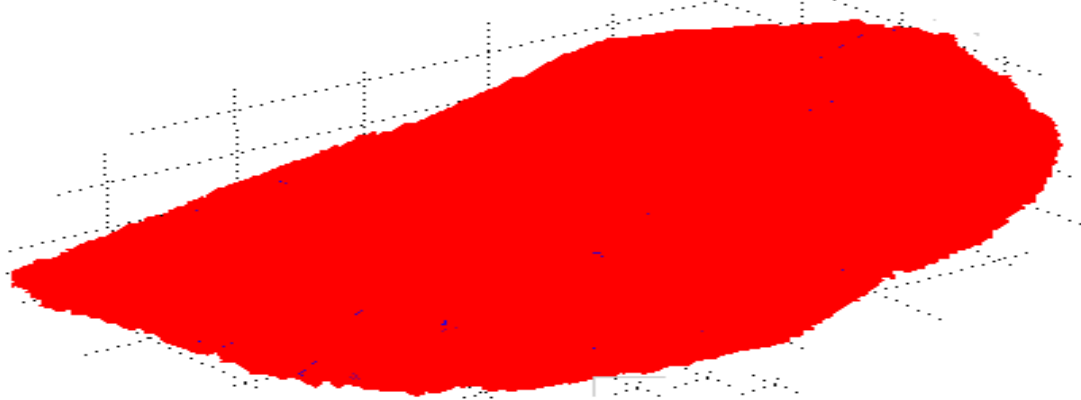


(c) Reconstruction using convex hull; volume = 927 mm^3

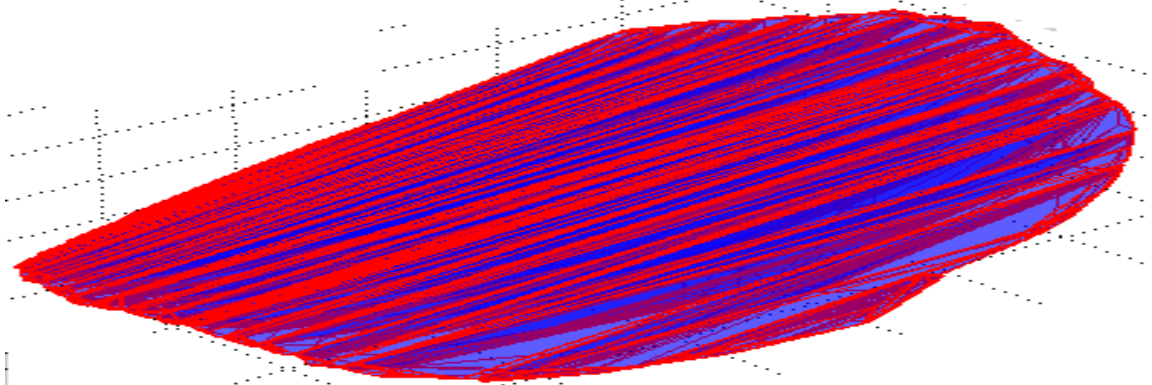
Figure 5.21: Wound model reconstructed from wound surface (Ulcer 6)



(a) Surface scan of ulcer 14



(b) Reconstruction using midpoint; volume = 9803 mm³



(c) Reconstruction using convex hull; volume = 9227 mm³

Figure 5.22: Wound model reconstructed from wound surface (Ulcer 14)

The following Table 5.5 provides wound size measurement obtained from two moulded surfaces using invasive and noninvasive techniques.

Table 5.5: Size measurement on two moulded wounds

Ulcer/ Method	Parameters				
	Top Area (mm ²)	True Surface area (mm ²)	Average Depth	Volume I (mm ³)	Volume II (mm ³)
Ulcer6 / invasive	412	568	-	Saline	Alginate paste
				950	1000
Ulcer6 / noninvasive	314	632	3	Mid - point	Convex hull
				929	927
Ulcer14 / invasive	2952	3472	-	Saline	Alginate paste
				-	10000
Ulcer14 / noninvasive	1795	3144	5.5 – 5.1	Mid - point	Convex hull
				9803	9227

From the table the invasive methods for estimating area and volume produced quantities that are larger than the quantities obtained by noninvasive methods. While true surface area measurement using noninvasive method could be larger than when using the invasive methods (acetate sheet) since this methods will not closely follow the fine changes at the wound surface. The percentage differences in the results between invasive and noninvasive methods computed using:

$$\% Diff = \frac{|Invasive_method - Noninvasive_method|}{|Invasive_method|} \times 100\% \quad \text{Eq. 5.3}$$

The percentage differences are:

- Top area= {(23.8%; ulcer 6) (39%; ulcer 14)}
- True surface area: {(11.2%; ulcer 6) (9.4%; ulcer 14)}
- Volume using midpoint method: {(7.1%; ulcer 6) (2.0%; ulcer 14)}
- Volume using convex hull: {(7.3%; ulcer 6) (7.7%; ulcer 14)}

CHAPTER 6: CONCLUSION

The effectiveness of a treatment regime can be estimated by measuring changes in the ulcer wound. The assessment of wounds covers a range of observations of the wound to determine the wound status at different times. Wound measurements that include top area, true surface area, depth and volume represent objective parameters that can be used to determine progression or regression of the wound.

Invasive methods for wound measurements are time consuming and often results in inconsistency in patient care. When computing wound area, overestimation occurs due to the fixed size of the squares composing the grid used for calculation. The overestimation is solved by digitizing the wound boundary and dividing the area to smaller units for better accuracy. Overestimation in volume calculation is due to overfilling the wound with material such as saline or alginate paste. In addition, invasive methods for volume estimation might cause infection or disturbance to the wound tissue and therefore are limited in practical use. Invasive methods for measuring volume are not suitable for large wounds, wounds that lay on limb with high curvature and shallow wounds.

Noninvasive methods for wound measurements from 3D surface scan will help in obtaining measurements that are more objective and eliminate the problems associated with the invasive methods. Current noninvasive methods for volume computation suffer from limitation such as overestimation due to existence of irregularities around the wound surface, handling large and high curvature areas and dealing with depressed edges wounds.

The objective of this research is to develop noninvasive computer algorithms that objectively determine ulcer wound parameters such as top area, true surface area, average depth, and volume. The algorithms are based on 3D surface scans and the wound of interest is limited to leg ulcers. The methods should overcome the problems faced by invasive and noninvasive methods.

3D laser scanner is used in the research to scan wounds surfaces using the triangulation concept (discussed in section 3.1.2.3) in which the depth of large number of points

located at the scanned surface is accurately obtained. In this thesis, algorithms for measuring wound top area, true surface area, average depth and volume from 3D surface scans are developed and investigated.

Wound attributes that describe the wounds are modelled based on real ulcer wound surface images. Wound models (refer section 4.5) representing possible ulcer wounds are created using AutoCAD software, are used to investigate the performance of solid reconstruction methods. In addition, moulded surfaces of wounds created using Rapid prototyping (RP), to verify the wound parameters (top area, true surface area, average depth and volume) measured using invasive and noninvasive methods.

Digitizing or obtaining the measurement from the scanned surface can solve inaccuracies in determining top area and true surface area. The top area of the wound is calculated as the area of the polygon created by extracting the wound boundary and projecting it to the XY plane ($z=0$). It turns out that, noninvasive method produces lower top area values compared to invasive method in the moulded surfaces. Using the same algorithm on large wounds that cover area larger than half of the leg circumference (refer to section 4.4 and section 4.6.1), boundary projection will result in underestimation for top area. This is overcome by decomposing the surface into 2 smaller surfaces so that the surface does not go beyond half of the leg circumference.

True surface area is obtained directly from the meshed surface. The area of all the triangles constructing the surface that is impeded in 3D space is computed and totalled to obtain the true surface area as such computing true surface area is not affected by surface alignment and the size of the wound. It is found, that underestimation/overestimation for true surface area can happen when using invasive method for moulded surfaces. The overestimation when using the invasive methods is expected (same reason as top area) but underestimation is found to occur in irregular base shape. Underestimation is because the plastic used in the invasive method resulted in surface smoothing, while the noninvasive method follows all the surface details.

In this work a method called midpoint projection has been developed to reconstruct solids from surfaces. In addition the convex hull approximation is investigated. These methods do not require large area around the wound for surface interpolation. Thus these methods

are not affected by the irregularities (swelling and scales) in the surrounding skin surface. The volume is computed from scattered data to handle depressed edges.

In the developed midpoint projection method, a solid is reconstructed from surface scans in which a point at the top missing surface is calculated by averaging several points selected at the wound boundary and then all the triangles composing the surface is projected to the midpoint composing several tetrahedra shapes. In the convex hull approximation (Delaunay tetrahedralization) all the vertices composing the wound surface is enclosed inside the nearest convex shape. In this work, the convex hull method is improved by performing surface division along the length prior to convex hull approximation to handle large leg curvature. Both algorithms produce solid shape composed of several tetrahedra; the volume of the shape is computed by totalling the volume of all the tetrahedra in the shape.

It is found that, both algorithms (midpoint and convex hull) produce overestimation when computing the volume of ulcer wounds having elevated base. The elevation at the base is normally due to limb curvature (global) and/or irregularity at the base (local).

From observations, midpoint projection outperforms convex hull approximation for all the models except for models with elevated base. The percentage error for midpoint method ranges from 0.0% - 6.5% and for convex hull the range is from 0.0% - 28.2%. It is concluded that midpoint projection can construct solids for wound surfaces having local curvature accurately, while for surfaces with large global curvature the error can be high. However, for elevated base models, the error in solid reconstruction and volume computation using midpoint projection increases with the decrease in distance between the base and the midpoint (higher error for shallow wounds). Elevation at the base from local curvature is not as high as the elevation from global curvature. Midpoint projection is not affected by local curvature but significantly affected by global curvature.

For convex hull approximation, lower errors in volume computation are produced in case of regular boundary models compared to irregular boundary models. Overestimation in volume for convex hull method can either be due to irregular boundary and/or elevation at the base (both global and local). To overcome the problems associated with convex hull, the 3D surface is divided into equal distance surfaces producing parallel surfaces in the leg length. This is done so that the high curvature of the leg and irregularity at the

boundary can be represented using a number of linear segments. Convex hull approximation (Delaunay tetrahedralization) is then applied for the vertices within the sub surfaces. With the increase in surface division, error in volume computation is reduced. The percentage error in volume computation when using convex hull approximation in all the models excluding models with elevated base ranges (0-28.2) and when using surface division of 20 sections prior to convex hull approximation the error ranges (-2.7-7.2). Local curvature will still produce overestimation in volume computation.

In this work, the shape reconstructed using convex hull approximation preceded by surface division simulates large leg curvature. Surface division prior to convex-hull approximation can model limbs that have cylindrical shape (e.g. legs and arms) or flat surfaces (wounds having small area). Analysis has shown that midpoint projection is suitable for approximately flat body parts and deep wounds. However it is not suitable for shallow wounds or wound covering high curvature areas.

For wounds that are located at the leg, the performance of volume computation algorithm is not only based on the wound area but it is also significantly affected by the increase in Y_{range} value (leg width covered by the wound). In case of wounds with $Y_{range} < 20$, mm midpoint projection is preferable for volume computation for both shallow and deep wounds. And in the case of wounds that are having Y_{range} of (20 - 50) mm, both algorithms can be used but convex hull with division is preferable for shallow wound (average depth < 3 mm). In case of large wounds with $Y_{range} > 50$ mm convex hull with surface division is preferable to midpoint due to the effect of global curvature.

From the results of volume computation obtained from moulded surfaces, invasive methods for volume measurement produce higher values compared to noninvasive methods. This indicates that invasive methods reduce the overestimation in volume computation due to overfilling the wound surface with material (saline or alginate paste).

Wound depth varies along the wound; it is more meaningful to measure average depth for wound assessment. Here the average depth is calculated by dividing wound volume by wound top area.

This work can be used to create a cast of any mold. This is possible if the top estimated using tabulated surface.

FUTURE WORK

When using convex hull approximation method, local curvature will produce overestimation since any dents at the base will be covered in the constructed part. For more accurate volume computation volume subtraction is proposed. The elevated part should be extracted and used in generating another solid. The volume of the dent solid must be subtracted to get the wound volume.

The system can be extended to cover other aspect of wound assessment including:

- a. Segmenting the wound boundary from the colored image aligned to surface.
- b. Performing tissue classification to analyze and quantify the different tissue composing wound bed.
- c. Using surface inspection to detect the exact locations for changes at the surface.
- d. Implement improvement on midpoint projection method to handle leg curvature.

REFERENCES

- Ahn, C. Salcido, R., *Advances in Wound Photography and Assessment Methods, Advances in Skin & Wound Care*, February 2008, 21(2):85-93.
- Albouy, B., Lucas, Y., Treuillet, S., '3D Modeling from Uncalibrated Color Images 3D Modeling from Uncalibrated Color Images for a Complete Wound Assessment Tool', Conference of the IEEE EMBS Cité Internationale, Lyon, France 2007.
- Albouy, B., Treuillet, S. & Lucas, Y. a. J., 'Volume Estimation from Uncalibrated Views Applied to Wound Measurement', Springer , ICIAP 2005, LNCS 3617, pp. 945 – 952.
- AutoCAD 2007, *Command Reference - Autodesk, Inc.*, U.S.A., 2006.
- Baranoski, S., & Ayello, E. A., *Wound Care Essentials: Practice Principles*, Lippincott Williams & Wilkins; Second Edition edition 2007.
- Barber, C.B., Dobkin, D.P., and Huhdanpaa, H.T., 'The Quickhull algorithm for convex hulls', *ACM Trans. on Mathematical Software*, Dec 1996, 22(4):469-483
- Berg, M. d., Cheong, O., Kreveld, M. v., & Overmars, M., *Computational Geometry Algorithms and Applications*, Springer; 3rd ed. Edition, 2008.
- Boersma, S.M., Heuvel, F.A., Cohen, A.F. and Scholtens, R.E.M., 'Photogrammetric Wound Measurement with a Three- Camera Vision System', XIXth Congress of ISPRS, Amsterdam, The Netherlands, Vol. XIXIII, Part B5/1, 2000, pp. 84-91.
- Callieri, M., Cignoni, P., Pingi, P., Scopigno, R., Coluccia, M., Gaggio, G., 'Romanelli, M.N., Derma, Monitoring the evolution of skin lesions with a 3D system', 8th Int. Workshop, Modeling, and Visualization Conf., Munich, 2003 ,pp. 167–174.
- Chivate, P.N., Jablokow, A.G., 'Review of surface representations and fitting for reverse engineering', *Computer Integrated Manufacturing Systems* 8 (3) 1995, 193-204.
- Conti, J., n.d., Retrieved 5 2008, from <http://www.mathworks.com/matlabcentral/fileexchange/1241>.
- Dealey, C., *The Care of Wounds a Guide for Nurse*, Edition 2, Blackwell Science Ltd, July 1999
- Fette AM., 'A clinimetric analysis of wound measurement tools', *World Wide Wounds*. January 2006. Retrieved 3 2009, from: <http://www.worldwidewounds.com/2006/january/Fette/Clinimetric-Analysis-Wound-Measurement-Tools.html> .
- Finkelstein, E., *AutoCAD 2007*, Wiley 2006.

- Flanagan M., 'Improving accuracy of wound measurement in clinical practice', *Ostomy Wound Manage*, 2003;49: 28-40 .
- Goldman RJ, Salcido R., 'More than one way to measure a wound: an overview of tools and techniques', *Advances in skin & wound care* 2002;15:236-43.
- Hachenberger, P., 'Exact Minkowski sums of polyhedra and exact and efficient decomposition of polyhedra in convex pieces', *Proc. 15th Annual European Symposium on Algorithms (ESA)* , 2007, pp. 669--680
- Halim, S., 'Measurement and analysis techniques for precise engineering and medical applications', *International Symposium and Exhibition on Geoinformation (ISG)*, 21-23 2004, Kuala Lumpur, Malaysia
- HARTMANN., 'Phase-specific wound management of decubitus ulcer' and 'Phase-specific wound management of venous leg ulcer', *PAUL HARTMANN AG D-89522 Heidenheim*, 2006.
- Hess, C.T., 'The Art of Skin and Wound Care Documentation tools', *Advances in skin & wound care* 2005;18:43-53.
- Hoffmann, C. M., *Geometric and Solid Modeling*, Morgan Kaufmann, 1989.
- Honrado, C. P., & Wayne F. Larrabee, J., 'Update in three-dimensional imaging in facial plastic surgery', *Lippincott Williams & Wilkins* ,2004 , pp. 1068-9508.
- Hsu, Y.-L. 1998. Retrieved 6 2008, from [http://designer.mech.yzu.edu.tw/article/articles/course/\(2000-10-23\)%20Analytic%20surfaces.htm](http://designer.mech.yzu.edu.tw/article/articles/course/(2000-10-23)%20Analytic%20surfaces.htm). Course Geometric modeling and computer graphics, Yuan Ze University
- INUS Technology, 'Rapidform2006 Tutorial'; 2005.
- Jon, I., http://www.cs.umbc.edu/~squire/cs455_l23.html. Numerical Computations Course, University UMBC ,2009.
- Kampel, M., 'Sablatnig, R., 3D Data Retrieval of Archaeological Pottery', *VSMM 2006*: 387-395.
- Kazhdan, M., 'Seminar on 3D Model Reconstruction', *JOHNS HOPKINS University* , 2005
- KONIKA, www.konicaminolta-3d.com, '3D Digitizing KONICA MINOLTA 3D Laser scanner Applications in medical science', 2004
- Kumar, P., and Yildirim, E. a., 'Computing Minimum Volume Enclosing Axis-Aligned Ellipsoids', *Journal of Optimization Theory and Applications*, Vol: 136 (2), 2008, pp: 211–228.

- Langemo D, Anderson J, Hanson D, Hunter S, Thompson P., ‘Measuring Wound Length, Width, and Area: Which Technique?’, *Advances in skin & wound care*, January 2008, vol. 21 no. 1.
- Lee, Y. T. and Requicha, A. A. G., ‘Algorithms for Computing the Volume and other Integral Properties of Solids’, Part I and Part II, *Comm. ACM*, Vol. 25, No. 9, 1982, pp. 635-641, and pp. 642-650.
- LEVOY, M., ‘Digital Michaelangelo Project: Creating Virtual Sculpture by David Salisbury’, *Stanford Campus Report*, January 1999.
- Li, X., Feng, J., Zha, H., ‘3D Modelling of Geological Fossils and Ores by Combining High-resolution Textures with 3D Scanning Data’, *Ninth International Conference on Virtual Systems and MultiMedia 2003*, Montreal, Canada, October 2003.
- Lien, J. m., Amato, N. m., ‘Approximate convex decomposition of polyhedra and its applications’, *Computer Aided Geometric Design*, 2008, 25(7): 503-522.
- Liepa, P., ‘Filling Holes in Meshes’, *Proc. Eurographics/ACM SIGGRAPH Symp, Geometry Processing*, 2003, pp. 200–205
- Lim, C. G., ‘A Univresal Parametrization in B-Spline Curve and Surface Interpolation and its Performance Evaluation’; PhD thesis, Louisiana State University and Agricultural and Mechanical College ;May 1998.
- London, N. J., & Donnelly, R., ‘ABC of arterial and venous disease Ulcerated lower limb’. *BMJ*, 2000, 320, 1589-1591.
- Malian, A., Azizi, A., Heuvel van den, F. A., ‘MEDPHOS: A New Photogrammetric System for Medical Measurements’, *Proceedings of ISPRS Congress*, Istanbul, Turkey, Vol. XXXV, 2004, pp. 311-316.
- Matlab documentation / matlab reference
- NHS, Centre for Research and Dissemination, ‘Compression therapy for venous leg ulcers’, *Effective Health Care Bulletin* 1997; 3: 4.
- Ohanian, O. J., ‘Mass Properties Calculation and Fuel Analysis in the Conceptual Design of Uninhabited Air Vehicles’; MSc thesis, Virginia Polytechnic Institute and State University : 2003.
- Persson, P.-O., Strang, G., ‘A Simple Mesh Generator in MATLAB. *SIAM Review*’, Volume 46 (2), pp. 329-345, June 2004
- Pflipsen, B., ‘VOLUME COMPUTATION - a comparison of total station versus laser scanner and different software’; MSc thesis , UNIVERSITY OF GAVLE 2006

- Plassmann, P., Harding, K.G., Melhuish, J.M., 'Methods of Measuring Wound size - A Comparative Study', *WOUNDS* March/April 1994, vol.6, no.2, p.54-61
- Plassmann, P., Jones, B.F., Ring, E.F.J., 'A structured light system for measuring wounds', *Photogrammetric Record* Vol.15 No86 pp.197- 203,1995.
- Ralph W. L. Ip, Angela C. W. Yeung, Felix T. S. Chan and Henry C. W. Lau, 'Select the Best Surface Fitting Approach for the Reconstruction of High Quality 3-D Objects from Range-image Data', November 2006, *IAENG International Journal of Computer Science*, 32:4, IJCS_32_4_4
- Registered Nurses Association of Ontario (RNAO), 'Assessment and management of venous leg ulcers', Toronto (ON): Registered Nurses Association of Ontario (RNAO); 2004.
- Requicha, A. and Rossignac, J., 'Solid Modeling and Beyond', Tech. Report RC 17676, IBM, Yorktown Heights, 1992.
- Sansoni, G., Docchio, F., Trebeschi, M., Scalvenzi, M., Cavagnini, G., Cattaneo, C., 'Application of three-dimensional optical acquisition to the documentation and the analysis of crime scenes and legal medicine inspection', *Proc. of the 2nd IEEE International Workshop on Advances in Sensors and Interfaces (IWASI)*, Bari, 2007, pp.217-226.
- Séquin, C. H., 'Rapid prototyping: a 3d visualization tool takes on sculpture and mathematical forms', *Commun. ACM* 48, 6 (Jun. 2005), 66-73.
- Serup, B. J., Jemec, G. B., & Grove, G. L., *Handbook of Non-Invasive Methods and the Skin*, Informa HealthCare; 2 edition, 2006.
- Shai, A., & Maibach, H., *Wound Healing and Ulcers of the Skin Diagnosis and Therapy – The Practical Approach*, ISBN 3-540-21275-2 Springer Berlin Heidelberg New York, 2005.
- Shewchuck, J. R., 'Lecture Notes on Delaunay Mesh Generation'; University of California at Berkeley: 1999
- Simonovits, M., 'How to compute the volume in high dimension?', *ISMP, 2003 Copenhagen. Math. Program.* 97, no. 1-2, Ser. B, 2003, 337-374.
- Simonsen, H., Coutts, P., Bogert-Janssen, S van den., Knight, S., 'Assessing and Managing Chronic Wounds', *Wound Care Reference Guide*.
- Sirakov, N.M., Iwanowski, M., D. R. Hack, M. L. Fever, 'Morphological approach to volume calculation of complex 3D geological objects', *Proc. of the Int. Sym. on*

- Application of Computers and Operations Research in the Mineral Industries, Cape Town, South Africa, 2003.
- Smith & Nephew, 'Visitrak', Retrieved 7 2009, from <http://wound.smith-nephew.com>
- Stroud, I., *Boundary Representation Modelling Techniques*, Springer-Verlag New York Inc, 2006.
- Sun, X., Rosin, P.L., Martin, R.R. and Langbein, F.C., 'Noise in 3D laser range scanner data', Proc. IEEE Int. Conf. on Shape Modeling and Applications 2008 , IEEE. pp. 37-45.
- Thomson, A., & Miles, A., *Manual of Surgery ,General Surgery*, Sixth Edition, 2006.
- Unimatic Engineers Ltd , Rapid prototyping, rapid 3D printing and rapid manufacturing, 2006 , <http://www.machinebuilding.net/ta/t0005.htm>.
- Unten, H., Ikeuchi, K., 'Virtual Reality Model of Koumokuten Generated from Measurement', 10th International Conference on Virtual Systems and Multimedia(VSMM2004), 2004.
- Wannous, H., Lucas, Y., Treuillet, S., Albouy, B.,
'A complete 3D wound assessment tool for accurate tissue classification and measurement',ICIP08(2928-2931).
- Weisstein, E.W, "Triangle Area." From MathWorld--A Wolfram Web Resource.
<http://mathworld.wolfram.com/TriangleArea.html>
- Weisstein, E. W., Surface of Revolution. From MathWorld--A Wolfram Web Resource.
<http://mathworld.wolfram.com/SurfaceofRevolution.html>
- Wendelken, M. E., Markowitz, L., Patel, M., Alvarez, O. M., Objective, noninvasive, wound assessment using B-mode ultrasonography. *Wounds*. 2003;15((11)):351–360.
- Wilhelm, K.-P., Elsner, P., Berardesca, E., & Maibach, H. I., *Bioengineering of the Skin: Skin Imaging & Analysis*, 2nd Edition, 2006, Informa HealthCare; 2 edition .
- Wilson, J. E., *3D modeling in AutoCAD*, CMP; 2nd edition,2001.
- Zhang, X., Morris, J., and Klette, R., CITR, 'Volume Measurement Using a Laser Scanner , 2005', Computer Science Department The University of Auckland, Private Bag 92019, Auckland
- Zhu, L. C., 'Non-invasive Optical Technologies to Monitor Wound Healing'; PhD thesis. Drexel University, December 2007.

APPENDICES

APPENDIX A: IMAGES OF THE SCANNED WOUNDS

In this study, 9 patients from Hospital Kuala Lumpur have been involved in providing 22 3D laser scanned surface images of ulcers at the legs. Each wound requires at least 3 scans to be aligned and registered to solve occlusion and coverage of large area.

Patient #: 1

Ethnic: Chinese

Gender: Male

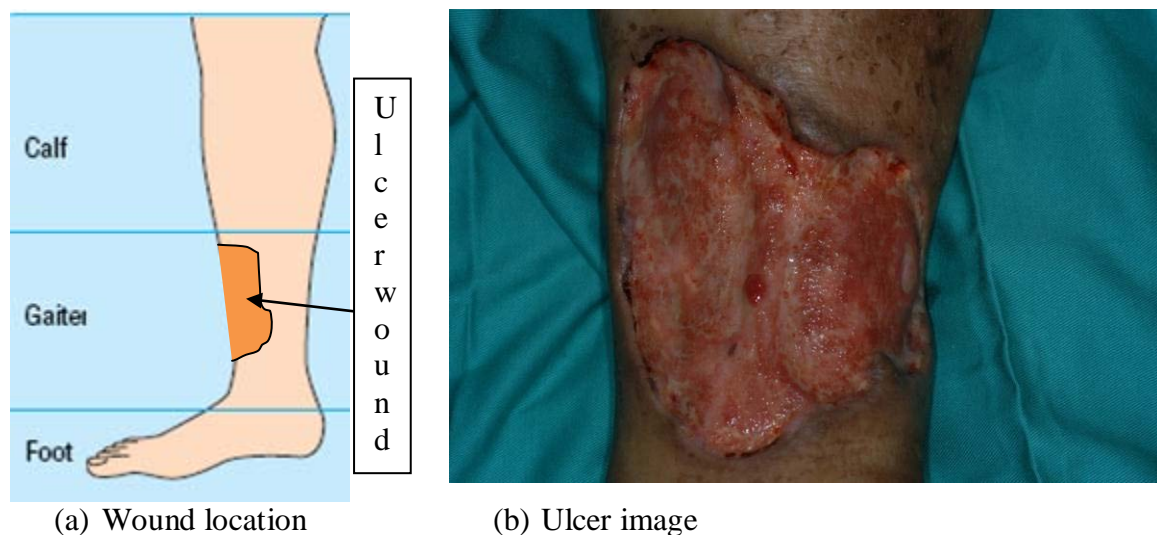
Ulcer type: Pyoderma Gangrenosum

Description: Large punched out deep ulcer on the left anterior shin, measuring approximately 12cm×15cm with punched out edges. There is large amount of slough with clear exudates. No granulation tissue. Surrounding skin erythematous. Irregular boundary.

Age: 46

Scanning date: 4-6-08

Scanning date: 24-6-08



(a) Wound location

(b) Ulcer image

Figure 1: The location and image of the ulcer of patient 1

Patient #: 2

Ethnic: Chinese

Gender: Female

Ulcer type: Venous ulcer

Description: Small shallow ulcer measuring approximately 3cm×4cm with slough and minimal granulation tissue. The edges are erythematous.

Age: 67

Scanning date: 4-6-08



(a) Wound location

(b) Ulcer image

Figure 2: The location and image of the ulcer of patient 2

Patient #: 3

Ethnic: Indian

Gender: Female

Ulcer type: Arterial recurrent ulcers

Age: 45

Scanning date: 5-6-08

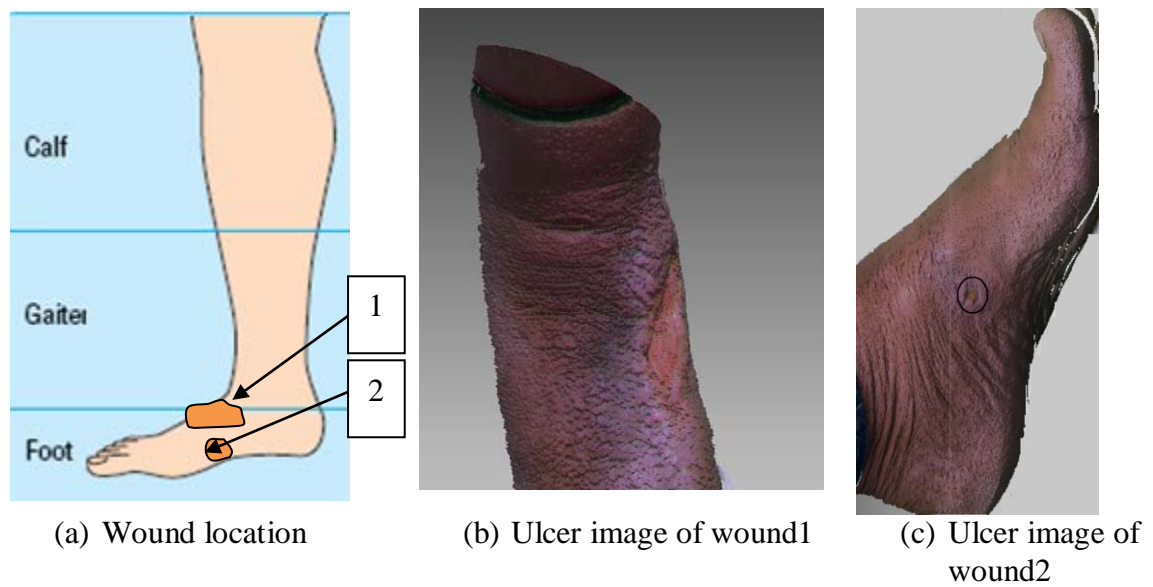


Figure 3: The locations and images of the ulcers of patient 3

Patient #: 4

Ethnic: Indian

Gender: Female

Ulcer type: Recurrent-stasis ulcer- **2 ulcers** both legs

Age: 65

Scanning date: 21-10-08

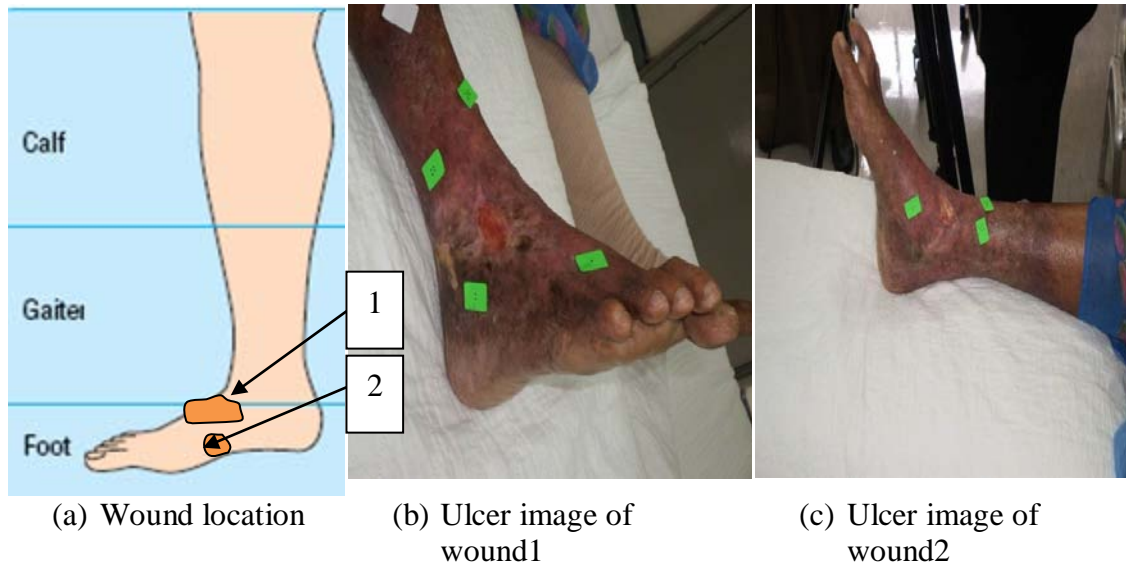


Figure 4: The locations and images of the ulcers of patient 4

Patient #: 5

Ethnic: Chinese

Gender: Female

Description: Deep ulcer, sharp punched out edge, dry, base with granulation tissue, normal surrounding skin. Location: right thigh - several burns

Age: 35

Scanning date: 21-10-08



Figure 5: The location and image of the ulcer of patient 5

Patient #: 6

Ethnic: Indian

Gender: Male

Ulcer type: Venous ulcer

Description: Superficial ulcer, sloping edge, dry, base with slough and granulation tissue, surrounding skin dry, pigmented and scaly. Recurrent ulcers started 1.5 years both legs having **several ulcers** with different sizes and locations both legs

Age: 36

Scanning date: 22-10-08



(a) Right foot



(b) Left leg



Right leg

Figure 6: Image of the ulcers of patient 6

Patient #: 7

Ethnic: Malay

Gender: Female

Ulcer type: Stasis ulcer

Description: Superficial ulcer, sloping edge, mild exudate, base with granulation tissue.

location: left leg.

Age: 57

Scanning date: 21-10-08

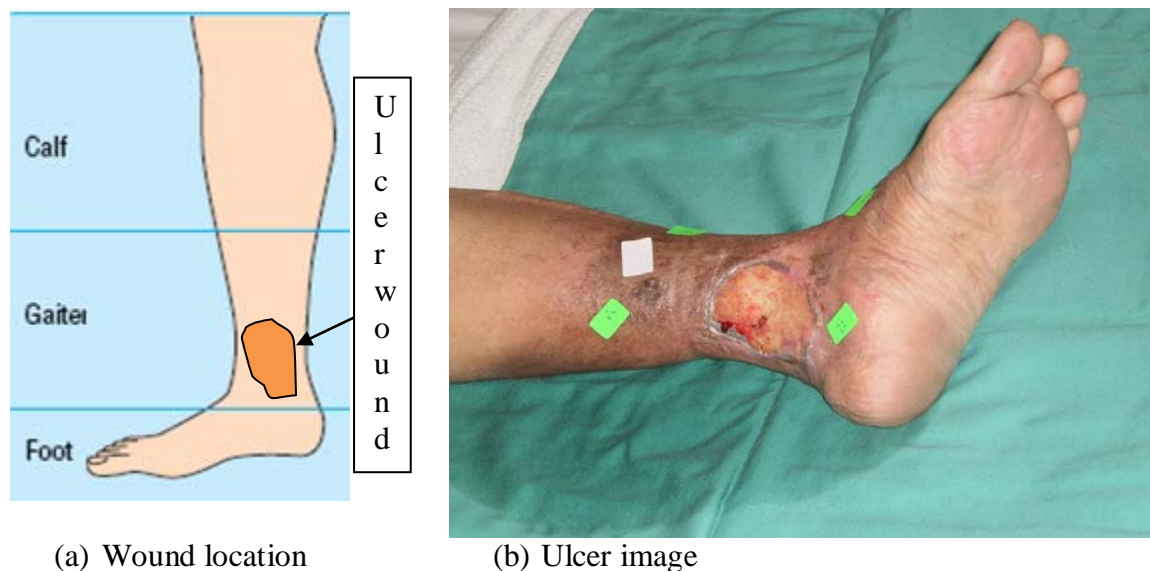


Figure 7: The location and image of the ulcer of patient 7

Patient #: 8

Ethnic: Malay

Gender: Male

Description: Several ulcers in both legs. Left leg - some liquid covering the wound surface. Right leg - after cleaning it dry wound

Age: 30

Scanning date: 4-12-08



Figure 8: The locations and images of the ulcers of patient 8

Patient #: 9

Ethnic: Indian

Gender: Female

Ulcer type: Arterial recurrent ulcers

Age: 45

Scanning date: 4-12-08



Ulcer 1 and 2

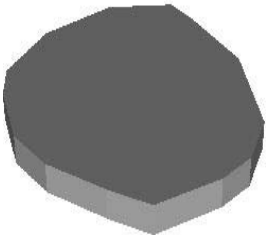

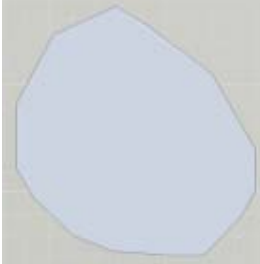

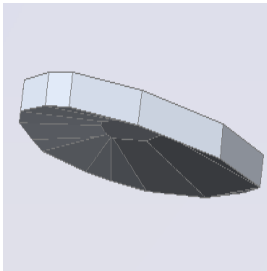
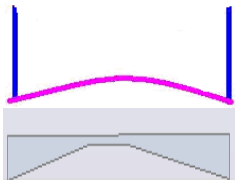
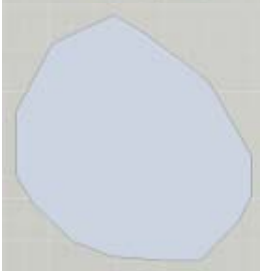
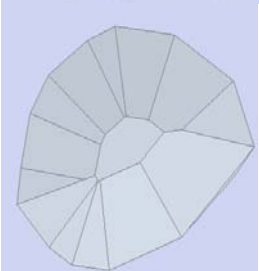
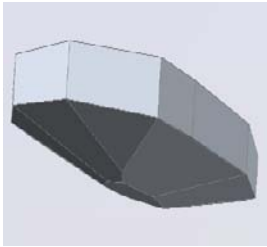
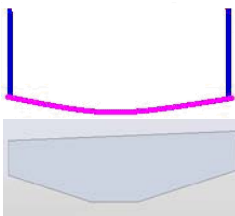

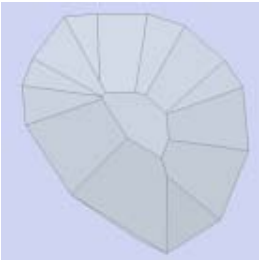
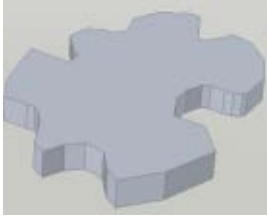
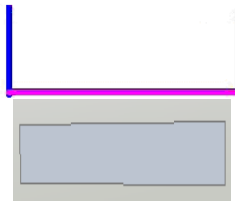


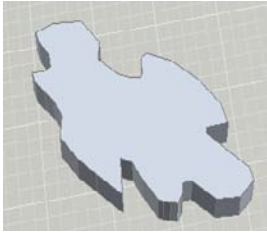
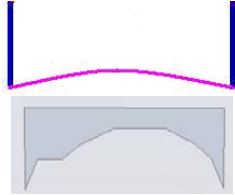




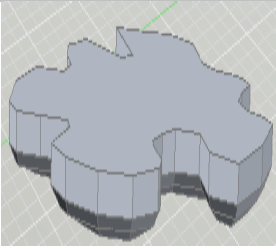
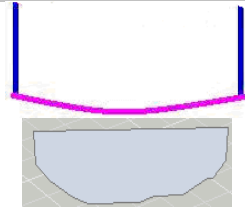


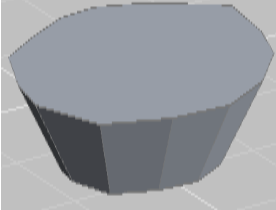
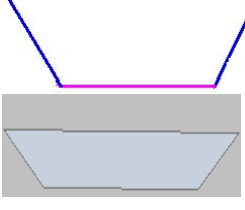

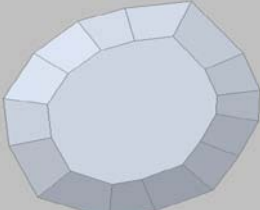
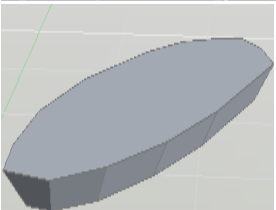
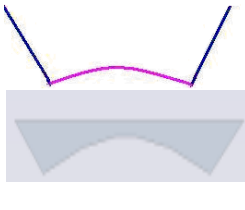

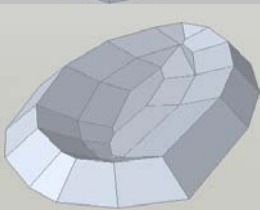
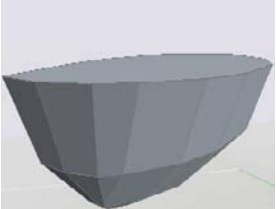
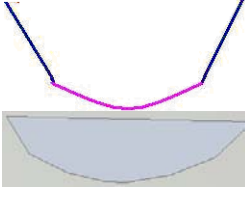

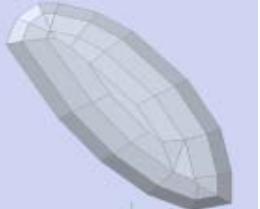
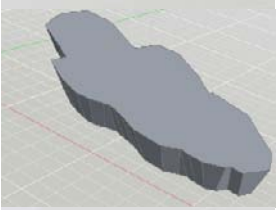
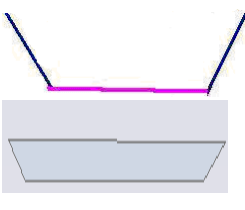


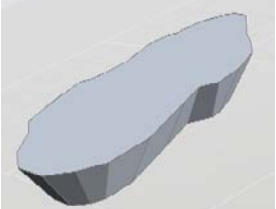
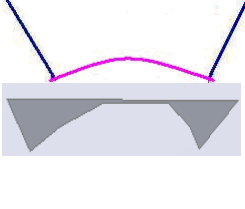

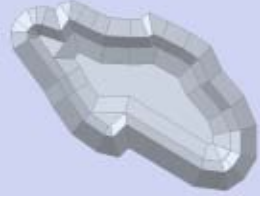
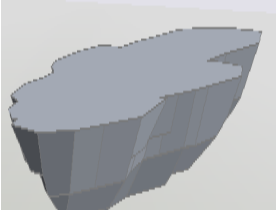
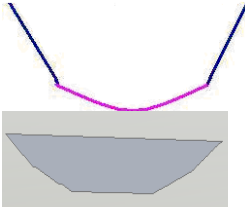


Ulcer 3

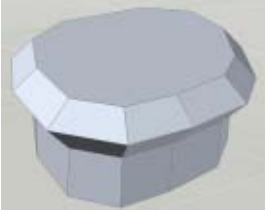
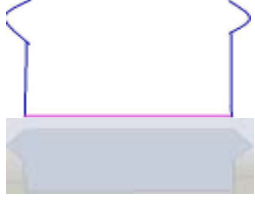
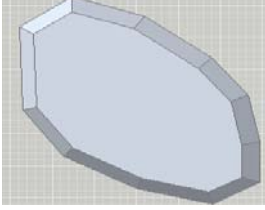
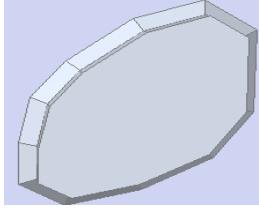
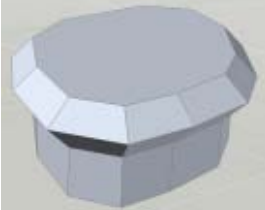
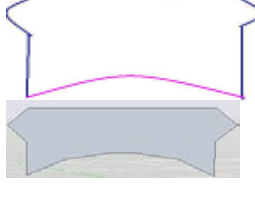
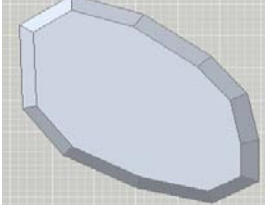
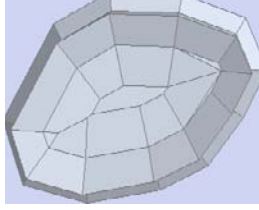
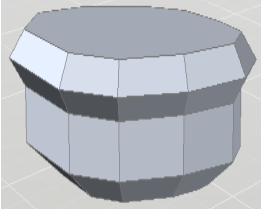
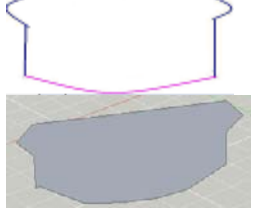
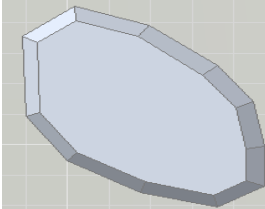
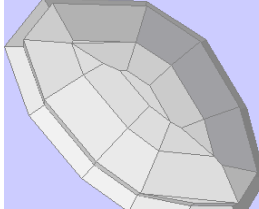
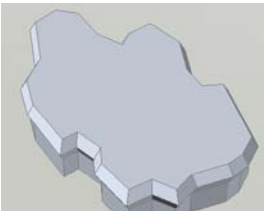
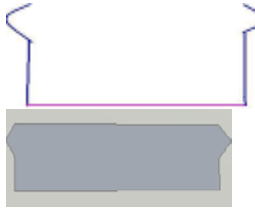
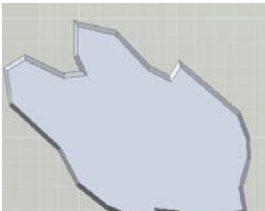

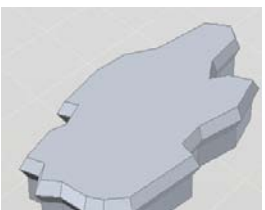
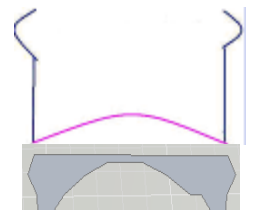
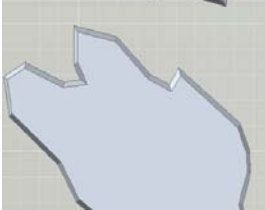

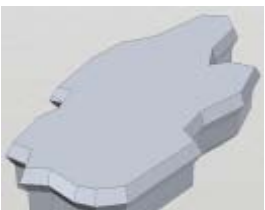
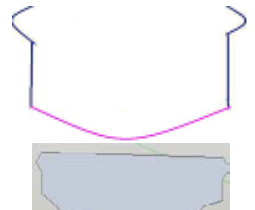

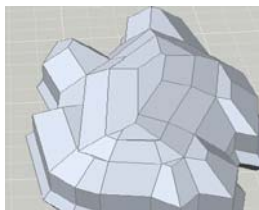
Figure 9: The locations and images of the ulcers of patient 9

APPENDIX B: WOUND MODELING USING AutoCAD

Table1: The 18 wound models created from a combination of edge, base and boundary descriptors

#	Model	Model	Cross Section	Top view	Bottom View
Model 1	M1h				
Model 2	M1a				
Model 3	M1b				
Model 4	M2h				
Model 5	M2a				

#	Model	Model	Cross Section	Top view	Bottom View
Model 6	M2b				
Model 7	M3h				
Model 8	M3a				
Model 9	M3b				
Model 10	M4h				
Model 11	M4a				
Model 12	M4b				

#	Model	Model	Cross Section	Top view	Bottom View
Model 13	M5h				
Model 14	M5a				
Model 15	M5b				
Model 16	M6h				
Model 17	M6a				
Model 18	M6b				

APPENDIX C: ALGORITHMS CODE

1- TopArea.m

```

%Remove the repeated vertices in the triangular mesh and rearrange the
%allocation table...
[B,ix,jx] = unique(y2,'rows');
%[B,I,J] = UNIQUE(...) also returns index vectors I and J such
    that B = A(I) and A = B(J) (or B = A(I,:) and A = B(J,:)).

[a,b]= size(y2);
c=1;
for i=1:a/3
    e1(i,1)=jx(c);
    e1(i,2)=jx(c+1);
    e1(i,3)=jx(c+2);
    c=c+3;
end

% The following function will return the vertices that belong to the
surface boundary (edge boundary)
e=boundedges(B,e1);
figure, simp_plot_2d(B, e);

% Re arrange the input matrix
[a,b]= size(e);
c=1;
c2=1;
for i=1:a
    v01(i,:)=B(e(i,1),:);
    v02(i,:)=B(e(i,2),:);

    XX(c2)=v01(i,1);
    XX(c2+1)=v02(i,1);
    YY(c2)=v01(i,2);
    YY(c2+1)= v02(i,2);
    c2=c2+2;
end

% compute the area of the polygon defined by the edge vertices
A = polyarea(XX,YY);

```

2- TrueSurfaceArea.m

```

function sr = Area(vertices,c)

% align the surface to the positive x,y,z plane by if the min of x,y,z
% is negative by subtracting min-1 from all the axes
% checking the the location of the minimum x,y,z dimensions

% x2=x;
% y2=y;
n1=min(vertices(:,1));
n2=min(vertices(:,2));
n3=min(vertices(:,3));

% if any of the dimensions lay in the negative axis we will performe
% translation for the whole object or surface
if n1<0
vertices(:,1)=vertices(:,1)-n1;
end

if n2<0
vertices(:,2)=vertices(:,2)-n2;
end

if n3<0
vertices(:,3)=vertices(:,3)-n3;
end

sur=0;
[a,b]= size(vertices);

for i=1:3:a-2 % for each triangle

a=[vertices(i,2),vertices(i,3),1;vertices(i+1,2),vertices(i+1,3),1;verti
ces(i+2,2),vertices(i+2,3),1];

b=[vertices(i,3),vertices(i,1),1;vertices(i+1,3),vertices(i+1,1),1;verti
ces(i+2,3),vertices(i+2,1),1];

c=[vertices(i,1),vertices(i,2),1;vertices(i+1,1),vertices(i+1,2),1;verti
ces(i+2,1),vertices(i+2,2),1];
d1=det(a);
d2=det(b);
d3=det(c);
sur = sur+sqrt(d1*d1+d2*d2+d3*d3);
end

sr=sur/2;

```

3- MidSelect.m

```

n1=min(y2(:,1));
n2=min(y2(:,2));
n3=min(y2(:,3));

% if any of the dimensions lay in the negative axis we will performe
% translation for the whole object or surface
if n1<0
y2(:,1)=y2(:,1)-n1;
end

if n2<0
y2(:,2)=y2(:,2)-n2;
end

if n3<0
y2(:,3)=y2(:,3)-n3;
end

% display the surface for edge points selection
figure
p = patch('faces', x2, 'vertices' ,y2);
C=1;
set(p, 'facec', 'b'); % Set the face color (force it)
set(p, 'facec', 'flat');% Set the face color flat
set(p, 'FaceVertexCData', C); % Set the color (from file)
%set(p, 'facealpha',.4) % Use for transparency
set(p, 'EdgeColor','none'); % Set the edge color
%set(p, 'EdgeColor',[1 0 0]);
% Use to see triangles, if needed.
grid on;
axis on;
axis tight;
light % add a default light
daspect([1 1 1]) % Setting the aspect ratio
view(3) % Isometric view
xlabel('X'),ylabel('Y'),zlabel('Z')

clear global B;
global B T;
% T = selected vertices count, B is the array of selected vertices
position
T=1; % initialize the point count, will be increased with each selection
select3dtool

```

4- MidProjection.m

```

figure;
[c cc]=size(y2);

% align the surface to the positive x,y,z plane by if the min of x,y,z
% is negative by subtracting min-1 from all the axes
% checking the the location of the minimum x,y,z dimensions
n1=min(y2(:,1));
n2=min(y2(:,2));
n3=min(y2(:,3));

% if any of the dimensions lay in the negative axis we will performe
% translation for the whole object or surface
if n1<0
y2(:,1)=y2(:,1)-n1;
end

if n2<0
y2(:,2)=y2(:,2)-n2;
end

if n3<0
y2(:,3)=y2(:,3)-n3;
end

% calculate the mid point
% the mid point lay in the center of the x, y of the object and having
% the
% maximum height.

xx=[x_value y_value z_value];

% Projection...add the midpoint as the 4th column in the vertices list to
% give the list of tetrahedra

y2(c+1,:)=xx;

x2(:,4)=c+1;

x2=uint32(x2);

t=simp_plot_3ddd(y2,x2);
vo=vol(y2);
vo=uint32(vo);

```


5- Vol.m

```

function vo = vol(vertices,T)

% receive ready tetrahedra
% vertices :,4
%v vertices , t triangles == faces, c count number of triangles

[c cc]=size(T);
% c = count is the number of triangles tetrahedra
volume=0;
for i=1:c % for each tetrahedron

    volume =
volume+abs(det([vertices(T(i,1),1),vertices(T(i,1),2),vertices(T(i,1),3)
,1;vertices(T(i,2),1),vertices(T(i,2),2),vertices(T(i,2),3),1;vertices(T
(i,3),1),vertices(T(i,3),2),vertices(T(i,3),3),1;
vertices(T(i,4),1),vertices(T(i,4),2),vertices(T(i,4),3),1])); %divide
by 6 later for efficiency
end
    vo= volume/6; %since the determinant give 6 times tetra
volume

```

6- Convex_div20.m

```

function [vol,s,Tes] = Convex_div20(y2)
% divide the surface to equally spaced subsurfaces using the Y
% coordiante...
% in this the surface is divides into 20 surfaces

yy = unique(y2,'rows');
% if any of the dimensions lay in the negative axis we will performer
% translation for the whole object or surface

[a b]=size(yy);

%   c1=1;
%   c2=1;
%   for in=1 :a
%       if yy(in,2)>=0
% yy1(c1,:)=yy(in,:);
% c1=c1+1;
%       else
% yy2(c2,:)=yy(in,:);
% c2=c2+1;
%       end

n1=min(yy(:,1));
n2=min(yy(:,2));
n3=min(yy(:,3));

% if any of the dimensions lay in the negative axis we will performe
% translation for the whole object or surface
if n1<0
yy(:,1)=yy(:,1)-n1;
end

if n2<0
yy(:,2)=yy(:,2)-n2;
end

if n3<0
yy(:,3)=yy(:,3)-n3;
end

% cs# = count for the vertices composing each of the 20 surfaces
cs1=1;
cs2=1;
cs3=1;
cs4=1;
cs5=1;
cs6=1;
cs7=1;
cs8=1;
cs9=1;
cs10=1;
cs11=1;
cs12=1;
cs13=1;
cs14=1;
cs15=1;
cs16=1;

```

```

cs17=1;
cs18=1;
cs19=1;
cs20=1;
dif= max(yy(:,2))-min(yy(:,2));
dis=dif/20;

for in=1 :a
if yy(in,2) < min(yy(:,2))+dis
s1(cs1,:)=yy(in,:);
cs1=cs1+1;
elseif yy(in,2) < min(yy(:,2))+dis*2
s2(cs2,:)=yy(in,:);
cs2=cs2+1;
elseif yy(in,2) < min(yy(:,2))+dis*3
s3(cs3,:)=yy(in,:);
cs3=cs3+1;
elseif yy(in,2) < min(yy(:,2))+dis*4
s4(cs4,:)=yy(in,:);
cs4=cs4+1;
elseif yy(in,2) < min(yy(:,2))+dis*5
s5(cs5,:)=yy(in,:);
cs5=cs5+1;
elseif yy(in,2) < min(yy(:,2))+dis*6
s6(cs6,:)=yy(in,:);
cs6=cs6+1;
elseif yy(in,2) < min(yy(:,2))+dis*7
s7(cs7,:)=yy(in,:);
cs7=cs7+1;
elseif yy(in,2) < min(yy(:,2))+dis*8
s8(cs8,:)=yy(in,:);
cs8=cs8+1;
elseif yy(in,2) < min(yy(:,2))+dis*9
s9(cs9,:)=yy(in,:);
cs9=cs9+1;
elseif yy(in,2) < min(yy(:,2))+dis*10
s10(cs10,:)=yy(in,:);
cs10=cs10+1;
elseif yy(in,2) < min(yy(:,2))+dis*11
s11(cs11,:)=yy(in,:);
cs11=cs11+1;
elseif yy(in,2) < min(yy(:,2))+dis*12
s12(cs12,:)=yy(in,:);
cs12=cs12+1;
elseif yy(in,2) < min(yy(:,2))+dis*13
s13(cs13,:)=yy(in,:);
cs13=cs13+1;
elseif yy(in,2) < min(yy(:,2))+dis*14
s14(cs14,:)=yy(in,:);
cs14=cs14+1;
elseif yy(in,2) < min(yy(:,2))+dis*15
s15(cs15,:)=yy(in,:);
cs15=cs15+1;

elseif yy(in,2) < min(yy(:,2))+dis*16
s16(cs16,:)=yy(in,:);
cs16=cs16+1;
elseif yy(in,2) < min(yy(:,2))+dis*17

```

```

        s17(cs17,:)=yy(in,:);
        cs17=cs17+1;
elseif yy(in,2) < min(yy(:,2))+dis*18
        s18(cs18,:)=yy(in,:);
        cs18=cs18+1;
        elseif yy(in,2) < min(yy(:,2))+dis*19
        s19(cs19,:)=yy(in,:);
        cs19=cs19+1;
else
        s20(cs20,:)=yy(in,:);
        cs20=cs20+1;
end
end

vol=0;
si=0;
if cs1>3
Tes1 = delaunay3(s1(:,1),s1(:,2),s1(:,3), {'Qt', 'Qbb', 'Qc', 'Qz'});
Tes=[Tes1];
v1=vol(s1, Tes1);
vol=vol+v1;
[si1 b]=size(s1);
si=si+si1;
s=s1;
end
if cs2>3
Tes2 = delaunay3(s2(:,1),s2(:,2),s2(:,3), {'Qt', 'Qbb', 'Qc', 'Qz'});
v2=vol(s2, Tes2);
vol=vol+v2;
[si2 b]=size(s2);
Tes=[Tes;Tes2+si];
si=si+si2;
s=[s;s2];
end
if cs3>3
Tes3 = delaunay3(s3(:,1),s3(:,2),s3(:,3), {'Qt', 'Qbb', 'Qc', 'Qz'});
v3=vol(s3, Tes3);
vol=vol+v3;
[si3 b]=size(s3);
Tes=[Tes;Tes3+si];
si=si+si3;
s=[s;s3];
end
if cs4>3
Tes4 = delaunay3(s4(:,1),s4(:,2),s4(:,3), {'Qt', 'Qbb', 'Qc', 'Qz'});
v4=vol(s4, Tes4);
vol=vol+v4;
[si4 b]=size(s4);
Tes=[Tes;Tes4+si];
si=si+si4;
s=[s;s4];
end
if cs5>3
Tes5 = delaunay3(s5(:,1),s5(:,2),s5(:,3), {'Qt', 'Qbb', 'Qc', 'Qz'});
v5=vol(s5, Tes5);
vol=vol+v5;
[si5 b]=size(s5);
Tes=[Tes;Tes5+si];
si=si+si5;
s=[s;s5];
end
end

```

```

if cs6>3
Tes6 = delaunay3(s6(:,1),s6(:,2),s6(:,3), {'Qt', 'Qbb', 'Qc', 'Qz'});
v6=vol(s6, Tes6);
vol=vol+v6;
[si6 b]=size(s6);
Tes=[Tes;Tes6+si];
si=si+si6;
s=[s;s6];
end
if cs7>3
Tes7 = delaunay3(s7(:,1),s7(:,2),s7(:,3), {'Qt', 'Qbb', 'Qc', 'Qz'});
v7=vol(s7, Tes7);
vol=vol+v7;
[si7 b]=size(s7);
Tes=[Tes;Tes7+si];
si=si+si7;
s=[s;s7];
end
if cs8>3
Tes8 = delaunay3(s8(:,1),s8(:,2),s8(:,3), {'Qt', 'Qbb', 'Qc', 'Qz'});
v8=vol(s8, Tes8);
vol=vol+v8;
[si8 b]=size(s8);
Tes=[Tes;Tes8+si];
si=si+si8;
s=[s;s8];
end
if cs9>3
Tes9 = delaunay3(s9(:,1),s9(:,2),s9(:,3), {'Qt', 'Qbb', 'Qc', 'Qz'});
v9=vol(s9, Tes9);
vol=vol+v9;
[si9 b]=size(s9);
Tes=[Tes;Tes9+si];
si=si+si9;
s=[s;s9];
end
if cs10>3
Tes10 = delaunay3(s10(:,1),s10(:,2),s10(:,3), {'Qt', 'Qbb', 'Qc',
'Qz'});
v10=vol(s10, Tes10);
vol=vol+v10;
[si10 b]=size(s10);
Tes=[Tes;Tes10+si];
si=si+si10;
s=[s;s10];
end

if cs11>3
Tes11 = delaunay3(s11(:,1),s11(:,2),s11(:,3), {'Qt', 'Qbb', 'Qc',
'Qz'});
v11=vol(s11, Tes11);
vol=vol+v11;
[si11 b]=size(s11);
Tes=[Tes;Tes11+si];
si=si+si11;
s=[s;s11];

end

```

```

if cs12>3
Tes12 = delaunay3(s12(:,1),s12(:,2),s12(:,3), {'Qt', 'Qbb', 'Qc',
'Qz'}));
v12=vol(s12, Tes12);
vol=vol+v12;
[si12 b]=size(s12);
Tes=[Tes;Tes12+si];
si=si+si12;
s=[s;s12];
end

```

```

if cs13>3
Tes13 = delaunay3(s13(:,1),s13(:,2),s13(:,3), {'Qt', 'Qbb', 'Qc',
'Qz'}));
v13=vol(s13, Tes13);
vol=vol+v13;
[si13 b]=size(s13);
Tes=[Tes;Tes13+si];
si=si+si13;
s=[s;s13];
end

```

```

if cs14>3
Tes14 = delaunay3(s14(:,1),s14(:,2),s14(:,3), {'Qt', 'Qbb', 'Qc',
'Qz'}));
v14=vol(s14, Tes14);
vol=vol+v14;
[si14 b]=size(s14);
Tes=[Tes;Tes14+si];
si=si+si14;
s=[s;s14];
end

```

```

if cs15>3
Tes15 = delaunay3(s15(:,1),s15(:,2),s15(:,3), {'Qt', 'Qbb', 'Qc',
'Qz'}));
v15=vol(s15, Tes15);
vol=vol+v15;
[si15 b]=size(s15);
Tes=[Tes;Tes15+si];
si=si+si15;
s=[s;s15];
end

```

```

if cs16>3
Tes16 = delaunay3(s16(:,1),s16(:,2),s16(:,3), {'Qt', 'Qbb', 'Qc',
'Qz'}));
v16=vol(s16, Tes16);
vol=vol+v16;
[si16 b]=size(s16);
Tes=[Tes;Tes16+si];
si=si+si16;
s=[s;s16];
end

```

```

if cs17>3
Tes17 = delaunay3(s17(:,1),s17(:,2),s17(:,3), {'Qt', 'Qbb', 'Qc',
'Qz'}));
v17=vol(s17, Tes17);
vol=vol+v17;

```

```

[si17 b]=size(s17);
Tes=[Tes;Tes17+si];
si=si+si17;
s=[s;s17];
end

if cs18>3
Tes18 = delaunay3(s18(:,1),s18(:,2),s18(:,3), {'Qt', 'Qbb', 'Qc',
'Qz'});
v18=vol(s18, Tes18);
vol=vol+v18;
[si18 b]=size(s18);
Tes=[Tes;Tes18+si];
si=si+si18;
s=[s;s18];
end

if cs19>3
Tes19 = delaunay3(s19(:,1),s19(:,2),s19(:,3), {'Qt', 'Qbb', 'Qc',
'Qz'});
v19=vol(s19, Tes19);
vol=vol+v19;
[si19 b]=size(s19);
Tes=[Tes;Tes19+si];
si=si+si19;
s=[s;s19];
end

if cs20>3
Tes20 = delaunay3(s20(:,1),s20(:,2),s20(:,3), {'Qt', 'Qbb', 'Qc',
'Qz'});
v20=vol(s20, Tes20);
vol=vol+v20;
Tes=[Tes;Tes20+si];
s=[s;s20];
end
vol=uint32(vol)
figure, simp_plot_3ddd(s,Tes);

```

APPENDIX D: CD

The attached CD contains related resources: (Data, Matlab code, Models and Soft copy of thesis).